DESIGNING HIERARCHICAL INFRASTRUCTURE-BASED TRAFFIC CONTROL FRAMEWORKS FOR LARGE-SCALE HETEROGENEOUS TRAFFIC NETWORKS

by

Pouria Karimi Shahri

A dissertation proposal submitted to the faculty of
The University of North Carolina at Charlotte
in partial fulfillment of the requirements
for the degree of Doctor of Philosophy in
Mechanical Engineering

Charlotte

2023

Approved by:

Dr. Amirhossein Ghasemi

Dr. Scott David Kelly

Dr. Srinivas Pulugurtha

Dr. Artur Wolek

Dr. Dipankar Maity

ABSTRACT

POURIA KARIMI SHAHRI. Designing Hierarchical Infrastructure-based Traffic Control Frameworks for Large-Scale Heterogeneous Traffic Networks. (Under the direction of DR. AMIRHOSSEIN GHASEMI)

This research aims to develop, enhance, and validate infrastructure-based hierarchical control framework designs for improving the mobility of large-scale heterogeneous traffic networks. This research defines heterogeneity as a multi-vehicle traffic network consisting of Human-Driven Vehicles (HDVs) and Autonomous Vehicles (AVs), distinguished by their operational characteristics and controllability. AVs have gained huge interest across private industry, academia, government, and the public because they promise higher road efficiency, improved safety, better energy consumption, and improved emissions. However, the widespread adoption of autonomous vehicle technology will likely take place over several years (if not decades) as the technology becomes more widely accepted by the general public and more cost-effective. Therefore, there will be a long period of time when we have both AVs and HDVs sharing the same road and it is essential to develop traffic management strategies that take the uncertainty associated with the heterogeneity in the traffic networks into account. Furthermore, it is crucial to understand the extent to which these control strategies improve the performance of the traffic network. To capture the realistic nature of large-scale heterogeneous traffic networks, we adopt the heterogeneous (multi-class) METANET model wherein the density and velocity dynamics of each vehicle class in each cell are described mathematically. In order to achieve a higher-fidelity traffic model, we considered state- and class-dependent model parameters to better capture the complex underlying dynamics of a heterogeneous traffic network. Moreover, in this research, we propose a hierarchical distributed infrastructure-based control framework to manage large-scale heterogeneous traffic networks. At the lower-level, we employed the Distributed Filtered Feedback Linearization (D-FFL) controller. The purpose of this

controller is to track the desired density of each vehicle class in the target cells which is set by the upper-level controller. D-FFL tracks the reference density by controlling the suggested velocity of vehicles in the target cell and its upstream cell. The D-FFL controller requires only limited model information, specifically, knowledge of the vector relative degree and the dynamic-inversion matrix, which is the nonlinear extension of the high-frequency-gain matrix for linear systems. The controller inputs derived by the classic feedback linearization control approach (ideal control inputs) and the control inputs generated by the D-FFL are mathematically equivalent. However, the feedback linearization method requires full knowledge of the plant model and measurement of the disturbance of the system which is hard to achieve based on the complex underlying dynamics of the heterogeneous traffic network. At the upper-level, in our initial design, a Distributed Extremum-Seeking (D-ES) controller is designed and implemented which aims to find the optimal operating densities of each vehicle class in the target cells over time. D-ES is a model-free, real-time adaptive control algorithm that is useful for adapting control parameters to unknown system dynamics and unknown mappings from control parameters to an objective function. The gradient-based D-ES comprises three essential components: the dither signals, the gradient estimator, and the optimizer operating at progressively slower time scales. The primary objective of the upper-level controller in our research is to achieve two main goals simultaneously: the maximization of the average flow of the target cell to mitigate traffic congestion and the minimization of the flow difference between the target cell and the upstream flow to prevent the propagation of congestion in the backward direction. The desired densities are then fed into the lower-level controller as the reference model. To improve the performance of the designed hierarchical controller and reduce the convergence time, we designed and implemented Newton Extremum Seeking (NES) at the upper level of the hierarchy to feed the optimal density of target cells to the lower-level controller. One of the key distinctions between the Newton al-

gorithm and the gradient algorithm is that the convergence of the former is not solely contingent on the second derivative (Hessian) of the cost map and it is user-assignable. In fact, this allows for the deliberate synchronization of all parameters to converge at a uniform pace, resulting in straightforward paths leading to the optimal point in a shorter time. Moreover, to address the potential loss in optimality that may arise due to continuous sinusoidal perturbations around the optimal point, we propose a switched control scheme to be added to the NES structure. The proposed switched control scheme involves reducing the amplitude of perturbations after convergence, specifically within a neighborhood around the desired state. The switch is determined by utilizing a Lyapunov function that is based on an averaged model of the NES feedback system. This Lyapunov function is designed to approximate the proximity to the desired state, and based on this estimate, the switch is activated to reduce the perturbation size. The enhanced upper-level controller design is named Lyupanov-based Switch Newton Extremum Seeking (LSNES) which is then combined with the FFL to form the hierarchical control framework. Finally, we established a MATLAB-VISSIM COM interface that allows closed-loop control of a simulated traffic scenario in PTV-VISSIM to test and validate the effectiveness of the distributed ES-FFL and LSNES-FFL control approaches in large-scale traffic networks. The simulation results show that our initial control framework design can effectively reduce congestion and prevent congestion back-propagation during peak hours in homogeneous and heterogeneous traffic networks. We further compare our novel control framework design with common model-free macroscopic traffic control approaches. By implementing our improved hierarchical control framework, we also show that the Lyupanov-based Switch Newton Extremum Seeking-FFL (LSNES-FFL) control framework has a %42 faster convergence rate with respect to the conventional ES-FFL method.

DEDICATION

To my best friend and partner, Kimia.

To the indomitable women of Iran, whose unwavering spirit and tireless pursuit of equality inspire us all.

ACKNOWLEDGEMENTS

I would like to express my deepest gratitude to my advisor and chair of my committee, Dr. Amirhossein Ghasemi, for his invaluable patience and guidance. I could not have undertaken this journey without his expertise and knowledge generously shared with me. I am also highly grateful to the Department of Mechanical Engineering and Science at UNC Charlotte, for providing me an opportunity to continue my education. I am also thankful for the support and guidance of my committee, UNC Charlotte faculty Drs. Srinivas Pulugurtha, Scott David Kelly, Artur Wolek, and Dipankar Maity. I extend my sincere gratitude to Drs. Azad Ghaffari and Baisravan HomChaudhuri for their invaluable contributions to our numerous collaborative endeavors, from which I have gained a wealth of knowledge and insights.

I am eternally thankful to my friends and family for their continued support and encouragement. I would not have made it so far without the bravery and persistence taught by my parents, Setareh and Mahmoud Reza, and my little sister, Parmida, whom I miss all so much since I have not seen them from the beginning of my Ph.D. journey in USA in 2018. Words cannot express my gratitude for my office friends who have been there for me when I needed heartening and someone to vent to, Daniel, Jacob, Ashish, Shubhankar, Joe, Navid, Arash, and all the other wonderful people I had the privilege to work, study, and thrive next to. I profoundly appreciate my friends Vahid I., Amirhossein Z., Masoumeh H., Mohammad M, Hamed A., Kimia K., Ali G. and all my friends in the Iranian Student Organization (ISO) at UNC Charlotte for keeping me sane during the challenging times in the past five years.

Lastly, I want to give a big thanks to my wife, Kimia Vahdat. This dissertation would not be here without her constant support and belief in me. Over the past five years, in the tapestry of our daily lives, we've shared meaningful conversations that have fueled my intellectual pursuits, cozy Netflix evenings that provided both relaxation and shared laughter, collaborative cooking adventures that turned ordinary

meals into cherished memories, and explorations across the diverse landscapes of the United States that offered us glimpses of beauty and wonder.

As my life partner, I am truly grateful for the journey we have shared. She has been a huge part of not just this academic accomplishment but also the happiness in my everyday life. I also want to give a shout-out to our cute little cats, Joey and Smokey, for bringing extra joy to our days with their playful antics and cozy company.

TABLE OF CONTENTS

LIST OF FIGURES

CHAPTER 1: INTRODUCTION

1.1 TRAFFIC MANAGEMENT STRATEGIES

As cities expand and people's mobility requirements rise, traffic congestion becomes a huge issue associated with urbanization. In 2021, Americans collectively wasted 3.4 billion hours as a result of congestion. [1]. The ongoing increase in the demand for current transportation infrastructure is placing strain on already nearly saturated road networks. Nevertheless, constructing new infrastructure is not a sustainable solution for alleviating congestion, as urban development and transportation infrastructure battle for the same limited space resources. In response to this challenge, a range of traffic control strategies, encompassing both infrastructure-based and vehicle-based traffic control measures, has been developed [2; 3; 4; 5; 6; 7; 8; 9]. The vehicle-based algorithms focus on controller synthesis for individual vehicles, where each vehicle evaluates its control solution with available information to improve its performance (such as energy consumption, travel time, or safety) [10; 11; 12; 13; 14; 15; 16; 17; 18; 19]. However, the egotistical nature (only focusing on its performance) of this type of controller and the availability of only local information can deteriorate the overall traffic network's traffic flow and overall performance [20; 21]. The infrastructure-based algorithms, using the macroscopic models of a traffic network, focus on improving the aggregated traffic behavior such as overall traffic flow, average density, total travel time, etc. [4; 5; 6; 7; 8; 9; 22; 23; 24; 25]. Examples of infrastructure-based controllers are ramp-metering [26], variable speed limit control [27], and lane management [28].

Among these initiatives, there is substantial interest in Autonomous Vehicle (AV) technologies from private industry, academia, government, and the public. This huge interest arises from the potential benefits AVs offer, including enhanced road efficiency,

increased safety, reduced energy consumption, and improved emissions [29; 30]. Nevertheless, the widespread adoption of AV technology is likely to unfold gradually over several years, if not decades, as the technology gains broader acceptance and becomes more cost-effective [29]. Therefore, it is essential to develop traffic management strategies that consider the uncertainty associated with the heterogeneity in the traffic network and understand the extent to which these strategies improve the network's performance and efficiency [31].

Researchers have been using various definitions of heterogeneity in traffic networks such as heterogeneity in operational characteristic [32], in controllability [33; 34] where AVs are considered as controllable agents that can follow the commands from the controller, in traffic properties [35] that both signalized and non-signalized intersections are available in the traffic network, in various sizes of vehicles in the traffic network [36], and in different vehicle types [37]. In this research, we consider the heterogeneity in terms of the operational characteristics and controllability of different types of vehicles; Human-Driven-Vehicles (HDVs) and Autonomous Vehicles (AVs).

1.1.1 DYNAMIC MODELS FOR HETEROGENEOUS TRAFFIC NETWORKS

The study of traffic flow modeling dates back to the 1950s, with notable contributions by researchers such as Lighthill and Whitham [38] and Richards [39]. These pioneers independently formulated mathematical models for freeway traffic flow, drawing parallels between traffic dynamics and fluid mechanics. Since that time, the mathematical modeling of traffic flow has gotten the attention of numerous researchers, as evidenced by the work of Ferrara and others [40]. Anticipating traffic patterns is integral to various practical applications in the realms of traffic and transportation, including travel information services, traffic management, decision-support systems, and freight and fleet management systems. At the network level, the most suitable tools for forecasting traffic conditions and potentially optimizing traffic measures are traffic simulation models. These models span from less detailed macroscopic

(infrastructure-based) models to highly detailed microscopic (vehicle-based) dynamic models [41].

Macroscopic models, whether categorized as first-order, second-order, or higher, describe how the traffic system's states change over time. This involves the consideration of two independent variables: i)time, and ii) space [42]. In the traffic dynamics mathematical model in continuous mode, these variables are presumed to demonstrate continuity, while discrete traffic models involve their discretization. In the latter scenario, a freeway segment is subdivided into multiple smaller road sections, and Time is divided systematically into a set number of intervals. This modeling approach, spanning from the evolution of aggregate quantities to the discretization of independent variables, offers a comprehensive understanding of traffic dynamics across temporal dimensions and spatial considerations [43].

The first-ever continuous macroscopic traffic model, the Lighthill Whitham Richards (LWR) model, was formulated in the 1950s by Lighthill and Whitham [38], along with Richards [39]. This model's core idea is that vehicles quickly adapt their speeds to a steady-state relation based on the current traffic density. Nevertheless, it has its downsides, one being the failure to account for the gradual changes in vehicle speeds caused by the lack of consideration for inertia effects[44]. This drawback can lead to vehicles experiencing unnaturally high accelerations or decelerations [44]. Furthermore, the model reliably predicts that the traffic leaving a congested cell matches the road's capacity flow if the downstream cell in the road is free from congestion. This stands in contrast to the real-world phenomenon of capacity drop that we see in traffic networks [45]. The widely known discretized version of the LWR model is the Cell Transmission Model (CTM), introduced by Daganzo in [46; 47]. Initially designed for roads without on-ramps or off-ramps, it was later expanded in [48] to accommodate traffic networks with complex features like intermediate exits or entrances, and intersections.

Analyzing and predicting traffic states in a heterogeneous (mixed) traffic network stands as a prominent research area in traffic and transport science [49]. Consequently, researchers have categorized multiclass traffic models to differentiate between various vehicle classes navigating the same traffic network [50]. Depending on the model's objectives, these vehicle classes may be specified as distinct types of vehicles or as specific characteristics of the drivers. Irrespective of the specific vehicle types under consideration, multiclass models possess a superior descriptive capacity compared to single-class models [26]. This enhanced capability enables them to better capture the dynamics of a large-scale traffic network in the real world. Multiclass models stand out in capturing important traffic phenomena that escape models concentrating solely on one vehicle class. This is especially true for interactions among diverse groups of vehicles sharing the same infrastructure. The majority of multiclass first-order traffic models derive from extending the LWR model, with only a limited number offering multiclass extensions of the CTM [51]. In specific scenarios, multi-lane models are employed to illustrate the characteristics of heterogeneous traffic flow, as exemplified in [52]. An alternative method is outlined in [53], where the model incorporates two vehicle classes and a set of lanes that are designated for each class. Expanding on this concept, a kinematic wave theory model of mixed traffic flow is introduced in [54] and further developed in [55] to accommodate lane-changing and lateral movement scenarios. These studies assume that vehicles follow predetermined paths, with vehicle class utilizing the same route. In a distinct approach, [56] introduces a novel dynamic model for the interaction of various vehicle classes in a non-cooperative manner, where the vehicles with slower velocities act as moving bottlenecks for vehicles with faster speeds trying to optimize their speed without affecting the slower vehicle classes. In this framework, each class of vehicles represents a homogeneous group of vehicles interacting with other vehicle groups within the overall traffic flow. Based on this model, each class is characterized by a unique Macroscopic Fundamen-

tal Diagram (MFD), which illustrates the relationship between road traffic flow and traffic density. The MFD is a concept used in transportation engineering and traffic flow theory to describe the relationship between traffic flow, density, and speed at a macroscopic level [47]. Unlike microscopic models that focus on individual vehicle movements, the MFD looks at aggregate traffic behavior over a larger spatial scale, such as a road network or an entire urban area. The MFD typically represents the relationship between the average network-wide flow and the average network-wide density. The fundamental diagram is often depicted as a curve showing how the flow or velocity changes with density. The MFD concept is useful for understanding the overall efficiency and performance of a transportation system [57]. A recent development in first-order macroscopic traffic models used in the multiclass context is the Fastlane model, first proposed in [58]. Subsequent improvements were implemented in [59], broadening the scope of Fastlane to include the integration of ramp metering, enabling the independent control of distinct vehicle classes.

To address the limitations of first-order continuous models, second-order traffic flow models emerged approximately two decades later. In addition to considering traffic density dynamics, these models explicitly incorporate a dynamic equation for the mean speed. The Payne–Witham (PW) model [60] belongs to the category of continuous traffic flow models at the macroscopic level, representing the dynamics of aggregate variables denoted as traffic flow. Key variables in macroscopic models include average mean speed, traffic density, traffic flow, location, and time. Continuous macroscopic models, particularly the PW model, utilize the analogy between traffic and fluids. However, as highlighted in [61], significant disparities exist between them, necessitating accurate representation in traffic models. Vehicles in traffic networks, unlike fluids, are anisotropic particles primarily responsive to the flow behind them and barely affected by the traffic flow ahead of them.

Furthermore, in contrast to molecules, drivers possess distinct personalities, con-

tributing to discrepancies within the PW model, and resulting in unrealistic behaviors like negative speeds. Aw, and Rascle in [62], along with Zhang [63], proposed modifications to the PW model to rectify these inconsistencies. Their adjustments involved incorporating anticipation and relaxation terms to enhance the model's representation of road networks. Another category of traffic models falls under discrete second-order models, exemplified by the METANET model [64; 65; 66]. The model adopts a discrete approach in both space and time, wherein the freeway stretch is segmented into distinct road portions, termed cells, and the time horizon is divided into equally spaced time intervals. In the METANET model, the presence of on-ramps and off-ramps is accounted for within the sections.

As emphasized earlier, there are various motivations to explicitly integrate multiple vehicle classes into traffic flow models, extending beyond first-order models to encompass second-order ones. In [43], modifications are made to the single-class METANET model to represent a mixed traffic flow, by considering a unique FD for each vehicle class. Another second-order traffic model accommodating multiple classes is introduced in [67; 68]. In this model, each class of vehicles adheres to its own MFD and is confined within a designated space. An extension of the METANET model to accommodate a multi-class (heterogeneous) framework is presented in [69], subsequently refined in [70; 71] for a freeway section, and further adapted in [72] for a whole network. In these subsequent models, interactions among various vehicle groups are characterized by class-specific MFDs, with the flow of each class dependent on the dynamic coupling term and the total density. In our proposal, we adopt the multiclass METANET model as presented in [68] for the heterogeneous traffic network. Additional insights into this model, examining its use in the heterogeneous traffic network containing AVs and HDVs, are elaborated in Chapter 2.

1.1.2 CONTROLLER DESIGN FOR HETEROGENEOUS TRAFFIC NETWORKS

The demand for creating monitoring and management plans for freeway traffic networks has risen in recent decades due to the ongoing rise in traffic congestion and its negative impacts on individuals and the environment. Despite being designed to accommodate substantial traffic volumes, freeway networks have faced challenges in coping with the growing demand, and conventional infrastructure interventions often fall short of addressing this issue [73]. Consequently, implementing targeted control measures frequently emerges as the optimal strategy for optimizing the efficiency of freeway traffic systems. Freeway traffic management can take various forms. One approach involves regulating the entry of traffic flows onto the freeway through the implementation of ramp metering. Another method entails controlling the movement of vehicles within the freeway itself, achieved through mainstream control. This entails guiding vehicles along designated paths and implementing efficient route guidance strategies [40; 74; 75].

The goals of traffic controllers are closely tied to enhancing traffic conditions on freeways, specifically aiming to reduce congestion and alleviate its negative impacts [76]. The primary aim of traffic controllers is to minimize total travel time, given its direct impact on travelers. However, recently, researchers have introduced additional control objectives to address environmental concerns, enhance safety, and consider issues related to the overall quality of life for people. Consequently, we can categorize the objective control functions into three main groups [40; 77; 78; 79; 80]: (I) Enhancement of system performance by reducing congestion and emissions, (II) Increasing safety, reducing the stop-and-go event in traffic, and preventing congestion back-propagation (III) Reducing the total travel time and total travel distance.

Numerous traffic controllers have been developed to regulate freeway traffic by tracking specific set-points as desired values for traffic states, specifically traffic den-

sity [81; 82]. The common approach is to establish reference densities for the traffic network and implement traffic control strategies to effectively track these reference densities by controlling the flow, velocity, or other terms of a large-scale traffic network[83; 84]. Desired values for traffic density, varying across different road sections and changing over time, represent a versatile and common scenario in homogeneous and heterogeneous traffic networks. In advanced control strategies, these set points can be dynamically defined based on current traffic conditions, especially in hierarchical control setups where an upper-level controller computes real-time set points [84]. However, the more straightforward approach is to maintain fixed values for these density targets. Often, the critical density of the vehicle class in the homogeneous traffic networks is the set desired density. Implementing a controller in the traffic network to track the critical density is synonymous with maximizing the flow, exploiting the road capacity as much as possible [85].

Traffic flow management in the mainstream based on local measurements of the traffic's states is a key aspect of flow control strategies. Various forms of mainstream control implementation exist, with [86] presenting a comprehensive concept of this control action. In this approach, traffic flow control is introduced as a tool for regulating mainstream traffic. The deployment of various actuators, including Variable Speed Limits (VSL), traffic lights, or advanced controllers providing instructions directly to drivers, is part of this control strategy.

As stated before, there is a lot of attention on heterogeneous traffic networks consisting of HDVs and AVs. Two main categories in controlling methods are closed-loop control, where a portion of the output signal is fed back to the input to reduce errors and improve stability, and open-loop control, which does not monitor or measure the condition of its output signal as there is no feedback. Now there are various subcategories in controlling methods such as optimal control, feedback control, robust control, phase control, and centralized and decentralized control which can all be used

in different heterogeneous traffic flow control methods like variable speed limit (VSL) control [87; 88; 89; 90; 91], ramp metering [92; 93; 94; 95], traffic signal control [96; 97], platooning [98; 99; 100; 101; 102], lane management [31; 103; 104], longitudinal and lateral control [105; 106].

In [87], researchers explored how to implement VSL in mixed-traffic highways with various penetration rates (levels of heterogeneity). Wu et al. developed a variable speed limit control strategy considering the relationship between headways and the visibility distance of autonomous vehicles [107]. In another study, the authors proposed a VSL algorithm to reduce the stop-and-go behavior of vehicles at traffic signals after finding out the relations among flow parameters by building a multiclass cell transmission model (CTM) [108]. Yu et al. presented an optimal variable speed limit control strategy for AVs in heterogeneous freeway corridors with multiple bottlenecks [90]. Another researcher addressed the VSL control problem for automated vehicles before they enter the speed reduction zone on freeways [91]. Ramezani et al. presented a two-level controller to reduce the congestion in the heterogeneous traffic network by controlling the lateral flows of AVs [33]. The first level controller finds the optimal density distribution upstream of the bottlenecks and the second controller controls the lane change advisory system in lateral movements. The same researcher presented a hierarchical perimeter flow control that operates on the border between urban regions to minimize the network delay and also to distribute the congestion more homogeneously by controlling the flow rate between regions [109]. In another study, researchers used AVs in a partial penetration rate traffic system to develop a variable speed limit control in order to reduce the time delay and improve the bottlenecks[110]. Talebpour et al. investigated the effect of lane dedication to AVs in two-lane and four-lane highways on congestion reduction and total travel time reliability [111]. They also showed that AVs' effectiveness in increasing the system's throughput is more than connected AVs with the same penetration rate. Moreover,

[112] stated that using intelligent control of AVs can dampen stop-and-go waves in a single-lane traffic network. As stated before, besides reducing congestion, increasing the throughput of the traffic network and its capacity is another aim of related papers. Chen et al. presented a theoretical framework to show how AVs will affect the heterogeneous traffic network capacity. Furthermore, they have investigated the optimal distribution of AVs across the lanes based on given network demand and penetration rate [113]. Additionally, another research has been conducted which discusses the optimal deployment of AV lanes in different penetration rates to increase the traffic system's capacity and throughput [114].

The main challenges associated with the design of infrastructure-based traffic controllers are due to (i) uncertainty and nonlinearity of the traffic system macroscopic dynamics and (ii) significant computational load of centralized macro-level controllers [115]. For instance, the model parameters of the METANET model are state-dependent and, thus, hard to characterize [68]. Furthermore, the optimal operating density of a congested cell in heterogeneous traffic networks with an unknown downstream bottleneck is not always known [116]. To address these issues, different control algorithms, including model-free based control algorithms have been investigated [31; 116; 117; 83]. Model-free control approaches require limited or even no information from the dynamics of the traffic network, such as Extremum Seeking (ES) control and Filtered Feedback Linearization (FFL) [83; 118; 119; 120].

Feedback linearization (FL) controller has been widely used as a set-point tracking (density tracking) controller for traffic management [121; 122]. However, the main drawback of FL is that it requires full model information and the measurement of the network disturbance. The traffic dynamics contain uncertainties associated with the unmodeled dynamics of a traffic system, which can intrinsically be state- and control-dependent, making it impractical to get the required model information for the FL controller [122]. This research addresses this shortcoming by introducing the

Filtered Feedback Linearization (FFL) approach. FFL is a high-parameter-stabilizing control technique that addresses both command following and disturbance rejection for Multi-Input-Multi-Output (MIMO) nonlinear systems where the equilibrium of the zero dynamics is locally asymptotically stable [123; 124]. FFL is mathematically equivalent to filtering a standard feedback linearization controller. However, unlike the standard FL, the controller only requires limited model information, specifically, knowledge of the vector relative degree and the dynamic-inversion matrix. As a result, FFL makes the $\mathcal{L}_\infty$ of the command following error arbitrarily small despite the presence of unknown disturbances[123; 125].

As discussed earlier, prior studies on traffic control rely on feedback control [126; 127; 85]. These studies utilize a predefined constant set-point based on historical traffic data, often the critical density at which the traffic network achieves its maximum flow. However, the critical density may not always be optimal due to the complex dynamics of heterogeneous traffic networks [84; 120]. In [85], we used the FFL approach for the first time in a non-signalized heterogeneous traffic network to reach the desired density for AVs and HDVs in the target cell. However, the desired densities for AVs and HDVs were set equal to the critical density of each vehicle class based on simulation data. Therefore we introduce a hierarchical controller design which consists of two levels. At the lower level, we utilize the FFL controller to adjust the velocity of vehicles in the target cells in order to reach the desired density for each vehicle class. At the upper level, we implement an ES controller to determine the optimal densities of each vehicle class and feed that into the lower-level controller as a reference density.

Extremum Seeking (ES) control has been intensively studied over the recent years [128; 129; 130; 131; 132; 133; 134; 135], especially after the theoretical work by Krstic and Wang [136] proving the convergence of cost function to a neighborhood of the optimal value using averaging analysis and singular perturbation. ES control is a

model-free optimization method that targets the steady-state performance of dynamic systems [136; 137]. An ES controller adjusts the input to a dynamic system to optimize the steady-state output, such as cost or performance, with minimal knowledge about the underlying dynamics [128; 138]. Gradient-based ES comprises three essential components: the dither signals, the gradient estimator, and the optimizer operating at progressively slower time scales [139]. ES has been applied to various control scenarios, including traffic light control and trajectory optimization [119; 140; 141]. ES leverages a small periodic excitation, usually sinusoidal, to stimulate the tuning parameters and quantifies the impact of the parameters using the output of a nonlinear map [142]. It is a real-time control method that seeks to optimize the steady-state dynamic of a system whose characteristics are not fully known [129; 136]. The method achieves this by approximating the gradients of the input-output mapping [128; 143]. Despite being studied in various contexts, ES has not received much attention for traffic congestion and flow control. In [144], ES control is employed for traffic congestion control with a downstream bottleneck. In this study, an unknown flow-density relationship is considered at the bottleneck area, and the optimum density of the upstream cell is determined to mitigate the congestion. Moreover, they assumed the traffic flow to be the control input; however, direct traffic flow control is not practical. To address this issue, a set-point tracking controller shall be integrated into the design of an ES-based controller [119]. In our paper [119; 85], a novel hierarchical control framework consisting of distributed ES and FFL is designed to mitigate the congestion in a homogeneous traffic network. In this framework, FFL updates the velocity communicated to the vehicles so that the desired density, which ES determines, is achieved. Furthermore, in this study, we enhance the performance of the novel hierarchical control framework by incorporating Lyapunov-based Switched Newton Extremum Seeking (LSNES) at the upper level of the control hierarchy and FFL at the lower level [120]. One of the key distinctions

between the Newton algorithm and the gradient algorithm is that the convergence of the former is not solely contingent on the second derivative (Hessian) of the cost map and it is user-assignable. In fact, this allows for the deliberate synchronization of all parameters to converge at a uniform pace, resulting in straightforward paths leading to the optimal point in a shorter time [128; 132]. The effectiveness of the Newton algorithm becomes particularly evident in the realm of multi-input optimization challenges. This advantage is most pronounced when dealing with problems in which the Hessian matrix notably deviates from the identity matrix. In such scenarios, the gradient algorithm frequently leads to the convergence of distinct input vector elements at notably disparate rates [145]. The issue of divergent convergence rates among different input vector elements presents an inherent challenge in gradient-based optimization schemes. To tackle this challenge, a potential solution involves adjusting the algorithm using the inverse of the Hessian matrix. However, this approach can be impractical in situations where the system model remains unknown. In contrast, the Newton algorithm offers a compelling solution by enabling uniform convergence rates for all input vector elements or allowing for rate customization if equipped with a convergent Hessian matrix estimator. This underscores the Newton algorithm's advantage in scenarios where gradient-based methods may grapple with disparate convergence rates, primarily stemming from limited knowledge about the Hessian matrix properties [128]. Consequently, addressing limit cycle concerns and achieving asymptotic convergence to the optimal set point stands as a notable issue in Newton-based Extremum Seeking (NES). To overcome this challenge, we implemented a Lyapunov-based switched approach that ensures asymptotic convergence to the optimal set point [146]. This ensures stable and robust convergence behavior of the control system, even in the presence of uncertainties. The utilization of a Lyapunov-based switching mechanism provides a rigorous mathematical framework for stability analysis, significantly enhancing the control system's reliability and ro-

bustness. The switched approach further offers adaptability and flexibility in selecting the appropriate control actions based on the system's current state. This adaptability proves particularly advantageous in the context of intricate and dynamic systems, such as heterogeneous traffic networks.

1.2 PROBLEM STATEMENT

This thesis aims to develop a hierarchical infrastructure-based control algorithm to control homogeneous and heterogeneous large-scale traffic networks. Although many previous works have developed infrastructure-based controllers for traffic networks, several **major challenges**, particularly for heterogeneous traffic networks, are yet to be addressed – that is the focus of this dissertation. In this research, we aim to address three objectives. In particular,

Aim 1: Modeling a Heterogeneous Traffic Network. The first aim of this research is to develop a modeling framework that can describe and predict the behavior of a heterogeneous traffic network. To capture the realistic nature of heterogeneous traffic systems, a proper way of coupling the dynamics of AVs and HDVs must be determined to achieve a high-fidelity mathematical model. Furthermore, to avoid implementing extensive inter-flow constraints which results in a more complex controller design, we need to consider class- and state-dependent model parameters in the heterogeneous traffic model and calibrate them with field data.

Aim 2: Developing and Enhancing Traffic Management Strategies for Large-scale Traffic Networks. The second aim of this research is to enhance mobility in homogeneous and heterogeneous traffic networks. We will design non-model-based hierarchical control approaches to examine to what extent mobility can be improved for different levels of heterogeneity when facing congestion during traffic peak hours. The main goal of our infrastructure-based

control framework is to reduce the congestion in target cells and prevent back-propagation of the congestion. Furthermore, we will also improve the performance and the convergence speed of the designed macroscopic controller.

Aim 3: Test and Validation. The effectiveness of the proposed infrastructure-based scalable control framework will be validated on an integrated model of heterogeneous traffic network highway scenarios using PTV-VISSIM software.

The proposed study will bridge different fields of study, establish new results for an important subclass of traffic, control, and optimization problems, establish a new fundamental theory in hierarchical control, and significantly advance state-of-the-art heterogeneous multi-vehicle traffic networks.

This dissertation is organized as follows. Chapter 2 provides an overview of the homogeneous and heterogeneous macroscopic traffic model, which is a descriptive tool for macroscopic highway traffic system dynamics. Chapter 3 elaborates on the development of a multi-level control platform for the purpose of realizing desirable traffic dynamics. Chapter 4 details the simulation results of the hierarchical control design, showcasing its proficiency in managing homogeneous and heterogeneous traffic networks. Finally, Chapter 5 serves as a conclusion, summarizing the research's key findings and presenting suggestions for future research directions.

CHAPTER 2: TRAFFIC DYNAMICS MODELLING

This chapter is focused on modeling the dynamics of both homogeneous and heterogeneous traffic networks. First, we go through the details of the METANET model for a single-class traffic network and then we introduce the METANET model for mixed traffic networks.

2.1 HOMOGENEOUS METANET MODEL

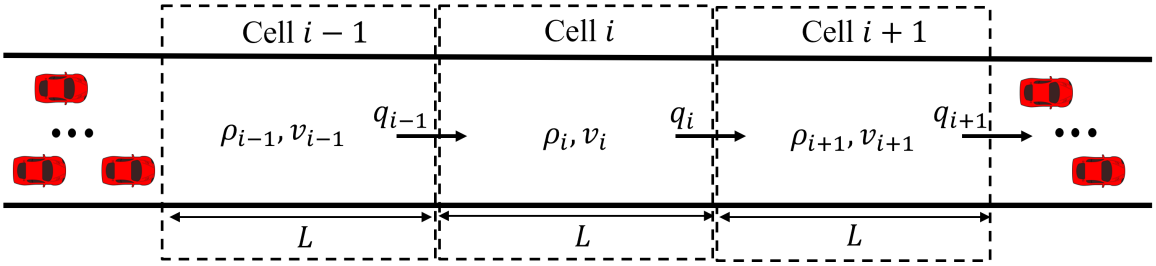

Figure 2.1: Schematic of a traffic network.

Consider a freeway traffic network, as shown in Fig. 2.2, wherein the road is discretized into multiple cells. The following assumptions are made throughout the rest of the discussion. A freeway corridor is divided into links; a link could be divided into cells if necessary; however, for simplicity, each link is considered as a cell in this research; and each link contains at least one traffic sensor. Consider the following notations in the following table:

i- cell index

$\mathcal{C}_i$ cell i

T- time step for model update

L_i length of cell i

λ_i number of lanes in cell i

$\rho_i(k)$- density for cell i during time interval k

$v_i(k)$- distance mean speed for the cell i during time interval k

$q_i(k)$- flow for the cell i during time interval k

$U_i(k)$- suggested velocity (speed control variable) for cell i

Payne [147] inferred the speed dynamics by making specific assumptions, including the equilibrium state assumption $v(x, t+\tau) = U(\rho(x+\Delta x, t))$. This presumption suggests that the Macroscopic Fundamental Diagram's (MFD) speed-density $(v-\rho)$ relationship has anticipated the density over a distance Δx, with the average driver's response delayed by τ in time. Utilizing Taylor series expansion on both temporal and spatial dimensions of the equation and subsequently discretizing it, the resulting expression for speed dynamics is outlined below:

$$v_i(k+1) = v_i(k) + \frac{T}{\tau}(U_i(\rho_i(k)) - v_i(k)) - \frac{T}{L_i} v_i(k)(v_{i-1}(k) - v_i(k)) - \frac{\varepsilon T}{\tau L_i} \frac{\rho_{i+1}(k) - \rho_i(k)}{\rho_i(k) + \kappa}. \tag{2.1}$$

The parameters τ, ε, and κ are values to be determined through calibration using field data. Eq. (2.1) contains three main terms that are discussed as follows:

1. First item - relaxation term: The relaxation term functions as a high-gain filter in the context of dynamic systems, characterized by the expression $\frac{1}{\tau}$ with a small τ [148]. The objective of the drivers collectively is to attain the desired speed $U_i(\rho_i(k))$, which serves as the control variable. The careful selection of

this desired speed is pivotal in capturing the nuances of driver behavior.

2. Second item - convection term: The convection term represents the impact of traffic from the upstream cell on the downstream cell, indicating the speed changes resulting from incoming and outgoing vehicle speeds. Its adjustment can involve introducing a factor, typically expressed as $\frac{\rho_{i-1}}{\rho_i}$. This modification accounts for the driver's speed adjustment concerning the density difference between the two neighbor cells [149]. Notably, this term holds the highest sensitivity in speed dynamics.

3. Third item - The density gradient term signifies that as the downstream density rises or falls, the speed in the current cell will correspondingly decrease or increase;

$$-\frac{\varepsilon T}{\tau L_i}\frac{\rho_i(k)-\rho_{i+1}(k)}{\rho_i(k)+\kappa} = -\frac{1}{\tau}(\frac{\varepsilon T}{L_i}\frac{\rho_i(k)-\rho_{i+1}(k)}{\rho_i(k)+\kappa}). \tag{2.2}$$

Here, τ represents the time delay characterizing how swiftly a group of drivers responds to the perception of traffic density. Essentially, each driver's observation pertains to the inter-vehicle distance in the immediate surroundings, akin to the driver's localized density perception. Meanwhile, ε functions as a sensitivity factor. The expression within the brackets articulates the influence of downstream cell density: an elevation in the downstream density correlates with a reduction in speed within the current cell. The incorporation of $\rho_i(k)$ in the denominator serves the purpose of normalization.

The introduction of the parameter $\kappa > 0$ serves two primary objectives:

- Enhancing the model's performance, particularly in scenarios characterized by medium to high density;

- Mitigating the singularity or excessive sensitivity of the term to the model under low-density conditions.

Given that the suggested velocity, $U_i(\rho_i(k))$, essentially serves as the parameter for speed control, it can be customized with values unrelated to density ($\rho_i(k)$), or even excluded from parameterization entirely. These adjustments involve a simple transformation of coordinates. However, choosing direct parameterization with density establishes a direct connection between the control design and the shape of the Fundamental Diagram (FD). When we integrate the dynamics of density and speed, the METANET model emerges, as outlined in previous works [66; 147; 150]:

Specifically, the dynamics of cell $\mathcal{C}_i$ are shown in continuous form as follows:

$$q_i(t) = \rho_i(t)v_i(t), \tag{2.3a}$$

$$\dot{\rho}_i(t) = \frac{1}{L_i\lambda_i}\Big(q_{i-1}(t) - q_i(t) + d_i(t)\Big) \tag{2.3b}$$

$$\dot{v}_i(t) = \frac{1}{\tau}\Big(U_i(t) - v_i(t)\Big) + \frac{1}{L_i}\Big[v_i(t)\Big(v_{i-1}(t) - v_i(t)\Big) - \frac{\varepsilon}{\tau}\frac{\rho_{i+1}(t) - \rho_i(t)}{\rho_i(t) + \kappa}\Big] \tag{2.3c}$$

where $d_i(t)$ is a disturbance flow (e.g., uncontrolled traffic flow including the off-ramps and on-ramps). Here, if we assume the suggested velocity of each cell is following the FD diagram, the $U_i(t) = V_i(t)$ is considered the suggested velocity for the vehicles in each cell of the traffic network, where $V_i(t) = v_{\mathrm{FF}}.\exp\left[\frac{-1}{a_{\mathrm{m},i}}\left(\frac{\rho_i(t)}{\rho_{\mathrm{c}}}\right)^{a_{\mathrm{m},i}}\right]$ is the mathematical model of the steady-state velocity-density relationship in the Macroscopic Fundamental Diagram (MFD) [151]. v_{FF} is the free-flow velocity, and ρ_{c} is the critical density where the flow is at capacity on a given lane. Also, $a_{\mathrm{m},i}$ is another model parameter that can be determined from field data in the model calibration process. However, in this research, we consider $U_i(t) = (1 - \beta_i(t))V_i(t)$ where $\beta_i(t)$ is the control input and it is within the range of $0 \leq \beta_i(t) \leq 1$. In particular, when $\beta_i(t) = 0$, the controller is suggesting vehicles to follow their macroscopic steady-state

behavior based on the FD diagram. On the other hand, $\beta_i(t) = 1$ indicates that the controller is commanding the vehicles to stop. Now that we have covered the basics of the METANET model for homogeneous traffic networks, we deep dive into the details of the heterogeneous METANET model to capture the differences and explain the crucial extra terms when it comes to modeling mixed traffic networks. Also, the equations of motion for the traffic dynamic model are introduced.

2.2 HETEROGENEOUS METANET MODEL

Now consider a highway traffic network with mixed flow as shown in Fig. 2.2 wherein the road is discretized into multiple cells. We characterize cell $\mathcal{C}_i$, where $i \in \{1, 2, \cdots, n\}$, by the density of AVs and HDVs ($\rho_{i,\mathrm{A}}$, $\rho_{i,\mathrm{H}}$), space mean speed of vehicles in each class ($v_{i,\mathrm{A}}$, $v_{i,\mathrm{H}}$) within the cell, and the average flow rate ($q_{i,\mathrm{A}}$,$q_{i,\mathrm{H}}$) of the cell for AVs and HDVs.

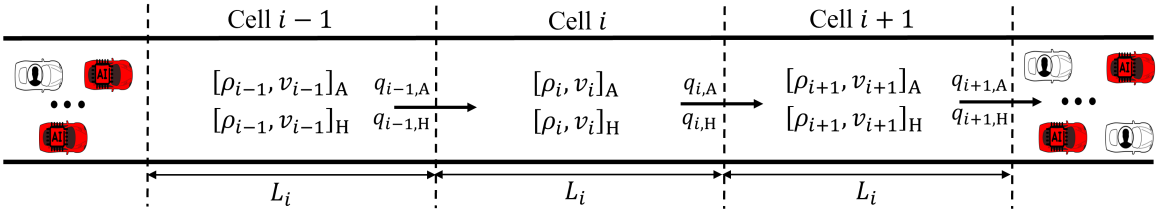

Figure 2.2: A schematic of a traffic network discretized into multiple cells with the length of L_i. The state variables of each cell are density ($\rho_{i,\mathrm{A}}$, $\rho_{i,\mathrm{H}}$), average velocity ($v_{i,\mathrm{A}}, v_{i,\mathrm{H}}$), and the flow ($q_{i,\mathrm{A}}, q_{i,\mathrm{H}}$) of each vehicle class.

The heterogeneous (multi-class) METANET model is an extension of the well-known METANET model [74] that we also discussed in the previous section. In this model, in cell $i \in \{1, \cdots, n\}$, for each class of vehicles, two sets of fundamental diagrams are defined that describe the macroscopic behavior of AVs and HDVs in a homogeneous (fully autonomous or fully human-driven) traffic network. Fig. 2.3 demonstrates two fundamental diagrams wherein a higher free-flow speed ($v_{\mathrm{A,FF}} > v_{\mathrm{H,FF}}$), larger critical density ($\rho_{\mathrm{c,A}} > \rho_{\mathrm{c,H}}$), higher capacity ($C_{\mathrm{A}} > C_{\mathrm{H}}$) and larger jam density ($\rho_{\mathrm{J,A}} > \rho_{\mathrm{J,H}}$) are assumed for AVs with respect to HDVs.

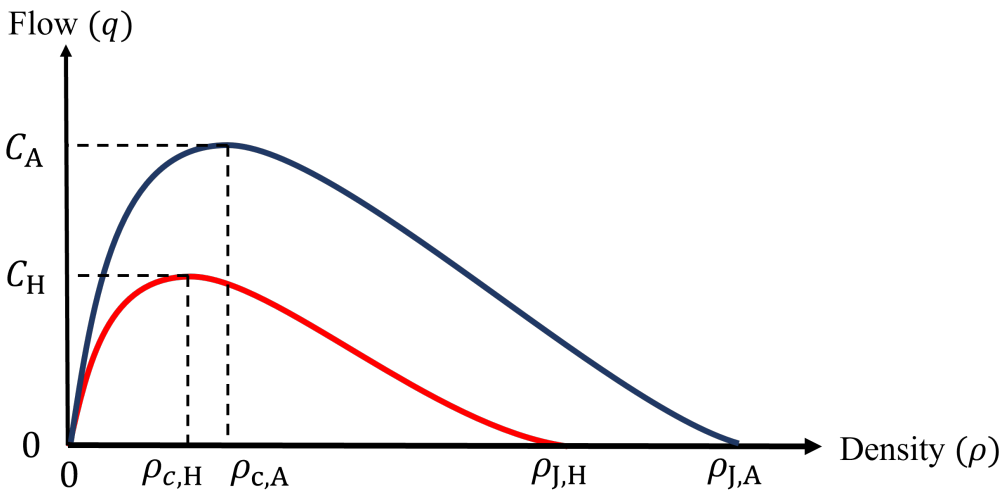

Figure 2.3: The flow-density relationship of AVs and HDVs.

For the heterogeneous METANET model, the dynamic equations for each vehicle class in the freeway cells are written in continuous form as follows:

$$q_{i,\mathrm{A}} = \rho_{i,\mathrm{A}} v_{i,\mathrm{A}}, \tag{2.4a}$$

$$q_{i,\mathrm{H}} = \rho_{i,\mathrm{H}} v_{i,\mathrm{H}}, \tag{2.4b}$$

$$\dot{\rho}_{i,\mathrm{A}} = \frac{1}{L_i \gamma_i}(q_{i-1,\mathrm{A}} - q_{i,\mathrm{A}} + d_{i,\rho_\mathrm{A}}), \tag{2.5a}$$

$$\dot{\rho}_{i,\mathrm{H}} = \frac{1}{L_i \gamma_i}(q_{i-1,\mathrm{H}} - q_{i,\mathrm{H}} + d_{i,\rho_\mathrm{H}}), \tag{2.5b}$$

$$\dot{v}_{i,\mathrm{A}} = \frac{1}{\tau_\mathrm{A}}\Big(U_{i,\mathrm{A}}(t) - v_{i,\mathrm{A}}(t)\Big) + \frac{1}{L_i}\Big[v_{i,\mathrm{A}}(t)\Big(v_{i-1,\mathrm{A}}(t) - v_{i,\mathrm{A}}(t)\Big) - \frac{\varepsilon_\mathrm{A}}{\tau_\mathrm{A}}\frac{\rho_{i+1,\mathrm{A}}(t) - \rho_{i,\mathrm{A}}(t)}{\rho_{i,\mathrm{A}}(t) + \rho_{c,\mathrm{A}}\kappa_\mathrm{A}}\Big], \tag{2.6a}$$

$$\dot{v}_{i,\mathrm{H}} = \frac{1}{\tau_\mathrm{H}}\Big(U_{i,\mathrm{H}}(t) - v_{i,\mathrm{H}}(t)\Big) + \frac{1}{L_i}\Big[v_{i,\mathrm{H}}(t)\Big(v_{i-1,\mathrm{H}}(t) - v_{i,\mathrm{H}}(t)\Big) - \frac{\varepsilon_\mathrm{H}}{\tau_\mathrm{H}}\frac{\rho_{i+1,\mathrm{H}}(t) - \rho_{i,\mathrm{H}}(t)}{\rho_{i,\mathrm{H}}(t) + \rho_{c,\mathrm{H}}\kappa_\mathrm{H}}\Big]. \tag{2.6b}$$

$d_i = [d_{i,\rho_\mathrm{A}}\ d_{i,\rho_\mathrm{H}}]$ represents the disturbance that includes unregulated traffic flow

for both AVs and HDVs. Additionally, the suggested velocities for AVs and HDVs in the traffic network are represented by $U_{i,\mathrm{A}}(t) = (1 - \beta_{i,\mathrm{A}}(t))V_{i,\mathrm{A}}(t)$ and $U_{i,\mathrm{H}}(t) = (1 - \beta_{i,\mathrm{H}}(t))V_{i,\mathrm{H}}(t)$, where

$$V_{i,\mathrm{A}}(t) = v_{\mathrm{FF,A}} \exp\left[\frac{-1}{a_{\mathrm{m,A}}}\left(\frac{\rho_{i,\mathrm{A}}(t)}{\rho_{\mathrm{c,A}}\alpha_{i,\mathrm{A}}(t)}\right)^{a_{\mathrm{m,A}}}\right], \tag{2.7a}$$

$$V_{i,\mathrm{H}}(t) = v_{\mathrm{FF,H}} \exp\left[\frac{-1}{a_{\mathrm{m,H}}}\left(\frac{\rho_{i,\mathrm{H}}(t)}{\rho_{\mathrm{c,H}}\alpha_{i,\mathrm{H}}(t)}\right)^{a_{\mathrm{m,H}}}\right]. \tag{2.7b}$$

$\alpha_{i,\mathrm{A}}$ and $\alpha_{i,\mathrm{H}}$ in (2.7a) and (2.7b) are the dynamic coupling terms specific to individual vehicle classes within each cell. These terms play a crucial role in interconnecting the dynamic behaviors of HDVs and AVs. A comprehensive discussion of the dynamic coupling terms can be found in Section 2.2.2 for further insights. Next, we introduce the control inputs $\beta_{i,\mathrm{A}}(t)$ and $\beta_{i,\mathrm{H}}(t)$, where $0 \leq \beta_{i,\mathrm{A}}(t), \beta_{i,\mathrm{H}}(t) \leq 1$, as a means to adjust the suggested (recommended) velocity of each cell for each vehicle class. In the absence of any local controller, denoted by $\beta_{i,\mathrm{A}}(t) = 0$ or $\beta_{i,\mathrm{H}}(t) = 0$, the system operates without intervention, and its macroscopic dynamics conform to the steady-state velocity-density behavior. Conversely, when $\beta_{i,\mathrm{A}}(t) = 1$ or $\beta_{i,\mathrm{H}}(t) = 1$, it indicates that the controller recommends the vehicles come to a complete stop as per the prescribed control action. In traffic dynamic model equations (2.4a)-(2.7b), there are multiple model parameters for each class of vehicle such as τ_{H}, τ_{A}, ε_{H}, ε_{A}, κ_{H}, κ_{A}, $a_{\mathrm{m,H}}$ and, $a_{\mathrm{m,A}}$. All these parameters were introduced and their functionality was explained in the previous section for a single-class METANET model. In some research papers, researchers add an extension to the traffic model which improves the fidelity of the model in complex traffic networks with multiple bottlenecks. For example, in [152], they added multiple constraints on the inter-flow between each cell and its downstream cell based on the traffic phase of each cell. Although this approach will lead to a higher fidelity traffic model, it will cause a high level of complexity when it comes to designing a controller for the traffic networks. In this research, instead

of adding the flow constraints to the model, we considered the METANET model parameters to be class-and-state-dependent parameters instead of constant values. By calibrating these parameters using the field data for each class of vehicle in various traffic phases and traffic states, we improved the fidelity of the traffic model to capture all the complex traffic phenomena in a large-scale traffic network.

2.2.1 EQUATIONS OF MOTION

Traffic dynamics in (2.4)-(2.6) can be mathematically expressed as

$$\dot{x}(t) = f(x(t)) + g(x(t))\big(u(t)\big) + D(t), \tag{2.8a}$$

$$y(t) = Cx(t), \tag{2.8b}$$

where $t \geq 0$; $x = [\rho^{\mathrm{T}}\ v^{\mathrm{T}}]^{\mathrm{T}} \in \mathbb{R}^{4n}$ is the state vector where $\rho = [\rho_{1,\mathrm{A}}\ \rho_{1,\mathrm{H}}\ \cdots\ \rho_{n,\mathrm{A}}\ \rho_{n,\mathrm{H}}]^{\mathrm{T}}$ and $v = [v_{1,\mathrm{A}}\ v_{1,\mathrm{H}}\ \cdots\ v_{n,\mathrm{A}}\ v_{n,\mathrm{H}}]^{\mathrm{T}}$. $y = [\rho_{s,\mathrm{A}}(t), \rho_{s,\mathrm{H}}(t), \cdots, \rho_{m,\mathrm{A}}(t), \rho_{m,\mathrm{H}}(t)]^{\mathrm{T}} \in \mathbb{R}^{2m-2s+2}$ is the output vector where $2 \leq s \leq m \leq n$, $u = [\beta_{s-1,\mathrm{A}}\ \beta_{s-1,\mathrm{H}}\ \cdots\ \beta_{m,\mathrm{A}}\ \beta_{m,\mathrm{H}}]^{\mathrm{T}} \in \mathbb{R}^{2m-2s+4}$ is the input control vector, $f(x) = [\dot{\rho}_{1,\mathrm{A}}\ \dot{\rho}_{1,\mathrm{H}}\ \cdots\ \dot{\rho}_{n,\mathrm{A}}\ \dot{\rho}_{n,\mathrm{H}}\ \hat{v}_{1,\mathrm{A}}\ \hat{v}_{1,\mathrm{H}}\ \cdots\ \hat{v}_{n,\mathrm{A}}\ \hat{v}_{n,\mathrm{H}}]^{\mathrm{T}} \in \mathbb{R}^{4n}$ where by assuming a same length for all cells $L_i = L$ we have $\hat{v}_{i,\mathrm{A}}(t) = \frac{1}{\tau_{\mathrm{A}}}\Big(V_{i,\mathrm{A}}(t) - v_{i,\mathrm{A}}(t)\Big) + \frac{1}{L}\Big[v_{i,\mathrm{A}}(t)\Big(v_{i-1,\mathrm{A}}(t) - v_{i,\mathrm{A}}(t)\Big) - \frac{\varepsilon_{\mathrm{A}}}{\tau_{\mathrm{A}}}\frac{\rho_{i+1,\mathrm{A}}(t)-\rho_{i,\mathrm{A}}(t)}{\rho_{i,\mathrm{A}}(t)+\kappa_{\mathrm{A}}\rho_{\mathrm{c,A}}}\Big]$ and $\hat{v}_{i,\mathrm{H}}(t) = \frac{1}{\tau_{\mathrm{H}}}\Big(V_{i,\mathrm{H}}(t) - v_{i,\mathrm{H}}(t)\Big) + \frac{1}{L}\Big[v_{i,\mathrm{H}}(t)\Big(v_{i-1,\mathrm{H}}(t) - v_{i,\mathrm{H}}(t)\Big) - \frac{\varepsilon_{\mathrm{H}}}{\tau_{\mathrm{H}}}\frac{\rho_{i+1,\mathrm{H}}(t)-\rho_{i,\mathrm{H}}(t)}{\rho_{i,\mathrm{H}}(t)+\kappa_{\mathrm{H}}\rho_{rmc,H}}\Big]$, $g(x) = \Big[[0]_{(2m-2s+4\times 2n)}\ [0]_{(2m-2s+4\times 2s-4)}\ [\hat{g}(x)]_{(2m-2s+4\times 2m-2s+4)}\ [0]_{(2m-2s+4\times 2n-2m)}\Big]^{\mathrm{T}}$ where $\hat{g}(x) = \mathrm{diag}\{-\frac{1}{\tau}V_{s-1}, ..., -\frac{1}{\tau}V_m\}$ and, $D = [d_{1,\rho_{\mathrm{A}}}\ d_{1,\rho_{\mathrm{H}}}\ \cdots\ d_{n,\rho_{\mathrm{A}}}\ d_{n,\rho_{\mathrm{H}}}\ d_{1,v_{\mathrm{A}}}\ d_{1,v_{\mathrm{H}}}\ \cdots\ d_{n,v_{\mathrm{A}}}\ d_{n,v_{\mathrm{H}}}]^{\mathrm{T}} \in \mathbb{R}^{4n}$ is the unknown-and-unmeasured disturbance. The dimensionality of the input vector $u(t)$ is greater than that of the output vector $y(t)$ due to the constraints imposed on the control inputs ($0 \leq \beta_{i,\mathrm{A}}(t), \beta_{i,\mathrm{H}}(t) \leq 1$). Efficient regulation of vehicle density in cell $\mathcal{C}_i$ requires two control inputs for recommended velocities in $\mathcal{C}_{i-1}$ (upstream cell) and $\mathcal{C}_i$ (target cell). These commands can be adjusted to modify inflow and outflow, enabling dynamic density control within $\mathcal{C}_i$ based on the controllability matrix from [42].

2.2.2 DYNAMIC COUPLING TERMS

To simulate the interplay between human-driven vehicles and autonomous vehicles on a macroscopic scale, numerous approaches have been suggested to model the dynamic coupling terms α_{A} and α_{H} [56; 153; 154]. One widely adopted approach employs the user-equilibrium assumption to model the interaction between HDVs and AVs. This assumption posits that all vehicles aim to minimize travel time, equivalent to maximizing speed [67]. In a user-optimum scenario, vehicle classes distribute themselves across road space, preventing a vehicle from increasing speed without slowing down slower vehicles. This definition considers the anisotropic property [68], where a vehicle's speed depends solely on vehicles with equal or lower speeds. Faster vehicles cannot decrease the speed of slower ones, and approaching vehicles from behind has no influence. Additionally, vehicles are assumed to occupy only essential space. Therefore, the dynamic coupling terms α_{H} and α_{A} are defined as a fraction of road used assigned to each vehicle class [68].

In this research, we also adopted the user-equilibrium assumption. In particular, to determine α_{A} and α_{H}, first, we assume that the macroscopic and stationary behavior of each class (human-driven vehicles and autonomous vehicles) can be described by homogeneous flow-density fundamental diagrams, as illustrated in Fig. 2.3. Without loss of generality, as discussed earlier, we presumed that the class of human-driven vehicles has a smaller jam density, a lower traffic network capacity, and a less negative congestion-wave speed. By leveraging the user-equilibrium assumption, three distinct interaction modes can manifest. These interaction modes are categorized as free-flow, semi-congested, and congested phases, as depicted in Fig. 2.4. Below, we discuss how the dynamic coupling terms are defined in each one of these phases based on Algorithm 1.

Free-Flow Phase: The first traffic phase is when both AVs and HDVs drive at their

Algorithm 1 Traffic Phase Determination Algorithm

if $(\frac{\rho_{i,\mathrm{H}}}{\rho_{\mathrm{c,H}}} + \frac{\rho_{i,\mathrm{A}}}{\rho_{\mathrm{c,A}}} \leq 1)$ **then**
  Traffic phase: *Free-flow*
else if $(\frac{\rho_{i,\mathrm{H}}}{\bar{\rho}_{\mathrm{c,H}}} + \frac{\rho_{i,\mathrm{A}}}{\bar{\rho}_{\mathrm{c,A}}} \leq 1)$ **then**
  Traffic phase: *Semi-congested*
else if $(\frac{\rho_{i,\mathrm{A}}}{\rho_{\mathrm{J,A}}} + \frac{\rho_{i,\mathrm{H}}}{\rho_{\mathrm{J,H}}} \leq 1)$ **then**
  Traffic phase: *Congested*
end if

free-flow velocity. Therefore we have

$$v_{\mathrm{FF,H}} = V_{i,\mathrm{H}} < V_{i,\mathrm{A}} = v_{\mathrm{FF,A}}. \tag{2.9}$$

In the free-flow phase of the traffic network, it is assumed that the density of both HDVs and AVs within their respective allocated road space is at most equal to their critical density. In particular,

$$\frac{\rho_{i,\mathrm{H}}}{\alpha_{i,\mathrm{H}}} \leq \rho_{\mathrm{c,H}}, \quad \frac{\rho_{i,\mathrm{A}}}{\alpha_{i,\mathrm{A}}} \leq \rho_{\mathrm{c,A}}. \tag{2.10}$$

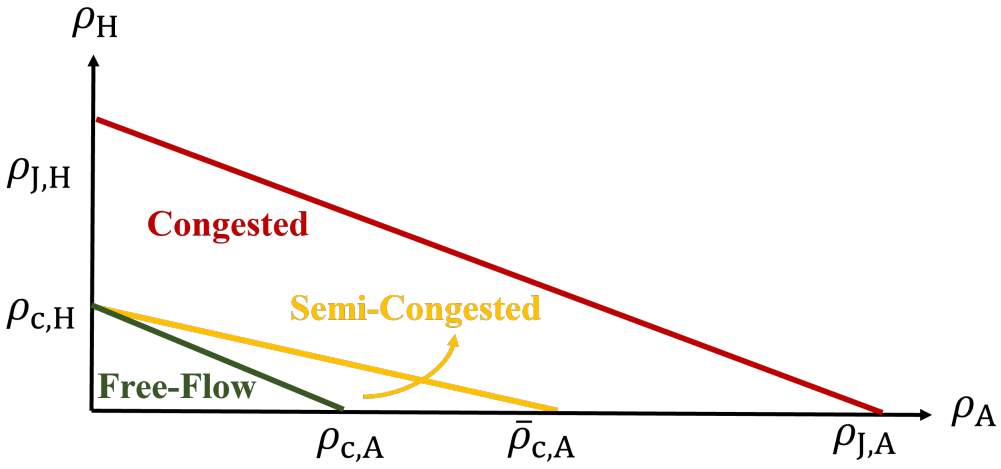

Figure 2.4: Traffic phases for heterogeneous traffic network.

Algorithm 1 demonstrates the criterion that sets apart the free-flow phase from the semi-congested phase. Since the sum of the fractions equals 1 ($\alpha_{i,\mathrm{A}} + \alpha_{i,\mathrm{H}} = 1$), we can determine the optimal allocation of road space to each vehicle category in the free-flow phase as follow:

$$\begin{aligned} \alpha_{i,\mathrm{H}} &= \frac{\rho_{i,\mathrm{H}}\rho_{c,\mathrm{A}}}{\rho_{i,\mathrm{H}}\rho_{c,\mathrm{A}} + \rho_{i,\mathrm{A}}\rho_{c,\mathrm{H}}}, \\ \alpha_{i,\mathrm{A}} &= \frac{\rho_{i,\mathrm{A}}\rho_{c,\mathrm{H}}}{\rho_{i,\mathrm{A}}\rho_{c,\mathrm{H}} + \rho_{i,\mathrm{H}}\rho_{c,\mathrm{A}}}. \end{aligned} \tag{2.11}$$

In real-world scenarios, during free-flow mode, the number of vehicles on the road is low enough that it allows them to navigate through various lanes, ensuring a path to maintain their free-flow velocity.

Semi-Congested Phase: In the heterogeneous traffic flow where the free-flow velocity of AVs is higher than HDVs, it is possible for HDVs to remain in the free-flow phase, while AVs have transitioned to the congested mode [57; 155]. In particular

$$v_{\mathrm{FF,H}} = V_{i,\mathrm{H}} \leq V_{i,\mathrm{A}} < v_{\mathrm{FF,A}}. \tag{2.12}$$

In this traffic phase, the effective density of HDVs is less than or equal to their critical density, and the effective density of AVs is larger than their critical density. The condition shown in Algorithm 1 determines the boundary constraint for the semi-congested phase. $\bar{\rho}_{\mathrm{c,A}}$ and $\bar{\rho}_{\mathrm{c,H}}$ are the "perceived" critical density of AVs and HDVs [156], defined as:

$$\bar{\rho}_{\mathrm{c,A}} = \rho_{\mathrm{c,A}} \left[-a_{\mathrm{m,A}} ln \left(\frac{v_{\mathrm{FF,H}}}{v_{\mathrm{FF,A}}} e^{(\frac{-1}{a_{\mathrm{m,H}}})} \right) \right]^{\frac{1}{a_{\mathrm{m,A}}}}, \tag{2.13a}$$

$$\bar{\rho}_{\mathrm{c,H}} = \rho_{\mathrm{c,H}}. \tag{2.13b}$$

The proof of the boundary condition and perceived densities in (2.13) are included in [68]. The optimal allocation of space fraction for AVs and HDVs in the semi-congested phase is calculated as follows:

$$\alpha_{i,\mathrm{H}} = \frac{\rho_{i,\mathrm{H}}}{\bar{\rho}_{\mathrm{c,H}}}, \quad \alpha_{i,\mathrm{A}} = 1 - \alpha_{i,\mathrm{H}} \tag{2.14}$$

Congested Phase: Here, both AVs and HDVs are in the congested phase, and the velocities of each class of vehicles are the same.

$$V_{i,\mathrm{H}} = V_{i,\mathrm{A}} < v_{\mathrm{FF,H}} < v_{\mathrm{FF,A}}. \tag{2.15}$$

Using (2.15), the space fraction of HDVs and AVs in the congested phase is calculated as follows:

$$\begin{aligned} \alpha_{i,\mathrm{A}} &= \frac{A}{B}, \quad \alpha_{i,\mathrm{H}} + \alpha_{i,\mathrm{A}} = 1, \\ A &= \Big((\rho_{\mathrm{c,H}} - \rho_{\mathrm{J,H}}) \rho_{\mathrm{c,A}} v_{\mathrm{FF,A}} - (\rho_{\mathrm{c,A}} - \rho_{\mathrm{J,A}}) \rho_{\mathrm{c,H}} v_{\mathrm{FF,H}} \Big) \rho_{\mathrm{A}} \rho_{\mathrm{H}} \\ &\quad + (\rho_{\mathrm{c,A}} - \rho_{\mathrm{J,A}}) \rho_{\mathrm{c,H}} \rho_{\mathrm{J,H}} v_{\mathrm{FF,H}}\ \rho_{\mathrm{A}}, \\ B &= (\rho_{\mathrm{c,A}} - \rho_{\mathrm{J,A}}) \rho_{\mathrm{c,H}} \rho_{\mathrm{J,H}} v_{\mathrm{FF,H}} \rho_{\mathrm{A}} + (\rho_{\mathrm{c,H}} - \rho_{\mathrm{J,H}}) \rho_{\mathrm{c,A}} \rho_{\mathrm{J,A}} v_{\mathrm{FF,A}} \rho_{\mathrm{H}}. \end{aligned} \tag{2.16}$$

The total average flow relationship in an MFD can be calculated through the following equation:

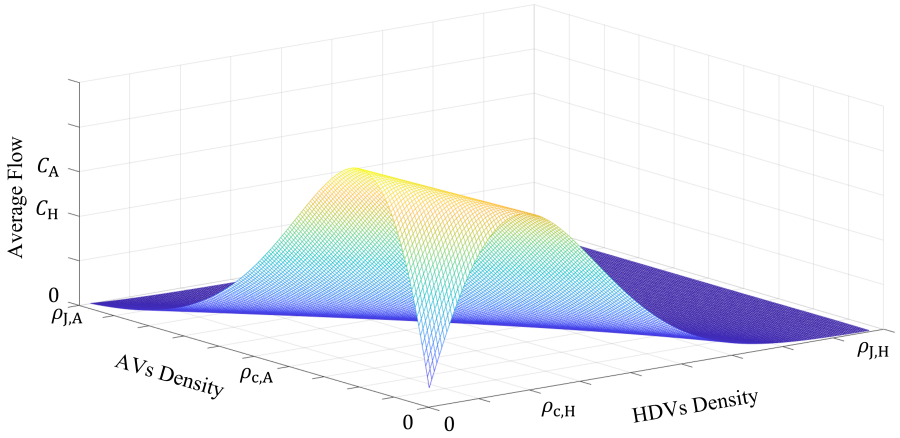

Figure 2.5: Total flow-density relationship of heterogeneous METANET model for AVs and HDVs.

$$Q_i = \rho_{i,\mathrm{H}} V\left(\frac{\rho_{i,\mathrm{H}}}{\alpha_{i,\mathrm{H}}}\right) + \rho_{i,\mathrm{A}} V\left(\frac{\rho_{i,\mathrm{A}}}{\alpha_{i,\mathrm{A}}}\right). \tag{2.17}$$

In Fig. 2.5 the average flow rate of the traffic network for a full spectrum of heterogeneity is shown.

CHAPTER 3: HIERARCHICAL CONTROLLER DESIGN

This section focuses on the design of a distributed hierarchical macroscopic traffic management controller to improve the performance of a large-scale traffic network in terms of mobility. It is important to note that this chapter only covers the control design details for heterogeneous traffic networks since it includes all the necessary calculations for either homogeneous or heterogeneous traffic networks. The designed control approach aims to (i) improve the system performance in terms of congestion reduction, and (ii) prevent congestion back-propagation. The initial controller design has a two-level structure with a Distributed Extremum Seeking (D-ES) algorithm at the upper level and a Distributed Filtered Feedback Linearization (D-FFL) at the lower level, acting as a VSL control in the traffic network, as shown in Fig. 3.1. The description of each level control algorithm is given below. However, crucial modifications have been made to the initial controller design to address the important research gaps that we will discuss in detail later. Further in this research, to improve the hierarchical controller performance, we introduce significant modifications to the initial controller design. Later in this thesis, a detailed discussion will highlight the specific enhancements made.

3.1 LOWER-LEVEL MACROSCOPIC CONTROLLER

3.1.1 DISTRIBUTED FILTERED FEEDBACK LINEARIZATION CONTROL

Within the introduced multi-level traffic control framework, we recommend implementing a Distributed Filtered Feedback Linearization (D-FFL) controller in the lower level to adjust the communicated recommended velocities for vehicles in order to achieve the targeted densities of AVs and HDVs in the target cells.

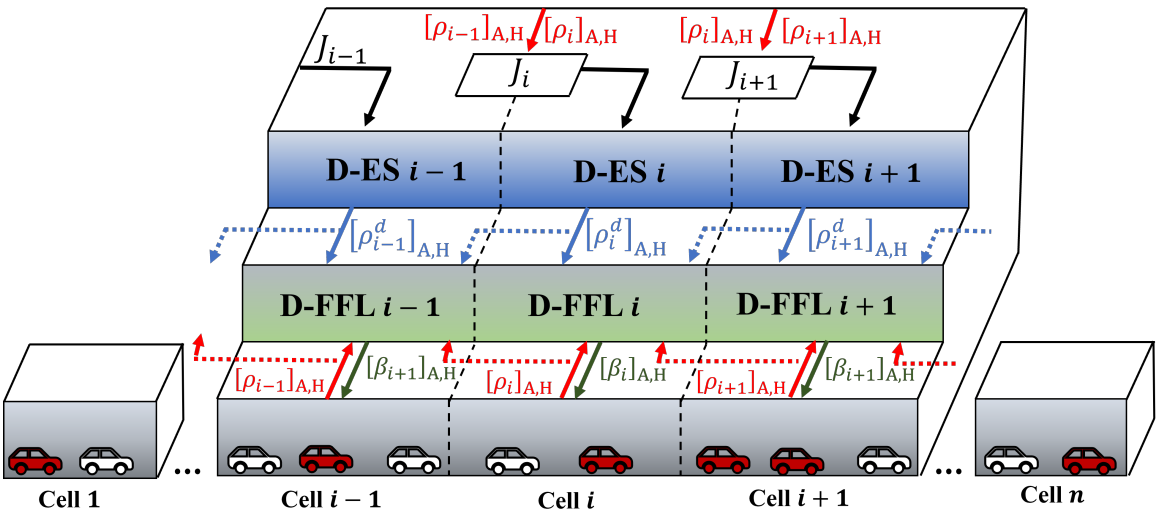

Figure 3.1: Schematic of a large-scale heterogeneous traffic network with n cells consisting of the hierarchical controller (Upper-level: D-ES, Lower-level: D-FFL). The cost function (J) is fed into the upper-level controller (D-ES), where the desired density (ρ^{d}) of the cell for each vehicle class is calculated and fed into the lower-level controller (D-FFL) as the reference model. D-FFL controller then generates the control inputs (β) to set the suggested velocity for each vehicle class in each cell.

The implementation of the D-FFL control is dependent on the relative degree and dynamic inversion matrix, as discussed in [125]. Specifically, the relative degree between the inputs u_{i-1} and u_i to the output y_i is established as 2 for a specific cell $\mathcal{C}_i$. The design of the D-FFL control approach is based on two underlying assumptions:

Assumption 1 *The disturbance function $D(t)$ is a continuous function and its derivative $\dot{D}(t)$ is accessible.*

Assumption 2 *The inputs of the reference model, $\rho^{\mathrm{d}}_{\mathrm{A}}(t)$ (desired density for AVs) and $\rho^{\mathrm{d}}_{\mathrm{H}}(t)$ (desired density for HDVs), and their derivatives $\dot{\rho}^{\mathrm{d}}_{\mathrm{A}}(t)$ and $\dot{\rho}^{\mathrm{d}}_{\mathrm{H}}(t)$ are assumed to be bounded.*

Now let us examine the output of the local reference model, denoted as y_{m}, which meets the requirements of the local reference model equation.

$$\varphi(\mathbf{p})y_{\mathrm{m}}(t) = \zeta(\mathbf{p})r(t), \tag{3.1}$$

where $y_{\mathrm{m}} = [y_{\mathrm{m,A}}\ y_{\mathrm{m,H}}]$, $r = [\rho^{\mathrm{d}}_{s,\mathrm{A}}\ \rho^{\mathrm{d}}_{s,\mathrm{H}}\ \cdots\ \rho^{\mathrm{d}}_{m,\mathrm{A}}\ \rho^{\mathrm{d}}_{m,\mathrm{H}}]^{\mathrm{T}} \in \mathbb{R}^{2m-2s+2}$ is the AVs and HDVs desired densities vector for the target cells, $\mathbf{p} = \frac{d}{dt}$ is the differential operator, and φ and ζ are $m \times m$ diagonal matrices.

By considering $e_i = [y_{\mathrm{m,A,i}} - y_{\mathrm{A,i}}\ y_{\mathrm{m,H,i}} - y_{\mathrm{H,i}}]^{\mathrm{T}}$ as the error vector, the square root of the average power of the density error can be calculated as follows

$$\mathcal{P}_e = \left[\frac{1}{t_1 - t_0}\int_{t_0}^{t_1} e^{\mathrm{T}}(\tau)e(\tau)d\tau\right]^{\frac{1}{2}}, \tag{3.2}$$

where the difference between t_0 and t_1 shows the convergence time of the output density reaching the desired density. The main goal is to develop a control input u that can achieve asymptotic stabilization of the closed-loop system (2.8) and minimize the error power $\mathcal{P}_e$ to an arbitrarily small value, even when the disturbance is unknown for each cell.

Assuming we have a perfect knowledge of the plant dynamics and measurement of the disturbance in (2.8), we derive the control input based on the Feedback Linearization (FL) approach. First, consider

$$\begin{bmatrix}\ddot{y}_{\mathrm{A}}\\ \ddot{y}_{\mathrm{H}}\end{bmatrix} = \psi(x, \Phi_D) + \begin{bmatrix}M_{\mathrm{u,A}} & 0\\ 0 & M_{\mathrm{u,H}}\end{bmatrix}\begin{bmatrix}u_{\mathrm{A}}\\ u_{\mathrm{H}}\end{bmatrix}, \tag{3.3}$$

where $u = [u_{\mathrm{A}}\ u_{\mathrm{H}}]^{\mathrm{T}}$ and $y = [y_{\mathrm{A}}\ y_{\mathrm{H}}]^{\mathrm{T}}$ are derived from (2.8a) and (2.8b) with minor

changes to better show the calculations towards the FL control input. Also, we have

$$\psi(x,\Phi_D) = C\frac{\partial f}{\partial x}(f(x)+D) + C\dot{D}, \Phi_D = [D\ \dot{D}]^{\mathrm{T}}$$

$$M_{\mathrm{u,A}} = \begin{bmatrix} (\rho V)_{s-1} & -(\rho V)_s & 0 & \cdots & 0 \\ 0 & (\rho V)_s & -(\rho V)_{s+1} & \cdots & 0 \\ 0 & 0 & 0 & \cdots & 0 \\ \vdots & \ddots & \ddots & \ddots & \vdots \\ 0 & \cdots & 0 & (\rho V)_{m-1} & -(\rho V)_m \end{bmatrix}_{\mathrm{A}}, \tag{3.4a}$$

$$M_{\mathrm{u,H}} = \begin{bmatrix} (\rho V)_{s-1} & -(\rho V)_s & 0 & \cdots & 0 \\ 0 & (\rho V)_s & -(\rho V)_{s+1} & \cdots & 0 \\ 0 & 0 & 0 & \cdots & 0 \\ \vdots & \ddots & \ddots & \ddots & \vdots \\ 0 & \cdots & 0 & (\rho V)_{m-1} & -(\rho V)_m \end{bmatrix}_{\mathrm{H}}. \tag{3.4b}$$

The standard FL control input (desired control input u^{d}) is designed as [122]:

$$u^{\mathrm{d}}_{\mathrm{A}}(x_{\mathrm{A}},\Phi_D,\Phi_{r_{\mathrm{A}}}) = -M^{-\dagger}_{\mathrm{u,A}}(M_{\mathrm{u,A}}M^{-\dagger}_{\mathrm{u,A}})^{-1}\big(\nu(x_{\mathrm{A}},\Phi_D,\Phi_{r_{\mathrm{A}}}) + \psi(x_{\mathrm{A}},\Phi_D)\big), \tag{3.5a}$$

$$u^{\mathrm{d}}_{\mathrm{H}}(x_{\mathrm{H}},\Phi_D,\Phi_{r_{\mathrm{H}}}) = -M^{-\dagger}_{\mathrm{u,H}}(M_{\mathrm{u,H}}M^{-\dagger}_{\mathrm{u,H}})^{-1}\big(\nu(x_{\mathrm{H}},\Phi_D,\Phi_{r_{\mathrm{H}}}) + \psi(x_{\mathrm{H}},\Phi_D)\big), \tag{3.5b}$$

where $\Phi_{r_{\mathrm{A}}} = [r_{\mathrm{A}}\ \dot{r}_{\mathrm{A}}\ \ddot{r}_{\mathrm{A}}]^{\mathrm{T}}$, $\Phi_{r_{\mathrm{H}}} = [r_{\mathrm{H}}\ \dot{r}_{\mathrm{H}}\ \ddot{r}_{\mathrm{H}}]^{\mathrm{T}}$, $x_{\mathrm{A}} = [\rho_{\mathrm{A}}\ v_{\mathrm{A}}]$, $x_{\mathrm{H}} = [\rho_{\mathrm{H}}\ v_{\mathrm{H}}]$, $M^{-\dagger}_{\mathrm{u,A}}$ and $M^{-\dagger}_{\mathrm{u,H}}$ are the pseudo inverse of $M_{\mathrm{u,A}}$ and $M_{\mathrm{u,H}}$ respectively, and $\nu(x_{\mathrm{A}},\Phi_D,\Phi_{r_{\mathrm{A}}}) = \varphi(\mathbf{p})y - \zeta(\mathbf{p})r - [\ddot{\rho}_{s,\mathrm{A}},\ \ddot{\rho}_{s,\mathrm{H}},\cdots,\ \ddot{\rho}_{m,\mathrm{A}},\ \ddot{\rho}_{m,\mathrm{H}}]^{\mathrm{T}}$.

It is shown in [123] that if $u_{\mathrm{A}} = u^{\mathrm{d}}_{\mathrm{A}}$ and $u_{\mathrm{H}} = u^{\mathrm{d}}_{\mathrm{H}}$, then $\lim_{t\to\infty} e(t) = 0$ and $\mathcal{P}_e = 0$. Thus, the ideal control inputs $u^{\mathrm{d}}_{\mathrm{A}}$ and $u^{\mathrm{d}}_{\mathrm{H}}$ accomplish reference density tracking as the lower-level control objective. However, these control inputs, $u^{\mathrm{d}}_{\mathrm{H}}$ and $u^{\mathrm{d}}_{\mathrm{A}}$ are not practically feasible since they rely on the complete state measurements $x_{\mathrm{A}}(t)$, $x_{\mathrm{H}}(t)$, uncertain dynamic function $f(x_{\mathrm{A}}(t), x_{\mathrm{H}}(t))$, and the and unmeasured and unknown disturbance $D(x(t),t)$.

A filter is designed to overcome the challenges mentioned by passing the FL control

inputs $u_{\mathrm{A}}^{\mathrm{d}}$ and $u_{\mathrm{H}}^{\mathrm{d}}$ through it to generate the control input u. Specifically,

$$[\mathbf{p}\bar{\sigma}_z(\mathbf{p})I + \bar{\sigma}_z(0)M'_{\mathrm{u,A}}M_{\mathrm{u,A}}]u_{\mathrm{A}} = \bar{\sigma}_z(0)M'_{\mathrm{u,A}}M_{\mathrm{u,A}}u_{\mathrm{A}}^{\mathrm{d}}, \tag{3.6a}$$

$$[\mathbf{p}\bar{\sigma}_z(\mathbf{p})I + \bar{\sigma}_z(0)M'_{\mathrm{u,H}}M_{\mathrm{u,H}}]u_{\mathrm{H}} = \bar{\sigma}_z(0)M'_{\mathrm{u,H}}M_{\mathrm{u,H}}u_{\mathrm{H}}^{\mathrm{d}}. \tag{3.6b}$$

Let $M'_{\mathrm{u,A}}$ and $M'_{\mathrm{u,H}}$ denote the transpose of $M_{\mathrm{u,A}}$ and $M_{\mathrm{u,A}}$, respectively. Additionally, let $\bar{\sigma}_z(s)$ be a monic polynomial with a degree of at least 2 ($r \geq 2$) and real coefficients that are dependent on a real parameter z. The polynomial σ_z can be represented as $\bar{\sigma}_z = s^r + \bar{\sigma}_{r-1,z}s^{r-1} + \cdots + \bar{\sigma}_{1,z}s + \bar{\sigma}_{0,z}$, where $\bar{\sigma}_{0,z}, \cdots, \bar{\sigma}_{r-1,z} \in \mathbb{R}$. $\bar{\sigma}_z$ is a critical design parameter that must meet specific requirements as outlined in [157]. Here, $u_{i,\mathrm{A}}^{\mathrm{d}}$ and $u_{i,\mathrm{H}}^{\mathrm{d}}$ are given by (3.5a) and (3.5b) which cannot be implemented due to their dependency on the full model information. Now by substituting (3.3) into (3.5a) and (3.5b), and substituting the result into (3.6a) and (3.6b), we have the D-FFL control inputs:

$$\mathbf{p}\bar{\sigma}_z(\mathbf{p})u_{\mathrm{A}} = \bar{\sigma}_z(0)M'_{\mathrm{u,A}}[\zeta(\mathbf{p})r_{\mathrm{A}} - \varphi(\mathbf{p})y_{\mathrm{A}}], \tag{3.7a}$$

$$\mathbf{p}\bar{\sigma}_z(\mathbf{p})u_{\mathrm{H}} = \bar{\sigma}_z(0)M'_{\mathrm{u,H}}[\zeta(\mathbf{p})r_{\mathrm{H}} - \varphi(\mathbf{p})y_{\mathrm{H}}]. \tag{3.7b}$$

The controller inputs (3.5a), (3.5b) and (3.7a), (3.7b) are mathematically equivalent if $z \to \infty$, $dt \to 0$ and there is no constraint on the control input u. The control inputs (3.7a) and (3.7b) are independent of the variables $\psi(x, \Phi_D)$ or the measurements of D and $\dot{D}$. Instead, the D-FFL input control design relies on various factors, including the knowledge of the dynamic inversion matrix M_{u}, the relative degree, and parameters of the reference model $\zeta_1, \zeta_0, \varphi_1, \varphi_0$, and $\bar{\sigma}_z$. By considering these factors, the D-FFL control input can be optimized and implemented effectively in the control system.

Proposition 1 *Assuming the minimum phase system is given by (2.8) and (3.7) and that assumptions 1-2 hold, it can be stated that for a sufficiently large value of the*

real parameter z in the filter polynomial $\bar{\sigma}_z(s)$, the closed-loop system (2.8) and (3.7) is asymptotically stable. The smallest value of z that stabilizes the system depends on the specific dynamics and parameters of the system.

Proof: The proof can be found in [123; 125].

Remark 1 *The selection of an adequately large value for the parameter z can lead to a significant reduction in the average power of the performance error, denoted as $\mathcal{P}_e$, to a desired level. However, in the quantified FFL with discrete time steps, the maximum z value is proportional to the inverse of the time step and larger z values will cause instability in the system.*

In real-world scenarios, it is common to use a nominal plant model to identify a suitable value for z that can guarantee stability while achieving the desired level of performance. It is important to note that $M_{\mathrm{u,A}}$ and $M_{\mathrm{u,H}}$ are non-square matrices, and their arrays are dependent on the measured densities $\rho_{j,\mathrm{A}}$, $\rho_{j,\mathrm{H}}$, and steady-state velocity-density relationship $V_{j,\mathrm{A}}$, $V_{j,\mathrm{H}}$ for $j \in \{s, \cdots, m\}$ as shown in (3.4a) through (3.4b). Here, $V_{j,\mathrm{A}}$, $V_{j,\mathrm{H}}$ are a function of $v_{\mathrm{FF,A}}$ and $v_{\mathrm{FF,H}}$ respectively which is predefined for each cell, parameters $a_{\mathrm{m,A}}$, $a_{\mathrm{m,H}}$, $\rho_{\mathrm{c,A}}$ and $\rho_{\mathrm{c,H}}$ that may not be necessarily known. However, numerical testing in our research suggests that the estimated values for these parameters, if their magnitudes are greater than the actual values and have the correct sign, can still yield stable and well-performing control. For practical purposes, $v_{\mathrm{FF,A}}$ and $v_{\mathrm{FF,H}}$ can be taken as upper bounds for $V_{j,\mathrm{A}}$ and $V_{j,\mathrm{H}}$ respectively, and used in place of these terms in $M_{\mathrm{u,A}}$ and $M_{\mathrm{u,H}}$. This observation is consistent with the robustness properties demonstrated in [157]. We define $\bar{M}_{\mathrm{u,A}}$ and $\bar{M}_{\mathrm{u,H}}$ as upper bounds of $M_{\mathrm{u,A}}$ and $M_{\mathrm{u,H}}$ since $V_{i,\mathrm{A}} \leq v_{\mathrm{FF,A}}$ and $V_{i,\mathrm{H}} \leq v_{\mathrm{FF,H}}$, in

particular:

$$\bar{M}_{\mathrm{u,A}} = \begin{bmatrix} \rho_{s-1}v_{\mathrm{FF}} & -\rho_s v_{\mathrm{FF}} & 0 & \cdots & 0 \\ 0 & \rho_s v_{\mathrm{FF}} & -\rho_{s+1}v_{\mathrm{FF}} & \cdots & 0 \\ 0 & 0 & 0 & \cdots & 0 \\ \vdots & \ddots & \ddots & \ddots & \vdots \\ 0 & \cdots & 0 & \rho_{m-1}v_{\mathrm{FF}} & -\rho_m v_{\mathrm{FF}} \end{bmatrix}_{\mathrm{A}}, \tag{3.8a}$$

$$\bar{M}_{\mathrm{u,H}} = \begin{bmatrix} \rho_{s-1}v_{\mathrm{FF}} & -\rho_s v_{\mathrm{FF}} & 0 & \cdots & 0 \\ 0 & \rho_s v_{\mathrm{FF}} & -\rho_{s+1}v_{\mathrm{FF}} & \cdots & 0 \\ 0 & 0 & 0 & \cdots & 0 \\ \vdots & \ddots & \ddots & \ddots & \vdots \\ 0 & \cdots & 0 & \rho_{m-1}v_{\mathrm{FF}} & -\rho_m v_{\mathrm{FF}} \end{bmatrix}_{\mathrm{H}}. \tag{3.8b}$$

Thus, it is not necessary for the D-FFL controller to receive the precise values of the class- and state-dependent parameters in the traffic model when $\bar{M}_{\mathrm{u}}$ is substituted for M_{u} in (3.7).

3.2 UPPER-LEVEL CONTROLLER

3.2.1 DISTRIBUTED EXTREMUM SEEKING CONTROL APPROACH

Distributed Extremum Seeking (D-ES) controller at the upper level of the hierarchical controller is designed to compute the optimal densities of vehicles in each class, denoted as $\rho^{\mathrm{d}}_{i,\mathrm{A}}$ and $\rho^{\mathrm{d}}_{i,\mathrm{H}}$, in the target cells. As discussed earlier, the primary objective of the upper-level controller is to achieve two main goals simultaneously: the maximization of the average flow of the target cell to mitigate traffic congestion and the minimization of the flow difference between the target cell and the upstream flow to prevent the propagation of congestion in the backward direction. Specifically, for each congested cell, an optimization problem is defined as follows

$$\max_{\rho_{i,\mathrm{A}},\rho_{i,\mathrm{H}}} J_i(t) = \bar{w}_{i,1}(t)Q_i^2(t) - \bar{w}_{i,2}(t)\Big[Q_i(t) - Q_{i-1}(t)\Big]^2. \tag{3.9}$$

The average flow rate $Q_i(t)$, which is subject to the dynamics equations, is defined in (2.17). In addition, $\bar{w}_{i,1}(t)$ and $\bar{w}_{i,2}(t)$ are each term's weight in the local objective function. We added the second term $-\bar{w}_{i,2}(t)\Big(Q_i(t) - Q_{i-1}(t)\Big)^2$ in the objective

function to prevent the creation of a fully autonomous traffic cell in a mixed traffic network. The rationale behind this is that it is assumed that a fully autonomous traffic network has a higher capacity than a mixed traffic network, as discussed in Chapter 2. The first term in (3.9) achieves its maximum value in a fully autonomous cell, however, if the HDVs in the upstream cell are stopped, congestion will start to back-propagate, resulting in a reduction of the overall average flow and performance of the whole traffic network.

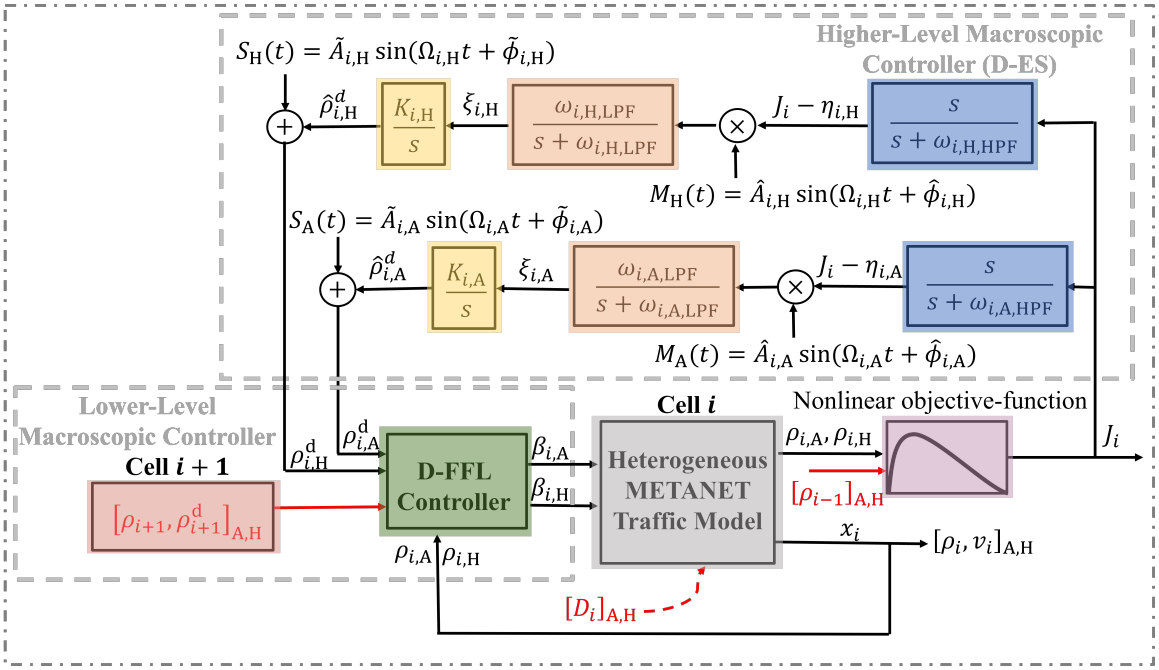

Figure 3.2: Hierarchical control architecture for cell i. D-ES at the upper level feeding the optimal densities of each class to the D-FFL as the reference model and D-FFL sets the suggested velocities of each vehicle class in the heterogeneous METANET model.

D-ES controller is designed and developed to tackle the problem stated in (3.9). The D-ES specifics are shown in Fig. 3.2. The optimization of the parameters, $\rho^{\mathrm{d}}_{i,\mathrm{A}}$ and $\rho^{\mathrm{d}}_{i,\mathrm{H}}$, is achieved through the perturbation of these values using low-amplitude sinusoidal signals, $S_{\mathrm{A}}(t) = \tilde{A}_{i,\mathrm{A}} \sin(\Omega_{i,\mathrm{A}} t + \tilde{\phi}_{i,\mathrm{A}})$ and $S_{\mathrm{H}}(t) = \tilde{A}_{i,\mathrm{H}} \sin(\Omega_{i,\mathrm{H}} t + \tilde{\phi}_{i,\mathrm{H}})$. In order to guarantee that the ES loop perceives the dynamics of the lower level as a fixed non-linear system, the frequencies of the perturbation signals denoted as $\Omega_{i,\mathrm{A}}$ and

$\Omega_{i,\mathrm{H}}$, should be selected to be sufficiently small [136]. Consider $\Omega_{i,\mathrm{A}} = \Omega_{i,\mathrm{H}} = \mathcal{O}(\omega)$, $\omega_{i,\mathrm{A,HPF}} = \omega_{i,\mathrm{H,HPF}} = \mathcal{O}(\omega\Delta)$ and, $\omega_{i,\mathrm{A,LPF}} = \omega_{i,\mathrm{H,LPF}} = \mathcal{O}(\omega\Delta)$ where $\mathcal{O}$ is the statistic order, ω and Δ are small positive constants.

Remark 2 *The D-ES controller's convergence time for the desired density estimation is notably slower (*10 *time slower) than the reaction time of the internal control loop. By choosing the best ζ and φ which gives us the fastest convergence in (3.7a) and (3.7b), the $\Omega_{i,\mathrm{A}}$ and $\Omega_{i,\mathrm{H}}$ will be maximized. Therefore, it is reasonable to consider that the reference for the density remains relatively constant in comparison to the dynamics of the inner loop for both AVs and HDVs.*

In D-ES, the rate of convergence can be improved by increasing the perturbation frequency. However, this improvement comes at the cost of a significant increase in the steady-state error [136]. In this case, we have opted for a small perturbation frequency (almost 10 times slower than the inner-loop dynamics). In order to guarantee stability and convergence of the D-ES controller, a specific set of assumptions must be satisfied [132].

Assumption 3 *A smooth function $\ell : \mathbb{R}^n \to \mathbb{R}^{m-s+1}$ exists such that $\mathcal{F}_{\mathrm{LL}}\big(X_{\mathrm{LL}}, \mathcal{G}(X_{\mathrm{LL}}, \rho_{\mathrm{A}}^{\mathrm{d}}, \rho_{\mathrm{H}}^{\mathrm{d}})\big) = 0$ if and only if $X_{\mathrm{LL}} = \ell(\rho_{\mathrm{A}}^{\mathrm{d}}, \rho_{\mathrm{H}}^{\mathrm{d}})$.*

Assumption 4 *For each $\rho_{\mathrm{A}}^{\mathrm{d}} \in \mathbb{R}^{m-s+1}$ and $\rho_{\mathrm{H}}^{\mathrm{d}} \in \mathbb{R}^{m-s+1}$, the equilibrium $x_{\mathrm{A}} = \ell(\rho_{\mathrm{A}}^{\mathrm{d}})$ and $x_{\mathrm{H}} = \ell(\rho_{\mathrm{H}}^{\mathrm{d}})$ of the system $\dot{X}_{\mathrm{LL}} = \mathcal{F}_{\mathrm{LL}}\big(X_{\mathrm{LL}}, \mathcal{G}(X_{\mathrm{LL}}, \rho^{\mathrm{d}})\big)$ is locally exponentially stable uniformly in $\rho_{\mathrm{A}}^{\mathrm{d}}$ and $\rho_{\mathrm{H}}^{\mathrm{d}}$.*

Assumption 5 *There exists $\rho_{\mathrm{A}}^{*} \in \mathbb{R}^{m-s+1}$ and $\rho_{\mathrm{H}}^{*} \in \mathbb{R}^{m-s+1}$ such that $\frac{\partial}{\partial \rho_{\mathrm{A}}^{\mathrm{d}}} J(\rho_{\mathrm{A}}^{*}) = 0$, $\frac{\partial}{\partial \rho_{\mathrm{H}}^{\mathrm{d}}} J(\rho_{\mathrm{H}}^{*}) = 0$ and $\frac{\partial^2}{\partial^2 \rho_{\mathrm{A}}^{\mathrm{d}}} J(\rho_{\mathrm{A}}^{*}) < 0$, $\frac{\partial^2}{\partial^2 \rho_{\mathrm{H}}^{\mathrm{d}}} J(\rho_{\mathrm{H}}^{*}) < 0$.*

In this research, we have confirmed the satisfaction of Assumptions 3 and 4, as the D-FFL controller has been shown to guarantee the asymptotic stability of the

inner-loop dynamics, as per Proposition 1. Furthermore, Assumption 5 has also been satisfied, given that the objective function in (3.9) takes a quadratic form according to the shape of the FD, which is depicted in Fig. 2.5.

The following proposition provides a concise summary of the convergence and stability characteristics associated with the D-ES:

Proposition 2 *Consider the closed-loop feedback system in Fig. 3.2 under Assumptions 3-5. Recall that Remark 2 is in place. There exists* $\bar{\omega} > 0$*, and for any* $\omega \in (0, \bar{\omega})$ *there exists* $\bar{\Delta}, \bar{A} > 0$ *such that for the given* ω *and any* $|\tilde{A}| \in (0, \bar{A})$ *and* $\Delta \in (0, \bar{\Delta})$ *there exists a neighborhood of the points* $(x_{\mathrm{A}}, \rho_{\mathrm{A}}^{\mathrm{d}}, \xi_{\mathrm{A}}, \eta_{\mathrm{A}}) = \big(\ell(\rho_{\mathrm{A}}^*), \rho_{\mathrm{A}}^*, 0, J(\rho_{\mathrm{A}}^*)\big)$ *and* $(x_{\mathrm{H}}, \rho_{\mathrm{H}}^{\mathrm{d}}, \xi_{\mathrm{H}}, \eta_{\mathrm{H}}) = \big(\ell(\rho_{\mathrm{H}}^*), \rho_{\mathrm{H}}^*, 0, J(\rho_{\mathrm{H}}^*)\big)$ *such that any solution of the feedback system (2.8) from the neighborhood exponentially converges to an* $\mathcal{O}(\omega+\Delta+|\tilde{A}|)$*-neighborhood of that point. Furthermore,* $y(t)$ *converges to an* $\mathcal{O}(\omega+\Delta+|\tilde{A}|)$*-neighborhood of* $J(\rho_{\mathrm{A}}^*)$ *and* $J(\rho_{\mathrm{H}}^*)$.

Consider the feedback system depicted in Fig. 3.6, subject to Assumptions 3-5. Note that Remark 2 is applicable. We can assert the existence of a positive number $\bar{\omega}$, such that for any ω within the range $(0, \bar{\omega})$, there exist positive constants $\bar{\Delta}$ and $\bar{A}$ such that, given any value of $|\tilde{A}|$ within the interval $(0, \bar{A})$ and Δ within $(0, \bar{\Delta})$, there exists a neighborhood around the points $(x_{\mathrm{A}}, \rho_{\mathrm{A}}^{\mathrm{d}}, \xi_{\mathrm{A}}, \eta_{\mathrm{A}}) = \big(\ell(\rho_{\mathrm{A}}^*), \rho_{\mathrm{A}}^*, 0, J(\rho_{\mathrm{A}}^*)\big)$ and $(x_{\mathrm{H}}, \rho_{\mathrm{H}}^{\mathrm{d}}, \xi_{\mathrm{H}}, \eta_{\mathrm{H}}) = \big(\ell(\rho_{\mathrm{H}}^*), \rho_{\mathrm{H}}^*, 0, J(\rho_{\mathrm{H}}^*)\big)$. In this neighborhood, any solution to the feedback system (2.8) will converge exponentially to an $\mathcal{O}(\omega + \Delta + |\tilde{A}|)$-neighborhood of these points. Additionally, the output signal $y(t)$ will converge to an $\mathcal{O}(\omega+\Delta+|\tilde{A}|)$-neighborhood of $J(\rho_{\mathrm{A}}^*)$ and $J(\rho_{\mathrm{H}}^*)$.

Proof: The proof is shown in [132; 136].

3.2.2 DISTRIBUTED NEWTON-BASED EXTREMUM SEEKING

In the previous section, we implemented a gradient-based ES at the upper level of the hierarchical control framework to determine the optimal density of vehicles in

target cells with unknown downstream bottlenecks. In this section, in order improve the performance of the traffic network and reduce the convergence time, a Newton-based ES (NES) is employed at the upper level to compute the optimal density of target cells for each vehicle class, denoted as $\rho^{\mathrm{d}}_{i,\mathrm{A}}$ and $\rho^{\mathrm{d}}_{i,\mathrm{H}}$ as shown in Fig. 3.3. The results obtained from our previous design give us the following expression in an average sense for the parameter variable error in a quadratic map:

$$\dot{\tilde{e}}_{\mathrm{A}} = K_{\mathrm{A}} H_{\mathrm{A}} \tilde{e}_{\mathrm{A}}, \tag{3.10a}$$

$$\dot{\tilde{e}}_{\mathrm{H}} = K_{\mathrm{H}} H_{\mathrm{H}} \tilde{e}_{\mathrm{H}}, \tag{3.10b}$$

where $\tilde{e}_{\mathrm{A}} = \hat{\rho}_{\mathrm{A}} - \rho^{\mathrm{d}}_{\mathrm{A}}$, $\tilde{e}_{\mathrm{H}} = \hat{\rho}_{\mathrm{H}} - \rho^{\mathrm{d}}_{\mathrm{H}}$, K_{A} and K_{H} are the proportional gains in each ES loop and H_{A}, H_{H} are the Hessian for each class. This revealed two significant insights: (i) the ES algorithm, which relies on gradient-based optimization, is locally convergent, and (ii) the speed of convergence $(\dot{\tilde{e}}_{\mathrm{A}}, \dot{\tilde{e}}_{\mathrm{H}})$ is impacted by the second derivative (Hessian matrix) of the map denoted as $\mathcal{H}$ which is unknown. The classic ES utilizes gradients for optimizing density in congested cells, and its convergence rate is contingent on the accurate estimation of the second-order derivative of the objective function. After deriving the estimation, the convergence speed is primarily regulated by the proportional gain denoted as K. However, the convergence rate is subject to limitations, as it must not exceed a specific range; otherwise, it results in oscillations or overly slow convergence.

As stated before, the major limitation in the gradient-based method is that it starts seeking the optimal point from an initial condition towards where it has a larger gradient, and eventually, as it gets closer to the optimal point since the gradient gets closer to 0, the convergence speed gets super slow. Furthermore, not only the transient behavior of the gradient estimate is dependent on the shape of the cost function and is not under our control, but also ρ_{A} and ρ_{H} as the two variables of the function can have

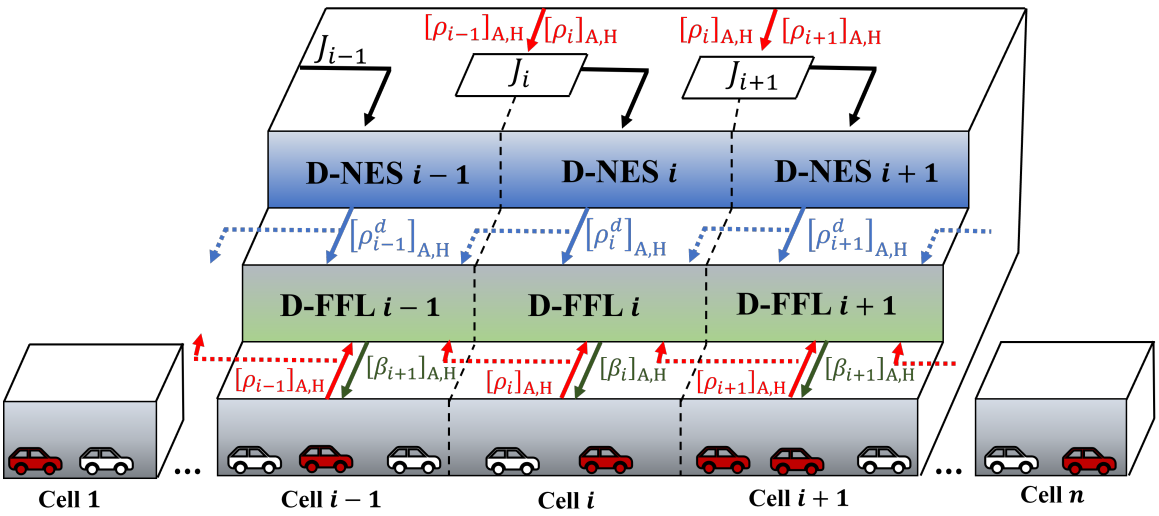

Figure 3.3: Distributed NES-FFL control scheme for a Heterogeneous traffic network.

different convergence rates which leads to non-uniform convergence. For example, consider a cost function similar to (2.17) and Fig. 2.5 with two input variables of AVs and HDVs densities for cell i. The curvature of the objective function can be more with respect to AVs density in comparison to HDVs density. The curvature of a cost function is determined by the Hessian, and when it is higher with respect to one variable than another, it signifies that the sensitivity or responsiveness of the cost function to changes in that particular variable is greater, indicating a steeper incline or decline in the optimization landscape along that variable. The issue in the previous example is that one variable (AVs density) may converge to its optimal density while the other variable (HDVs density) is not even close to its optimal point. Non-uniform convergence is a crucial challenge specifically when the unknown function has abrupt changes due to the noises or sudden changes in the shape of the function. Therefore, to improve the convergence speed and prevent the non-uniform convergence of the gradient-based ES at the upper level of the hierarchical controller, a novel Newton-based ES (NES) scheme is used to consider the effect of Hessian as shown in Fig. 3.4. The major improvement over the gradient-based ES is that an additional loop is attached to the former to obtain the estimate of the unknown Hessian matrix.

Moreover, the other obstacle in the way of designing the NES algorithm is that the inverse of the Hessian is also required in the Newton algorithm. Note that, since we are working on a multivariable NES, there will be transients from one optimal point to another, due to changes in the heterogeneity level of the target cell, and the estimation of Hessian may not always be accurate. Calculating the inverse of Hessian algebraically when the Hessian estimate may not be accurate due to changes in the function and noise of the system, can lead to a singular Hessian inverse which causes large transient gains and destabilizes the control system. Now since the Hessian matrix estimate, may not necessarily remain invertible, a dynamic system is designed to asymptotically generate the inverse. This dynamic system takes the form of a Riccati differential equation filter [132].

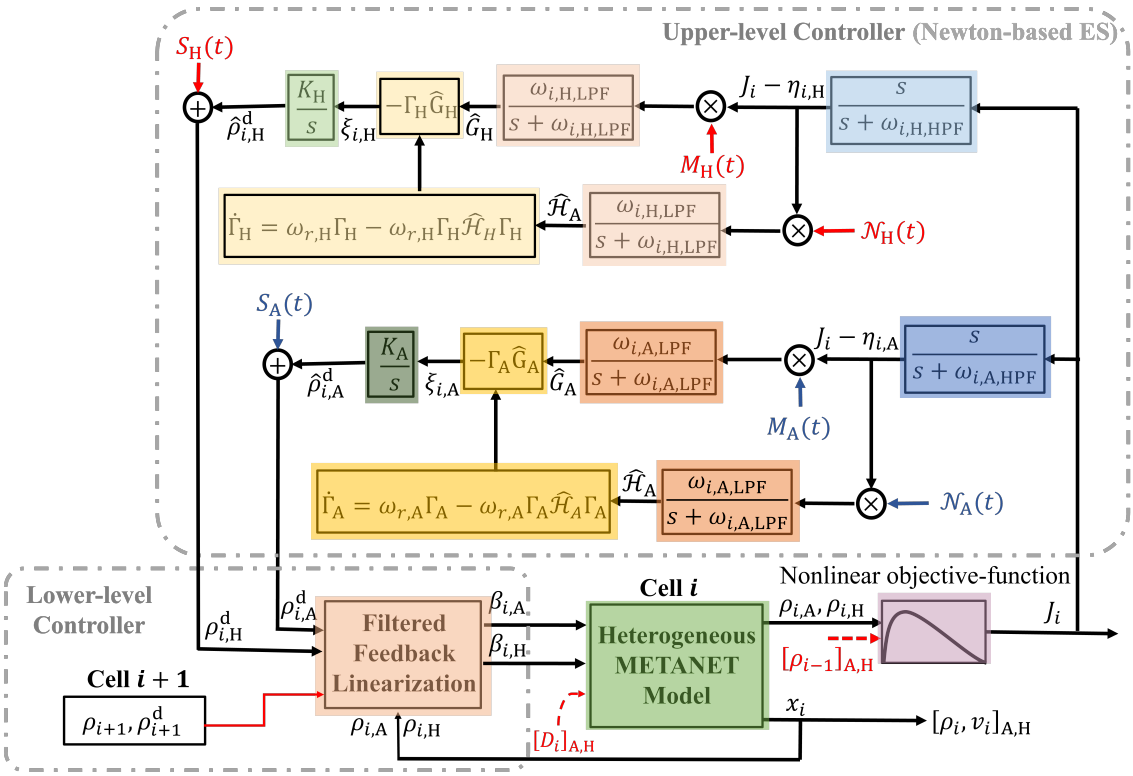

Figure 3.4: Distributed NES-FFL control scheme for a Heterogeneous traffic network.

The NES controller employs sinusoidal signals defined as $S_{\mathrm{A}}(t) = \tilde{A}_{i,\mathrm{A}}(t)\sin(\Omega_{i,\mathrm{A}}.t + \phi_{\mathrm{A}})$, $S_{\mathrm{H}}(t) = \tilde{A}_{i,\mathrm{H}}(t)\sin(\Omega_{i,\mathrm{H}}.t + \phi_{\mathrm{H}})$, $M_{\mathrm{A}}(t) = \frac{2}{\tilde{A}_{i,\mathrm{A}}(t)}\sin(\Omega_{i,\mathrm{A}}.t + \phi_{\mathrm{A}})$ and $M_{\mathrm{H}}(t) =$

$\frac{2}{\tilde{A}_{i,\mathrm{H}}(t)}\sin(\Omega_{i,\mathrm{H}}.t+\phi_{\mathrm{H}})$ to perturb the desired density values for each vehicle class and probe the objective function map. Moreover, the Newton-based algorithm encompasses two other critical elements as shown in Fig. 3.4: $\mathcal{N}(t)$, which represents another perturbation signal and gives us an approximation of the Hessian matrix ($\mathcal{H}(t)$), and the estimator of the inverse of the Hessian ($\Gamma(t)$) which has the form of a differential Riccati equation. The estimator yields an estimation of the inverse of $\mathcal{H}$, even in scenarios where the estimation of the $\mathcal{H}$ is singular. In [128], it has been shown that by carefully choosing an appropriate $\mathcal{N}(t)$ and calculating the average value of $\mathcal{N}(t)J$ over a full period denoted as $\frac{2\pi}{\Omega_i}$, an estimation of the Hessian matrix $\hat{\mathcal{H}}$ can be obtained. It is worth noting that the perturbation signal and the Riccati equation can be class-dependent [158] as depicted in Fig. 3.4. A feasible choice for $\mathcal{N}_{\mathrm{A}}(t)$ and $\mathcal{N}_{\mathrm{H}}(t)$, which satisfies all necessary constraints listed in [128], can be obtained as follow:

$$\mathcal{N}_{\mathrm{A}}(t)=\frac{16}{\tilde{A}_{\mathrm{A}}(t)^2}\big(\sin^2(\Omega_{i,\mathrm{A}}.t)-\frac{1}{2}\big), \tag{3.11a}$$

$$\mathcal{N}_{\mathrm{H}}(t)=\frac{16}{\tilde{A}_{\mathrm{H}}(t)^2}\big(\sin^2(\Omega_{i,\mathrm{H}}.t)-\frac{1}{2}\big), \tag{3.11b}$$

which lead us to

$$\hat{\mathcal{H}}_{\mathrm{A}}=\mathcal{N}_{\mathrm{A}}(t)J, \tag{3.12a}$$

$$\hat{\mathcal{H}}_{\mathrm{H}}=\mathcal{N}_{\mathrm{H}}(t)J. \tag{3.12b}$$

Next, we employ a dynamic estimator that calculates the inverse of $\hat{\mathcal{H}}_{\mathrm{A}}$ and $\hat{\mathcal{H}}_{\mathrm{H}}$,

denoted as Γ_{A} and Γ_{H}, utilizing a Riccati equation, as exemplified below:

$$\dot{\Gamma}_{\mathrm{A}} = \omega_{r,\mathrm{A}}\Gamma_{\mathrm{A}} - \omega_{r,\mathrm{A}}\Gamma_{\mathrm{A}}\hat{\mathcal{H}}_{\mathrm{A}}\Gamma_{\mathrm{A}}, \tag{3.13a}$$

$$\dot{\Gamma}_{\mathrm{H}} = \omega_{r,\mathrm{H}}\Gamma_{\mathrm{H}} - \omega_{r,\mathrm{H}}\Gamma_{\mathrm{H}}\hat{\mathcal{H}}_{\mathrm{H}}\Gamma_{\mathrm{H}}, \tag{3.13b}$$

where $\omega_{r,\mathrm{A}}$ and $\omega_{r,\mathrm{H}}$ are positive values and the equilibria of the Riccati in (3.13) are $\Gamma^*_{\mathrm{A}} = 0$, $\Gamma^*_{\mathrm{H}} = 0$ (unstable) and $\Gamma_{\mathrm{A}} = \hat{\mathcal{H}}^{-1}_{\mathrm{A}}$, $\Gamma_{\mathrm{H}} = \hat{\mathcal{H}}^{-1}_{\mathrm{H}}$ (exponentially stable; since the linearization of (3.13) has the Jacobian $-\omega_{r,\mathrm{A}}I$ and $-\omega_{r,\mathrm{H}}I$). The Riccati filter has two advantages in our design; i) It is stable in the $\Gamma_{\mathrm{A}} = \hat{\mathcal{H}}^{-1}_{\mathrm{A}}$, $\Gamma_{\mathrm{H}} = \hat{\mathcal{H}}^{-1}_{\mathrm{H}}$ which is the region of attraction since the goal of the dynamic estimator is to estimate the Hessian inverse, ii) It removes the unwanted transients that cause instability to the system. On the other side, the trade-off here is that the convergence speed will be reduced slightly by using this estimator which acts like a low-pass filter.

To ensure that the underlying dynamics exhibit a static nonlinearity when viewed from the NES loop perspective, it is crucial to select a perturbation frequency Ω_i that is sufficiently small, as discussed in [136]. Specifically, we consider $\Omega_i = \mathcal{O}(\omega)$, where $\omega_{\mathrm{i,H}} = \mathcal{O}(\Delta\omega)$ and $\omega_{i,\mathrm{L}} = \mathcal{O}(\Delta\omega)$, with $\mathcal{O}$ denoting statistical order, and ω and Δ representing small positive constants.

In order to uphold the stability of the NES controller, a series of assumptions must be satisfied, as discussed in Assumptions 3-5 and as posited in the literature [128].

The proposition presented in proposition 2 provides a summary of the stability and convergence characteristics of the upper-level NES controller as well.

3.2.3 DISTRIBUTED LYAPUNOV-BASED SWITCH NEWTON EXTREMUM SEEKING

The existing ES methods including NES, often converge to a limited cycle around the desired state instead of achieving precise convergence [146]. Thus, a significant challenge in utilizing the NES is eliminating the limit cycle behavior and achieving

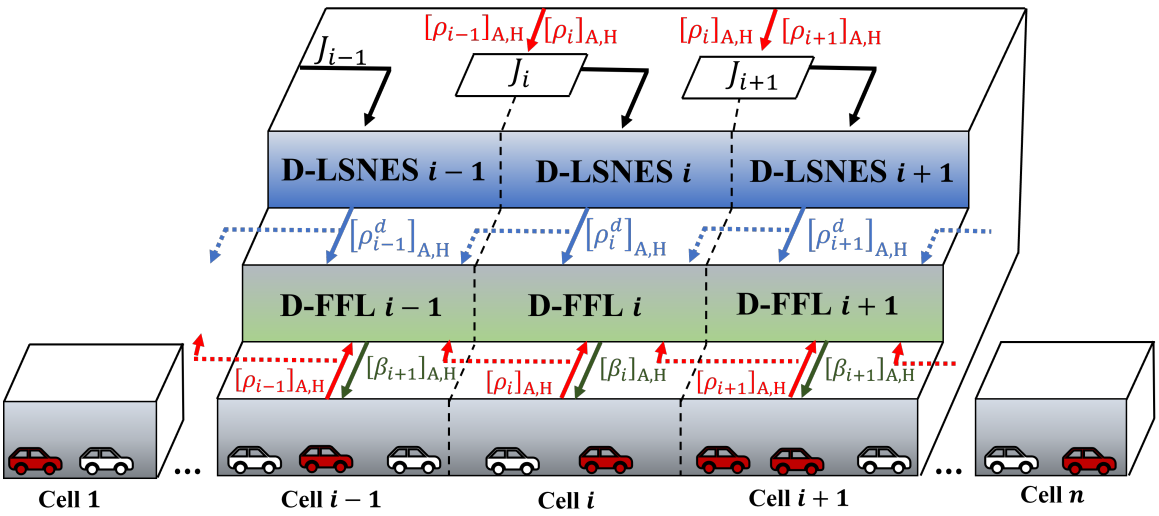

Figure 3.5: Distributed LSNES-FFL control scheme for a Heterogeneous traffic network.

asymptotic convergence to the optimal set-point. To address the potential loss in optimality that may arise due to continuous sinusoidal perturbations around the optimal point, we propose a switched control scheme to be added to the NES structure. The proposed switched control scheme involves reducing the amplitude of perturbations after convergence, specifically within a neighborhood around the desired state. We incorporated a Lyapunov-based Switch that was proposed by [146] into the NES (LSNES) approach, which is based on an averaged model of the NES feedback system and enables asymptotic convergence to the optimal set point. This Lyapunov function is designed to approximate the proximity to the desired state, and based on this estimate, the switch is activated to reduce the perturbation size. In Fig. 3.5, the hierarchical controller design consisting of distributed LSNES at the upper level and distributed FFL controller at the lower level is shown.

The Lyapunov function utilized in LSNES is a function of an averaged state variable, which is obtained by taking the average over one oscillation period as shown in

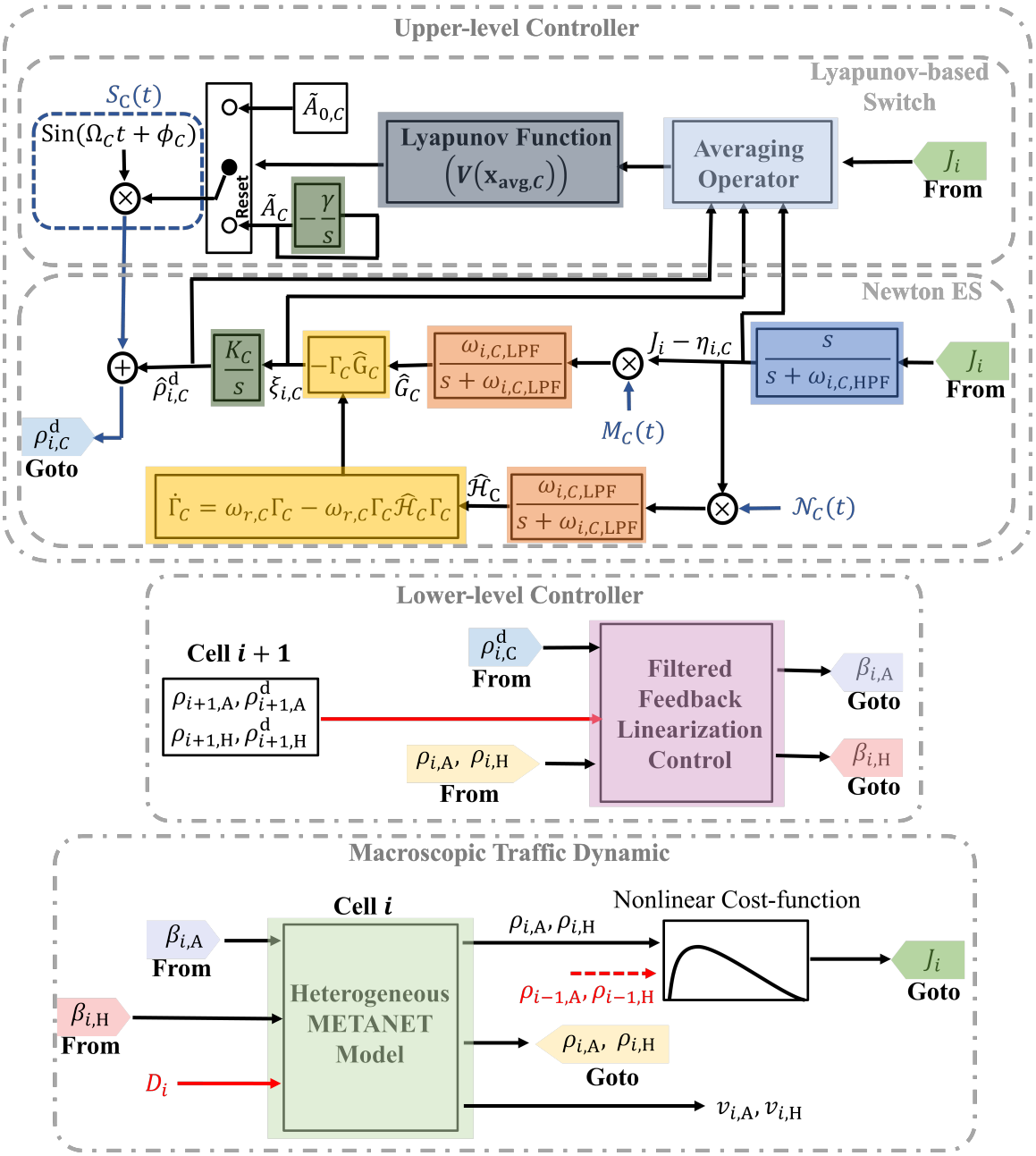

Figure 3.6: Comprehensive schematic of the control framework design for $\mathcal{C}_i$ consisting of the Newton ES, Lyapunov-based Switch, FFL, and heterogeneous METANET model. Subscript C at the upper-level controller represents different vehicle classes in the traffic network (A for AVs and H for HDVs). We are suggesting that all the perturbation signals, high-pass and low-pass filter frequencies, dynamic estimator, integrator gain, the Lyapunov function, and the switch are class-dependent.

Fig. 3.6. The Lyapunov functions are given by:

$$\tilde{x}_{\text{avg,A}} = \frac{\Omega_{\text{A}}}{2\pi} \int_{t-\frac{2\pi}{\Omega_{\text{A}}}}^{t} \tilde{x}_{\text{A}}(\tau) d(\tau), \tag{3.14a}$$

$$\tilde{x}_{\text{avg,H}} = \frac{\Omega_{\text{H}}}{2\pi} \int_{t-\frac{2\pi}{\Omega_{\text{H}}}}^{t} \tilde{x}_{\text{H}}(\tau) d(\tau), \tag{3.14b}$$

where $\tilde{x}_{\mathrm{A}} = [\tilde{\rho}^{\mathrm{d}}_{\mathrm{A}}, \xi_{\mathrm{A}}, \tilde{\eta}_{\mathrm{A}}]^{\mathrm{T}}$, $\tilde{x}_{\mathrm{H}} = [\tilde{\rho}^{\mathrm{d}}_{\mathrm{H}}, \xi_{\mathrm{H}}, \tilde{\eta}_{\mathrm{H}}]^{\mathrm{T}}$ as shown in Fig. 3.6. The switching mechanism illustrated in Fig. 3.6 utilizes a quadratic Lyapunov function denoted as $V(\tilde{x}_{\mathrm{avg,A}})$ and $V(\tilde{x}_{\mathrm{avg,H}})$, which serve as a metric for gauging the closeness of the averaged values (computed over one NES period) of $\rho^{\mathrm{d}}_{\mathrm{A}}$, $\rho^{\mathrm{d}}_{\mathrm{H}}$, η_{A} and η_{H} to their estimated desired values:

$$V(\tilde{x}_{\mathrm{avg,A}}) = \frac{1}{2}\tilde{x}^{\mathrm{T}}_{\mathrm{avg,A}}\bar{J}\tilde{x}_{\mathrm{avg,A}}, \tag{3.15a}$$

$$V(\tilde{x}_{\mathrm{avg,H}}) = \frac{1}{2}\tilde{x}^{\mathrm{T}}_{\mathrm{avg,H}}\bar{J}\tilde{x}_{\mathrm{avg,H}}. \tag{3.15b}$$

The construction of V involves solving the following Lyapunov equation for $\bar{J}$ considering $Q = Q^{\mathrm{T}} > 0$:

$$\bar{J}\Upsilon_{\mathrm{A}} + \Upsilon^{\mathrm{T}}_{\mathrm{A}}\bar{J} = -Q, \tag{3.16a}$$

$$\bar{J}\Upsilon_{\mathrm{H}} + \Upsilon^{\mathrm{T}}_{\mathrm{H}}\bar{J} = -Q, \tag{3.16b}$$

where the Jacobian matrices Υ_{A} and Υ_{H} are utilized to approximate the system dynamics near the equilibrium [146] as follows:

$$\Upsilon_{\mathrm{A}} = \begin{bmatrix} 0 & \hat{K}'_{\mathrm{A}} & 0 \\ \omega'_{\ell,\mathrm{A}} J''_{\mathrm{A}}(\rho^{\mathrm{d}}_{\mathrm{A}}) A_{0,\mathrm{A}} & -\omega'_{\ell,\mathrm{A}} & 0 \\ \omega'_{\mathrm{h,A}} J'_{\mathrm{A}}(\rho^{\mathrm{d}}_{\mathrm{A}}) & 0 & -\omega'_{\mathrm{h,A}} \end{bmatrix}, \tag{3.17a}$$

$$\Upsilon_{\mathrm{H}} = \begin{bmatrix} 0 & \hat{K}'_{\mathrm{H}} & 0 \\ \omega'_{\ell,\mathrm{H}} J''_{\mathrm{H}}(\rho^{\mathrm{d}}_{\mathrm{H}}) A_{0,\mathrm{H}} & -\omega'_{\ell,\mathrm{H}} & 0 \\ \omega'_{\mathrm{h,H}} J'_{\mathrm{H}}(\rho^{\mathrm{d}}_{\mathrm{H}}) & 0 & -\omega'_{\mathrm{h,H}} \end{bmatrix}, \tag{3.17b}$$

where $\hat{K}_{\mathrm{A}} = \frac{K_{\mathrm{A}}}{\Omega_{\mathrm{A}}}$, $\hat{K}_{\mathrm{H}} = \frac{K_{\mathrm{H}}}{\Omega_{\mathrm{H}}}$, $\omega'_{\ell,\mathrm{A}} = \frac{\omega_{\mathrm{LPF,A}}}{\Omega_{\mathrm{A}}}$, $\omega'_{\ell,\mathrm{H}} = \frac{\omega_{\mathrm{LPF,H}}}{\Omega_{\mathrm{H}}}$, $\omega'_{\mathrm{h,H}} = \frac{\omega_{\mathrm{H,H}}}{\Omega_{\mathrm{H}}}$, $J''_{\mathrm{A}}(\rho^{\mathrm{d}}_{\mathrm{A}}) < 0$ and, $J''_{\mathrm{H}}(\rho^{\mathrm{d}}_{\mathrm{H}}) < 0$. When the value of $V(\tilde{x}_{\mathrm{avg,A}})$ and $V(\tilde{x}_{\mathrm{avg,H}})$ are small enough, the perturbation signals, $A_{\mathrm{A}}(t)$ and $A_{\mathrm{H}}(t)$, will decay in size. However, if $V(\tilde{x}_{\mathrm{avg,A}})$ or $V(\tilde{x}_{\mathrm{avg,H}})$ are not sufficiently small, the perturbation signal will remain at its full size. The following relationship dictates how the size of $A_{\mathrm{A}}(t)$ and $A_{\mathrm{H}}(t)$ changes over time.

$$A_{\mathrm{A}}(t) = \begin{cases} A_{0,\mathrm{A}} & \text{if } V(\tilde{x}_{\mathrm{avg,A}}) > \epsilon, \\ -\gamma_{\mathrm{A}} \int_{t_{sw}}^{t} A_{\mathrm{A}}(\tau) d(\tau) & \text{if } V(\tilde{x}_{\mathrm{avg,A}}) \leq \epsilon, \end{cases} \tag{3.18a}$$

$$A_{\mathrm{H}}(t) = \begin{cases} A_{0,\mathrm{H}} & \text{if } V(\tilde{x}_{\mathrm{avg,H}}) > \epsilon, \\ -\gamma_{\mathrm{H}} \int_{t_{sw}}^{t} A_{\mathrm{H}}(\tau) d(\tau) & \text{if } V(\tilde{x}_{\mathrm{avg,H}}) \leq \epsilon, \end{cases} \tag{3.18b}$$

where t_{sw} is the switching time and γ determines the rate at which the perturbation amplitude shrinks in the proposed control scheme.

Remark 3 *In scenarios where the optimal density $(\rho^{\mathrm{d}}_{\mathrm{A}}, \rho^{\mathrm{d}}_{\mathrm{H}})$ and its corresponding cost function value $(J(\rho^{\mathrm{d}}_{\mathrm{A}}), J(\rho^{\mathrm{d}}_{\mathrm{H}}))$ are not known a priori, an estimation procedure is employed to approximate these values, for use in (3.16). This estimation process involves numerically differentiating J and J' based on the current and previous values to estimate J' and J'' at the current density for each vehicle class. Subsequently, extrapolation is utilized to estimate ρ^{d} for both AVs and HDVs using the values of J' and J'' at the current density of each vehicle class. Previous studies [146] have demonstrated the algorithm's robustness to estimation errors.*

CHAPTER 4: SIMULATION RESULTS

To demonstrate the effectiveness of the designed hierarchical controller, we conducted a series of case studies at the lower level and upper level. Fig. 4.1 is the schematic diagram of the freeway section used in these case studies using real-world traffic data. It is a subsection of I-485 inner highway, between Mallard Creek Rd and Harrisburg Rd, Charlotte, North Carolina. This section is approximately 10 miles long, with 4 lanes with a speed limit of 70 mph. We discretize this network into 10 cells, as shown in Fig. 4.1.

We use I-485 N of Exit 28 (Mallard Creek Rd, Mecklenburg County, NC in Fig. 4.1) traffic flow data which was reported on Tuesday, 22 December 2020, in peak hours between 4:00 to 6:00 PM, to calibrate the state- and class-dependent METANET model parameters. The calibrated model parameters are listed here: $\gamma_{\mathrm{A}} = 66, \gamma_{\mathrm{H}} =$

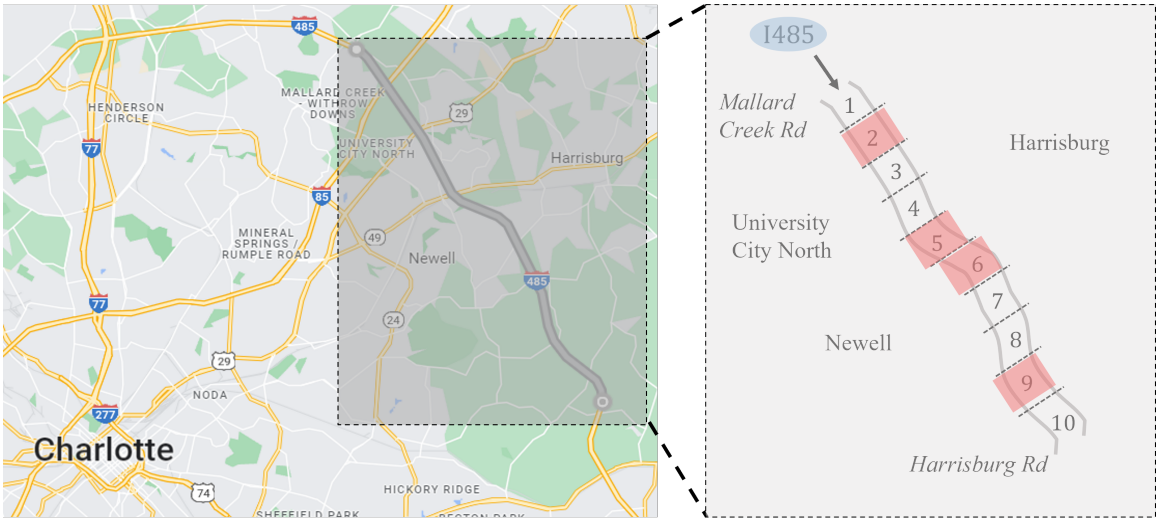

Figure 4.1: I485 inner highway between Mallard Creek Rd and Harrisburg Rd, Charlotte, North Carolina. Target cells 5 and 6 that are in the congested phase are highlighted.

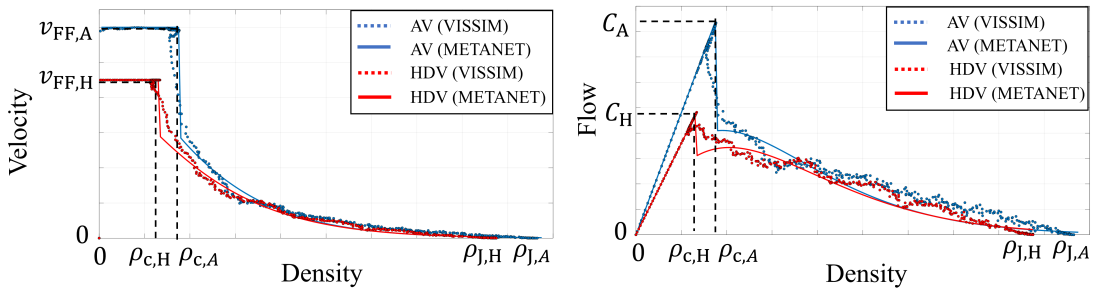

Figure 4.2: Exemplary MFD (Velocity-Density, Flow-Density) for full AVs and full HDVs networks using PTV-VISSIM traffic simulation data and METANET model.

$44\frac{mile^2}{h}$, $\kappa_{\mathrm{A}} = 18, \kappa_{\mathrm{H}} = 14\frac{veh}{mile.h}$, $\tau_{\mathrm{A}} = 3s, \tau_{\mathrm{H}} = 12s$ and $a_{m,\mathrm{A}} = \mathfrak{h}(\rho_{i,\mathrm{A}}), a_{m,\mathrm{H}} = \mathfrak{g}(\rho i, \mathrm{H})$ which are the only state varying parameters in this paper. In this research, we use brute-force search to find out the $\mathfrak{h}(k_{i,\mathrm{A}})$ function, which is equal to $[16, 11, 4, 2.1]$ if the density of cell is $[\rho_{i,\mathrm{A}} \leq \rho_{c,\mathrm{A}}, \rho_{c,\mathrm{A}} < \rho_{i,\mathrm{A}} \leq 1.5\rho_{c,\mathrm{A}}, 1.5\rho_{c,\mathrm{A}} < \rho_{i,\mathrm{A}} \leq 3\rho_{c,\mathrm{A}}, 3\rho_{c,\mathrm{A}} < \rho_{i,\mathrm{A}} \leq \rho_{J,\mathrm{A}}]$ respectively. In addition, $\mathfrak{h}(\rho_{i,\mathrm{H}})$ function which is equal to $[12, 8, 5, 1.5]$ if the density of cell is $[\rho_{i,\mathrm{H}} \leq \rho_{c,\mathrm{H}}, \rho_{c,\mathrm{H}} < \rho_{i,\mathrm{H}} \leq 1.5\rho_{c,\mathrm{H}}, 1.5\rho_{c,\mathrm{H}} < \rho_{i,\mathrm{H}} \leq 3\rho_{c,\mathrm{H}}, 3\rho_{c,\mathrm{H}} < \rho_{i,\mathrm{H}} \leq \rho_{J,\mathrm{H}}]$. Also, the critical density of AVs and HDVs is $\rho_{\mathrm{c,A}} = 38, \rho_{\mathrm{c,H}} = 29\frac{veh}{mile.lane}$, the jam density is $\rho_{\mathrm{J,H}} = 145, \rho_{\mathrm{J,H}} = 190\frac{veh}{mile.lane}$ and the free-flow velocity is $v_{\mathrm{FF,A}} = 90, v_{\mathrm{FF,H}} = 70mph$.

4.1 LOWER-LEVEL CONTROLLER (D-FFL) RESULTS

This section is dedicated to evaluating the efficacy of the lower-level controller (D-FFL) in both homogeneous and heterogeneous traffic networks. We have conducted a set of case studies specifically designed to gauge the effectiveness of the D-FFL controller, excluding any influence from the upper-level controller. As a result, the reference density for the target cells is determined by the infrastructure itself rather than the ES algorithm, aligning closely with the critical density of the vehicles.

4.1.1 CASE STUDY 1: QUANTIFYING FFL PERFORMANCE

In the first case study, we present a numerical example that demonstrates the D-FFL controller and the effect of z on the system's outputs. First, we consider a sce-

nario where the desired density is defined for cells 4 and 5 (i.e., $\xi = [\rho^{\mathrm{d}}_{4,\mathrm{A}}\ \rho^{\mathrm{d}}_{4,\mathrm{H}}\ \rho^{\mathrm{d}}_{5,\mathrm{A}}\ \rho^{\mathrm{d}}_{5,\mathrm{H}}]^{\mathrm{T}}$). This set of densities is a sequence of steps that are passed through a low-pass filter: $\frac{10^3}{(s+10)^3}$.

These distributed controllers can be implemented with knowledge of measurements of $\rho_{3,\mathrm{A}}$, $\rho_{3,\mathrm{H}}$, $\rho_{4,\mathrm{A}}$, $\rho_{4,\mathrm{H}}$, $\rho_{5,\mathrm{A}}$ and, $\rho_{5,\mathrm{H}}$. In this simulation, flow disturbances ($d_{4,\rho_{\mathrm{A}}}$, $d_{4,\rho_{\mathrm{H}}}$, $d_{5,\rho_{\mathrm{A}}}$ and, $d_{5,\rho_{\mathrm{H}}}$) are passed through a second-order Butter-worth filter that has a 30-Hz cutoff frequency. Fig. 4.3 shows closed-loop simulations for increasing values of z and demonstrates that as z increases, the error between the reference command (i.e., desired density) and the cell density decreases. Furthermore, Fig. 4.4 shows as z increases, the error between the suggested velocity and the velocity decreases.

Next, we examine the impact of discretizing the D-FFL control system for practical implementation on an infrastructure. In practice, there is limited bandwidth for measuring the density on the road or sending suggested velocity commands to the vehicles within a cell. We examine the digital implementation of D-FFL with sample frequencies of 1, 0.5, 0.2, and 0.1 Hz (i.e., sample times of 1, 2, 5, and 10 seconds). The dynamics of the traffic network and the D-FFL control, (2.8), (3.7a) and (3.7b), are discretized using a zero-order hold on the input and a uniform sample time $T_{s,\mathrm{A}} = T_{s,\mathrm{H}} = T_s$. In Fig. 4.5, the average power of density error of cell 5 as a function of z value is shown. In each time step, as z increases, the average power of density error decreases till it reaches its minimum value, and it increases afterward. Also, as the time step T_s decreases, the minimum value for the average power of density error decreases.

4.1.2 CASE STUDY 2: D-FFL VS MTFC-PID

Traffic control in large networks often involves using a PID feedback controller for Mainstream Traffic Flow Control (MTFC). This approach is similar to the design of the D-FFL controller, as outlined in [86]. To compare the performance of these two controllers, we consider a setpoint for the target cell 5, which is equal to the

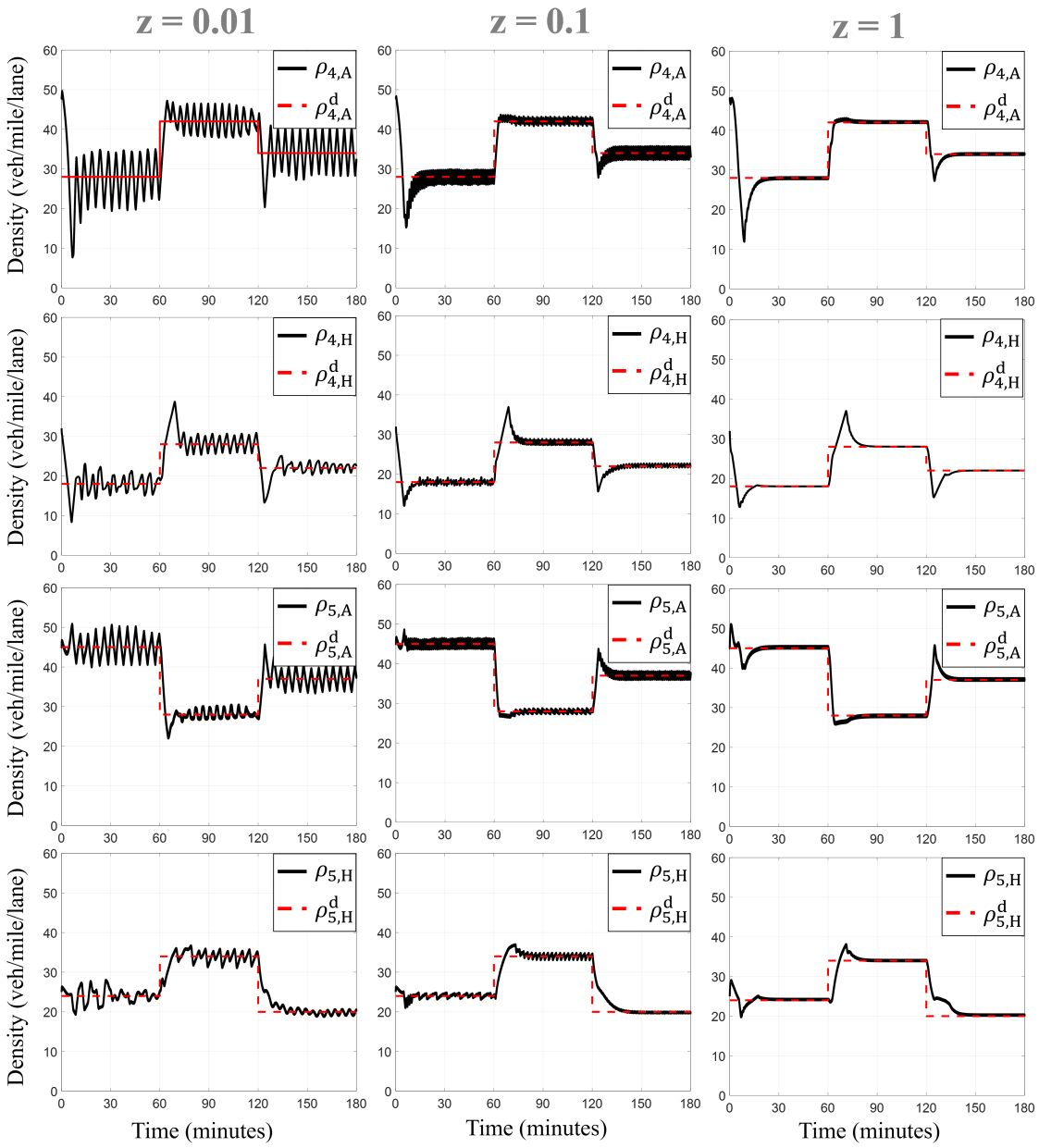

Figure 4.3: Densities of cells 4 and, 5 are shown for various z values $(1, 0.1, 0.01)$ for AVs and HDVs. By increasing the z value from $z = 0.01$ (first column) to $z = 1$ (third column), the output results improve. The density (solid black line) and the desired density (dashed red line) for target cells (4 and 5) are shown in each subplot.

critical density of AVs and HDVs, and feed it to both controllers. The PID gains are calculated to give us the best closed-loop command following for the problem. The calculated gains are Kp=10.2, Ki=0.35, and Kd=0.04. Fig. 4.6 compares the density of AVs and HDVs when using PID-MTFC and D-FFL controllers in the traffic

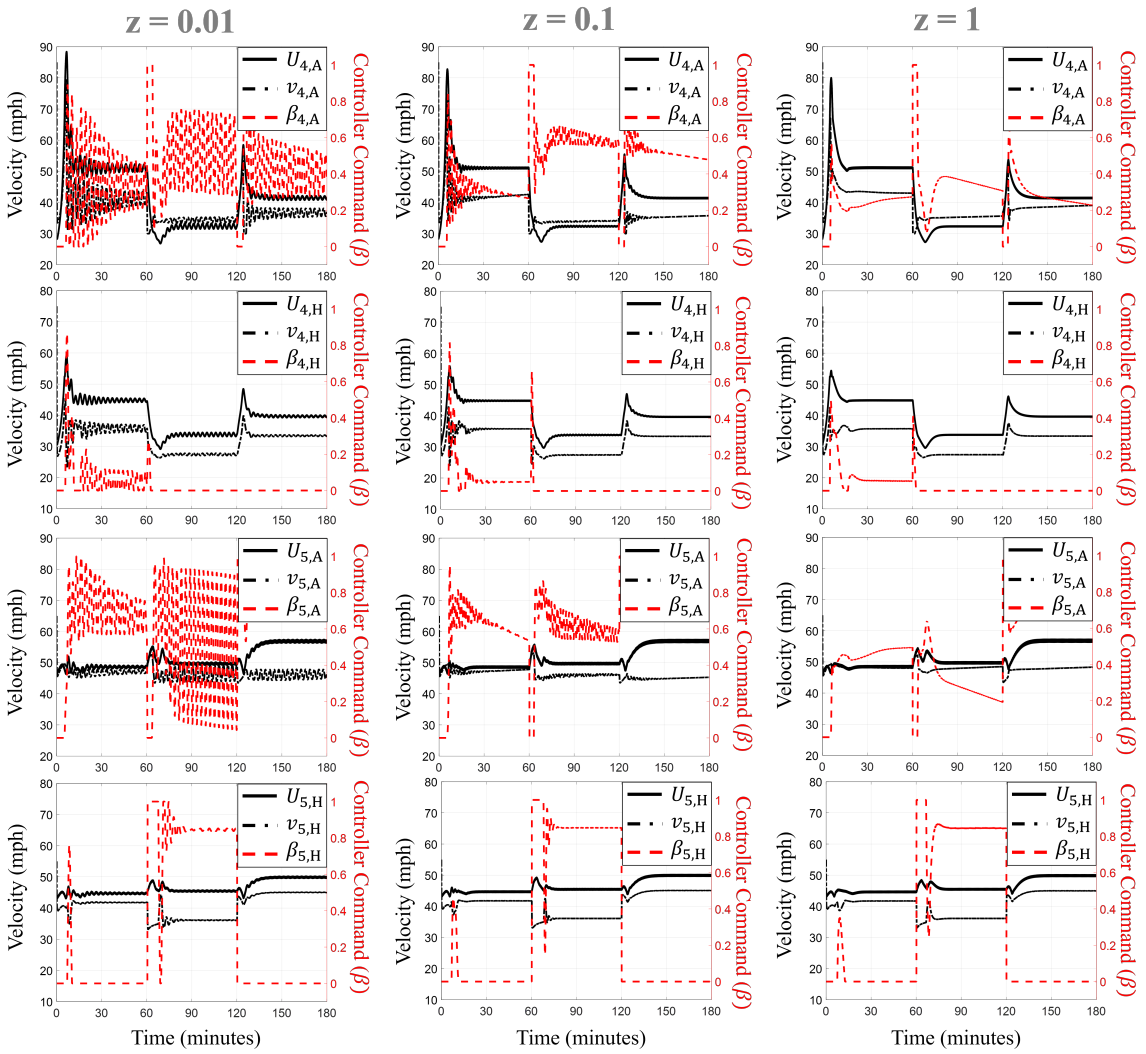

Figure 4.4: Velocities, suggested velocities and controller commands for cells 4 and, 5 are shown for various z values $(1, 0.1, 0.01)$ for AVs and HDVs. By increasing the z value from $z = 0.01$ (first column) to $z = 1$ (third column), the output results improve. Velocity (dashed-dot black line), suggested velocity (solid black line), and the controller command (dashed red line) for cells 4, and 5 are shown in each sub-plot

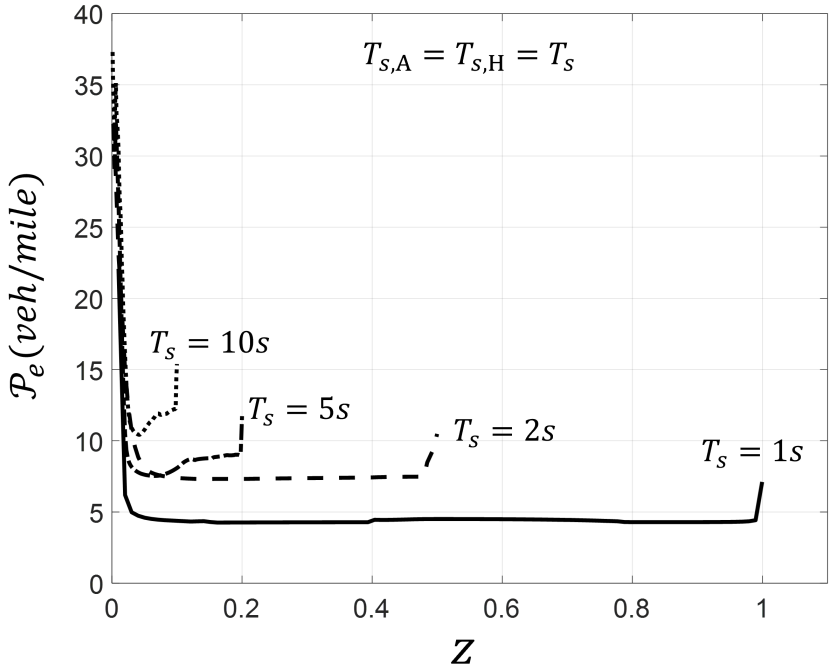

Figure 4.5: Average power of density error of cell 3 as a function of z in discrete D-FFL control system and sample time $T_s \in \{1, 2, 5, 10\}$. For each T_s, as z increases, the $\mathcal{P}_e$ decreases, reaches a minimum, and then increases.

network.

Upon comparing the outcomes obtained from the D-FFL controller and the PID-MTFC, it is found that the former exhibits a faster settling time. Specifically, the D-FFL controller can regulate the velocity of AVs in cell 5 and its upstream cell to attain the intended density within 85 seconds, whereas the PID-MTFC necessitates 188 seconds to achieve the desired set-point. Furthermore, the D-FFL controller regulates the density of HDVs more efficiently, achieving the desired density in only 80 seconds, while PID-MTFC takes 115 seconds. These findings indicate that the D-FFL controller is more effective in controlling the speed and density of both AVs and HDVs and holds promise for managing traffic flow in highly congested networks. It is important to note that in the designed multi-level control framework, the perturbation frequency of the D-ES is dependent on the time constant of the lower-level dynamics. As a result of this interdependence, the D-ES-FFL controller achieves a faster overall

convergence rate than the ES-PID-MTFC. This can be attributed to the hierarchical framework's ability to optimize control action by exploiting the system's underlying dynamics. By utilizing the time constant of the lower-level dynamics, the higher-level controller can adjust its perturbation frequency to more effectively regulate the system, resulting in superior performance compared to the ES-PID-MTFC controller.

4.1.3 CASE STUDY 3: IMPACT OF DISCRETIZATION, V2I COMMUNICATION RATES, AND LEVELS OF HETEROGENEITY

We will now evaluate the practical implementation of the D-FFL controller and the impact of discretization on transportation infrastructure. Real-world implementation poses limitations in terms of measuring road density and transmitting velocity suggestions to vehicles within a cell. In such scenarios, AVs are typically assumed to have a faster Vehicle-to-Infrastructure (V2I) communication rate than HDVs [159]. This enables AVs to receive velocity suggestions through direct V2I communication,

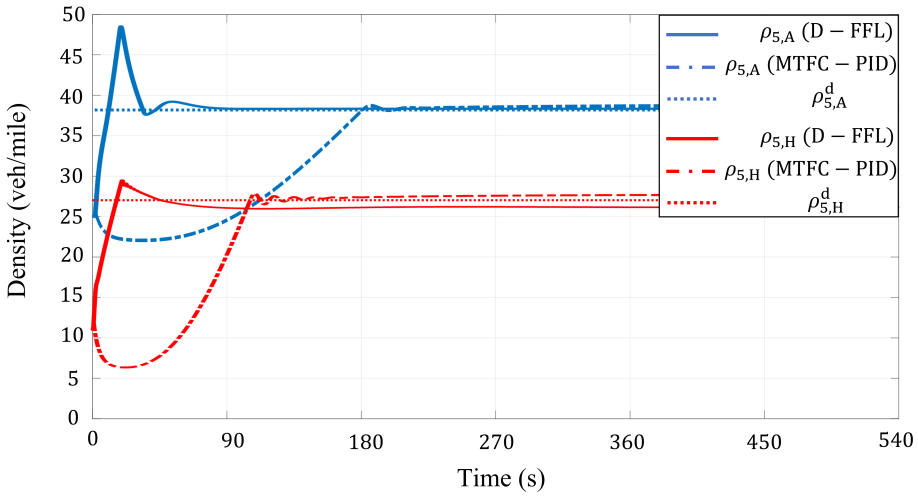

Figure 4.6: Density changes of AVs and HDVs in target cell 5 using PID-MTFC and D-FFL controllers, with the desired densities set equal to the critical density of each class.

reducing the time required to achieve the desired velocity compared to HDVs that rely on dynamic speed limit signs on the freeway. Specifically, we consider the V2I communication rate for AVs to be $T_{s,\mathrm{A}} = 1s$, while the HDV time step changes from $1s$ to ∞ in our analysis. It is crucial to understand these practical implementation challenges and their effect on the performance of the D-FFL controller, which is an essential aspect of its broader deployment in highly congested traffic networks. When the $\frac{T_{s,\mathrm{H}}}{T_{s,\mathrm{A}}} = 1$, dynamic speed limit signs update every $1s$, and when the $\frac{T_{s,\mathrm{H}}}{T_{s,\mathrm{A}}} = \infty$, HDVs only follow their steady-state speed density dynamic. We consider the density error of AVs ($e_{i,\mathrm{A}} = y_{\mathrm{m,A}} - y_{i,\mathrm{A}}$) in the target cell $i = 6$ to see the effect of various V2I rates for HDVs on one cell in a heterogeneous traffic network. Fig. 4.7 shows the average power of AVs' density error of target cell 6 for various V2I communication rates. The average power of AVs' density error is smaller when HDVs have a faster communication rate with the traffic network infrastructure, and it keeps increasing as the communication rate gets slower for HDVs. Furthermore, as the filter gain value z increases, the $\mathcal{P}_{e,\mathrm{A}}$ reduces. Also, it is important to note that high gain values make the discrete system unstable.

To investigate the effects of heterogeneity levels and different communication rates for HDVs, we analyzed the same traffic network displayed in Fig. 4.1, using identical boundary conditions and total inflow rate ($q_{\mathrm{in,TOT}}$). Five relative flow values ranging from fully human-driven traffic flow to fully autonomous traffic flow ($\frac{q_{\mathrm{in,A}}}{q_{\mathrm{in,TOT}}} = 0, 0.25, 0.5, 0.75, 1$) are considered to examine the effects of heterogeneity levels. We assumed that the V2I communication rate for AVs is $1s$ and we evaluated four different communication rates for HDVs ($\frac{T_{s,\mathrm{H}}}{T_{s,\mathrm{A}}} = 1, 10, 100, \infty$). For each scenario, we calculated the steady-state total average flow value for target cells 5 and 6 and the upstream cell 4 ($Q_{\mathrm{TOT}} = \sum_{i=5}^{i=6} Q_i$). The 3D plot of Q_{TOT} for each level of heterogeneity and V2I communication rate is illustrated in Fig. 4.8. As is shown, the total average flow rate is the lowest when the total inflow is fully HDVs, and there is

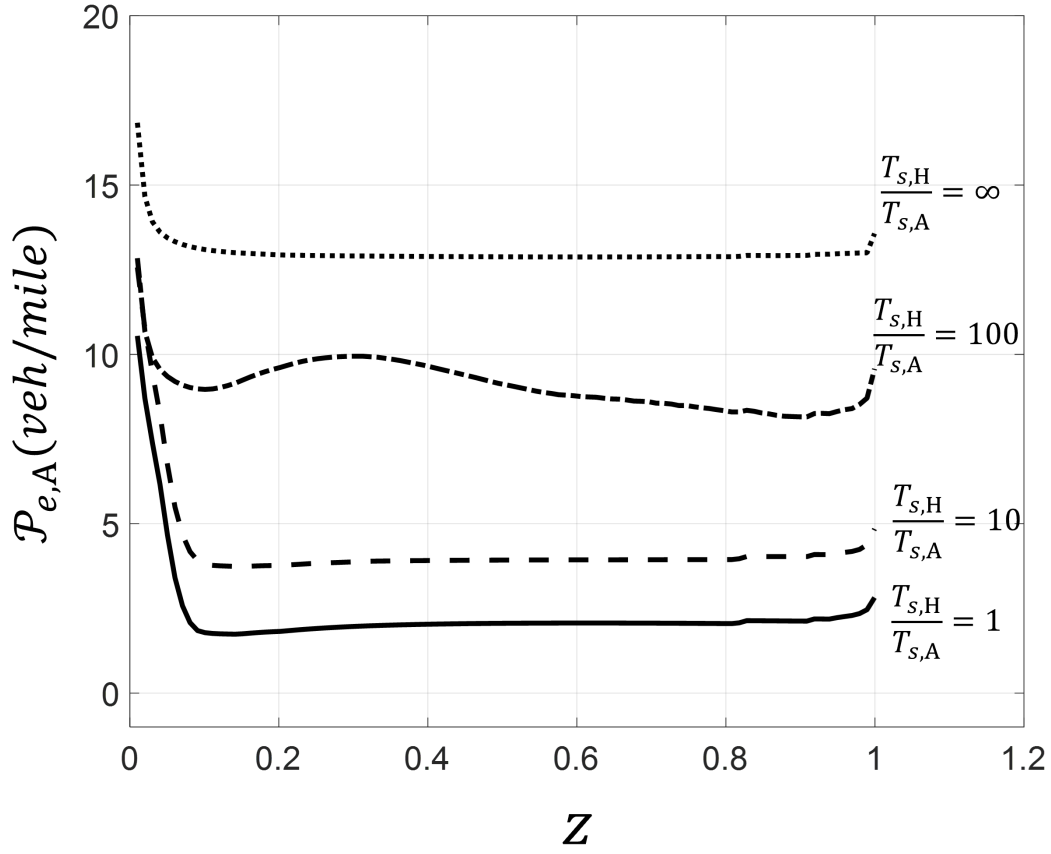

Figure 4.7: Average power of AVs' density error of cell 6 as a function of z in discrete D-FFL control system with various communication rates for AVs ($T_{s,\mathrm{A}}$) and HDVs ($T_{s,\mathrm{H}}$).

no control over them. On the other hand, when the traffic inflow is fully AVs, and the V2I communication rate is assumed to be $1s$ for all the scenarios, we reach the maximum total average flow value.

4.1.4 CASE STUDY 3: FFL WITH PTV-VISSIM

In this case study, we use a real-world traffic simulator, PTV Vissim, to show the effectiveness of FFL control in a real-world simulation. VISSIM serves as a widely employed microscopic traffic simulator, offering a graphical user interface for simulating both simple static controls (pre-timed or fixed-time) and the flexibility for dynamic simulation control through versatile programming languages [160]. Inte-

grating computational tools can streamline the implementation of various traffic control techniques, with MATLAB being a widely utilized tool that meets the essential requirements for dynamically controlling VISSIM simulations [160].

The entire process of establishing a direct MATLAB-VISSIM interface for online implementation of the FFL controller is illustrated in a flowchart (Fig.4.9). Initially, the traffic network and its corresponding settings are configured using the VISSIM GUI. Subsequently, the network and settings, such as the number of lanes and free flow speed, are saved in the VISSIM project (INP) and initialization file (INI), respectively. The MATLAB environment then dynamically controls the traffic network within the VISSIM microscopic simulator [160].

To create the direct MATLAB-VISSIM interface, two MATLAB codes were devel-

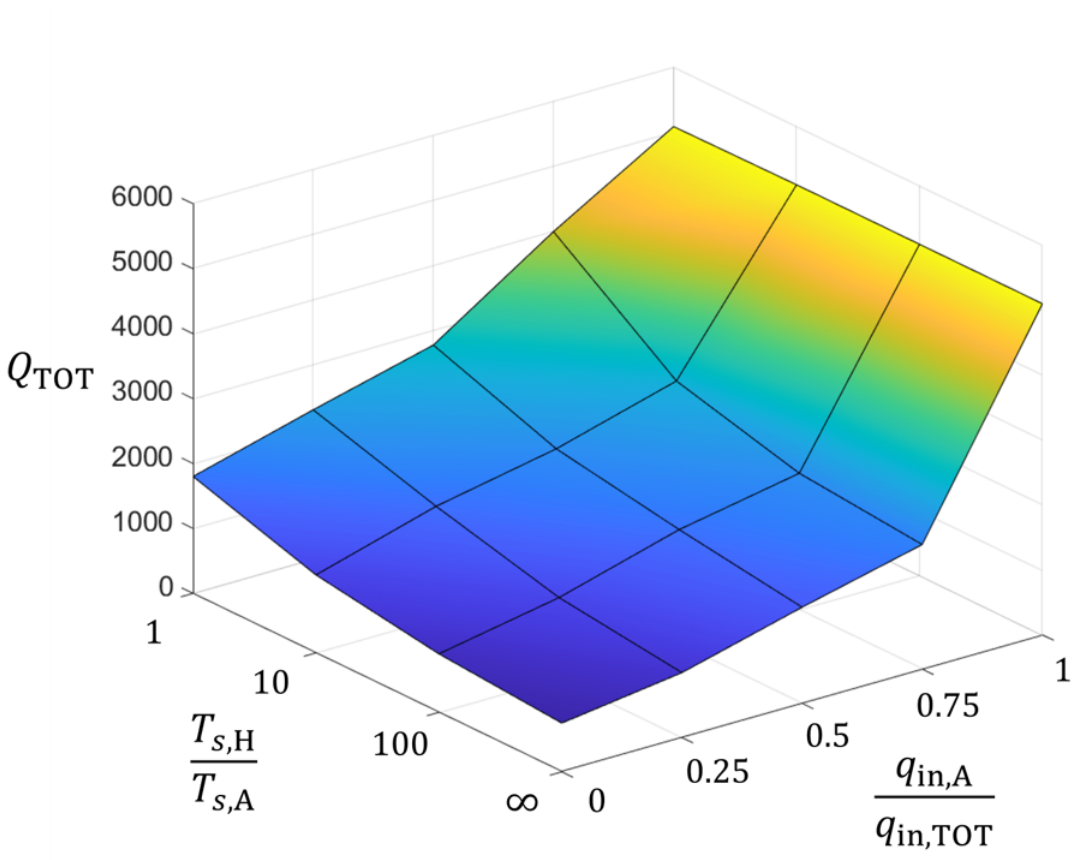

Figure 4.8: Total average flow value for the target cells 5 and 6 is shown for various levels of heterogeneity and communication rates.

oped. The first code, presented as a MATLAB script, issues commands to control the VISSIM simulator by sending instructions from MATLAB and receiving traffic information from VISSIM. This code activates the VISSIM server to establish the COM object, taking INP and INI files as input. It then accesses "network" and "simulation" through the COM object. The second code is a Simulink file containing a METANET model of the traffic network, a Luenberger observer, and the FFL controller. For this study, a single-step microscopic simulation with a step size of 10 minutes has been chosen to control and set the state of signal controllers dynamically. After completion of each cycle (duration = 10 minutes), the density of AVs and HDVs in each cell is recorded and passed to the MATLAB Simulink environment through the COM interface. Using the observer, the states of the METANET model are updated. Then, using the measured densities of the METANET model in the Simulink file, the suggested control commands are generated using the FFL controller. These commands are then passed to the first code and then applied to the VISSIM. The entire process continues till the end of the total simulation time, which was 120 minutes (12 cycles) for this study.

In this study, we considered the same case study in Case Study 1. The highway link has five cells with freeway link behavior type and 1mile length. The inflow on the traffic network was set equal to $q_{0,\mathrm{TOT}} = 3000\frac{veh}{h}$ with the stochastic volume type and vehicle composition of 0.6 for AVs and 0.4 for HDVs. Data collection points were put at the end of each cell to collect the flow and velocity information. The vehicle class of the vehicles in the traffic network was chosen to be "Car" for both HDVs and AVs, with the driving behavior of "Freeway" for HDVs and "AV normal (CoEXist)" for AVs. In order to have a distributed traffic control network, we put the variable speed limit signs every 0.1 mile for AVs, so all the vehicles in each cell get the suggested velocities information from the controller at almost the same time. The experimental results of the heterogeneous traffic network with five cells are shown in Fig.4.25

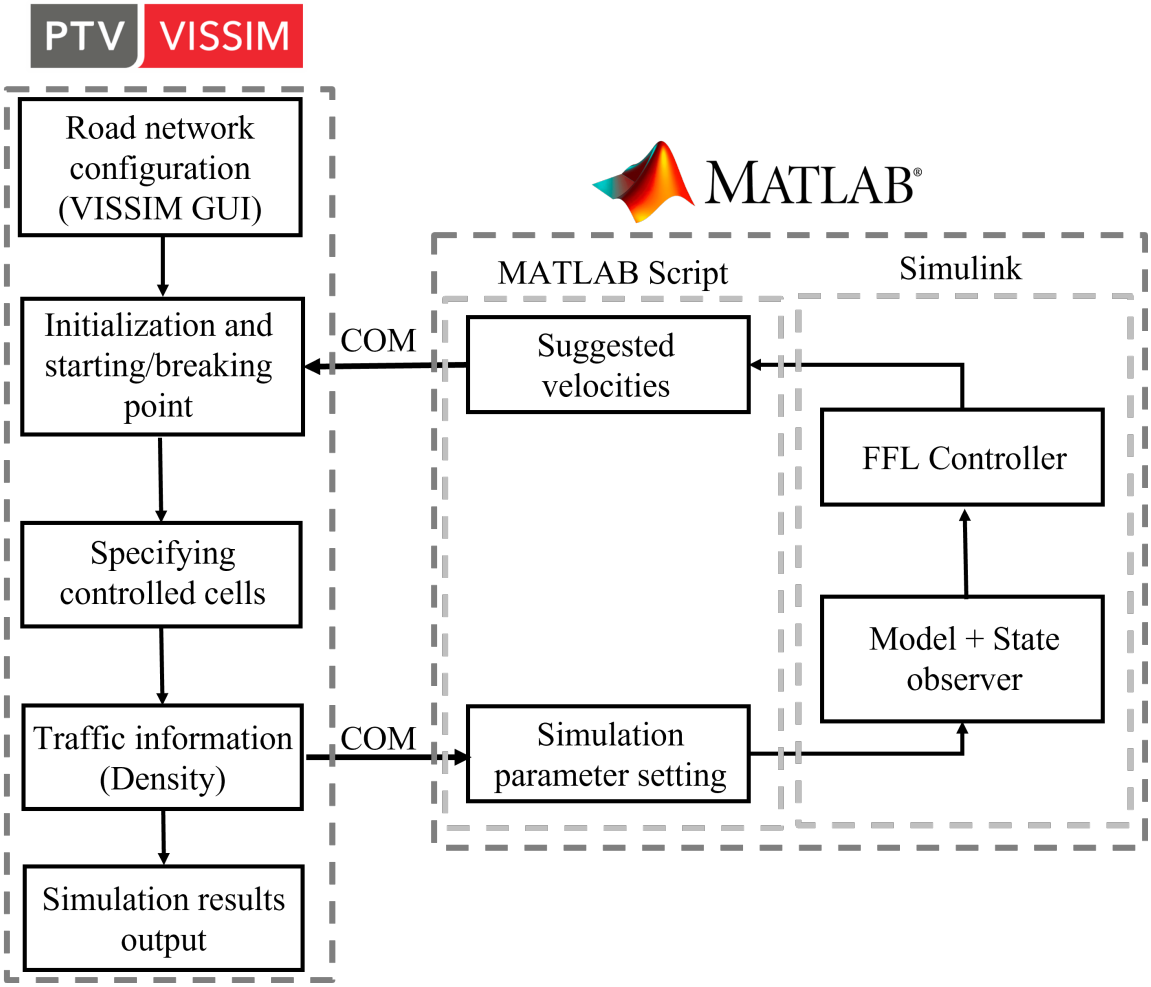

Figure 4.9: MATLAB-VISSIM simulation platform structure

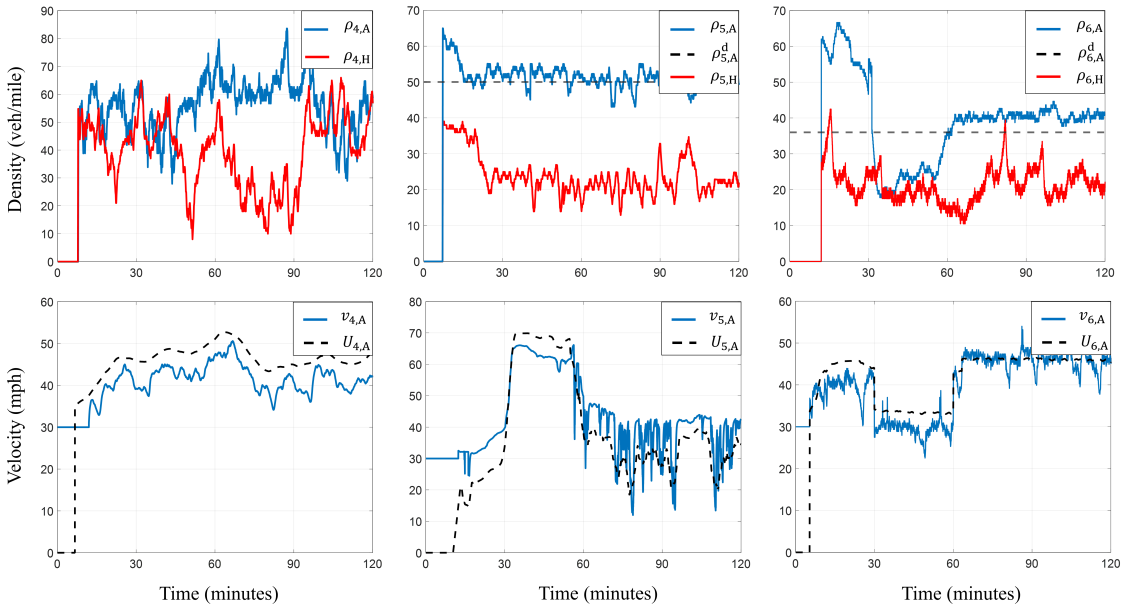

Figure 4.10: VISSIM Experimental Results. States (density and velocity) and suggested velocities for cells 5 and 6 are shown. The density (solid black line) and the desired density (dashed red line) for target cells (5 and 6) are shown in the first column. Velocity (solid black line) and suggested velocity (dashed red line) for cells 5 and 6 are shown in the second column.

In this experiment, the initial velocity was set equal to 30 mph for both AVs and HDVs, and the simulation was running for 12 minutes where the controller was inactive, and there was no data communication between VISSIM and MATLAB. After 12 minutes, the initial density of cells 3 and 4 was equal to 63 and $64 veh/mile$ for AVs and 40 and $30 veh/mile$ for HDVs, and the controller activated at the same time to control the speed of AVs in the traffic network. The desired densities for cells 3 and 4 were set equal to 50 and 38 $veh/mile$ respectively for AVs. By generating the proper suggested velocities for each cell and their upstream cell for AVs and sending it back to VISSIM, the control system reaches the desired densities after 30 minutes in cell 3 and 60 minutes in cell 4.

4.2 HIERARCHICAL CONTROLLER RESULTS

4.2.1 D-ES-FFL FOR HOMOGENEOUS TRAFFIC

In this section, we show the effectiveness of the proposed hierarchical controller, Distributed Extremum Seeking Filtered Feedback Linearization (D-ES-FFL) controller in a large-scale homogeneous traffic network.

4.2.1.1 CASE-STUDY 1:D-ES-FFL PERFORMANCE

In this section, we present a numerical example showing the D-ES-FFL controller's effectiveness in mitigating congestion and preventing back-propagating congestion using the METANET model. This case study compares two scenarios where there is no active infrastructure controller in the traffic network versus when there is an active local D-ES-FFL controller for target cells in the traffic network. As shown in Fig. 4.1, the target cells 2, 5, 6, and 9 are on the verge of getting heavily congested due to the traffic network inflow and unknown downstream bottleneck.

In Fig. 4.23, the states of the target cells 5 and 6 and the upstream cell 4 are shown for both "D-ES-FFL" and "No-Control" scenarios. As shown, in the No-Control scenario, the congestion starts back-propagating, and as the density increases, the congestion gets heavier, and the average velocity of each cell reduces. By activating the local "D-ES-FFL" controller, estimating the optimal densities of the cell, and finally tracking the optimal densities, the target cell avoids jam conditions. According to (3.9), the local objective function of each target cell is trying to maximize the average flow rate of the cell and minimize its flow difference with the upstream cell. In Fig. 4.12, the objective function values for cells 5 and 6 are shown in both scenarios. Furthermore, the total average flow of all cells upstream of the bottleneck ($Q_{\text{TOT}} = \sum_{i=1}^{6} Q_i$) is shown. Finally, in Fig. 4.13, a colormap of the velocity changes in the whole network for the full-time spectrum is shown in both "No-Control" and "D-ES-FFL" scenarios.

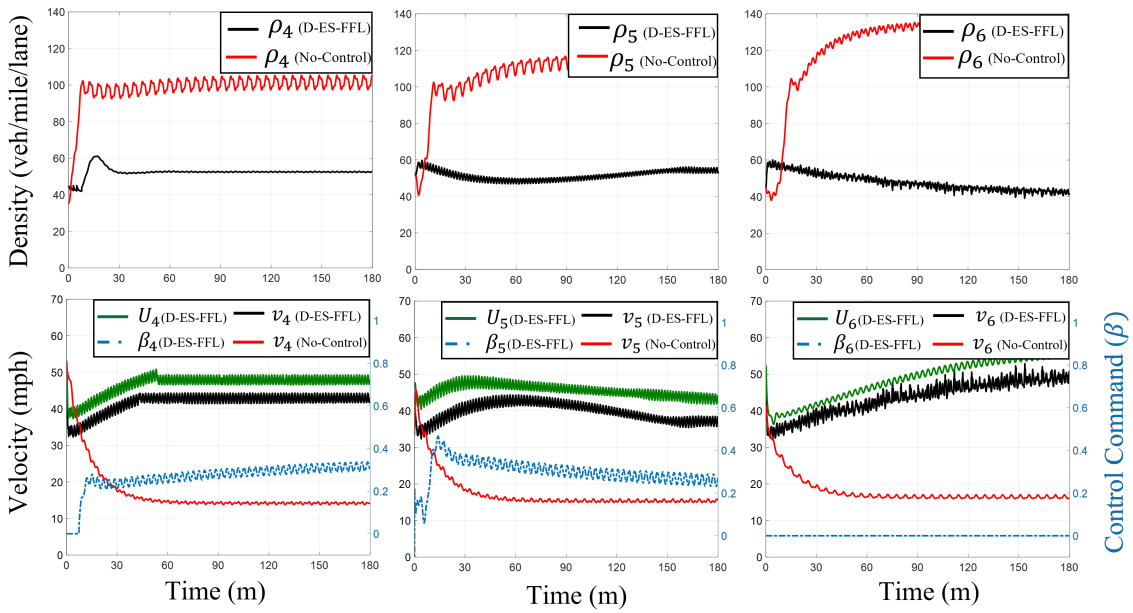

Figure 4.11: States, Suggested velocities (solid green line) and control commands (dashed-dotted blue line) for cells 4, 5, and 6 in both scenarios.

4.2.1.2 CASE-STUDY 2: D-ES-FFL WITH PTV-VISSIM

In the second case study, we use a real-world traffic simulator, PTV Vissim, to show the effectiveness of D-ES-FFL control in a real-world traffic simulation with real-world traffic data. For this study, after the completion of each cycle (duration = 10 minutes), the density of the target cells is recorded and passed to the MATLAB-

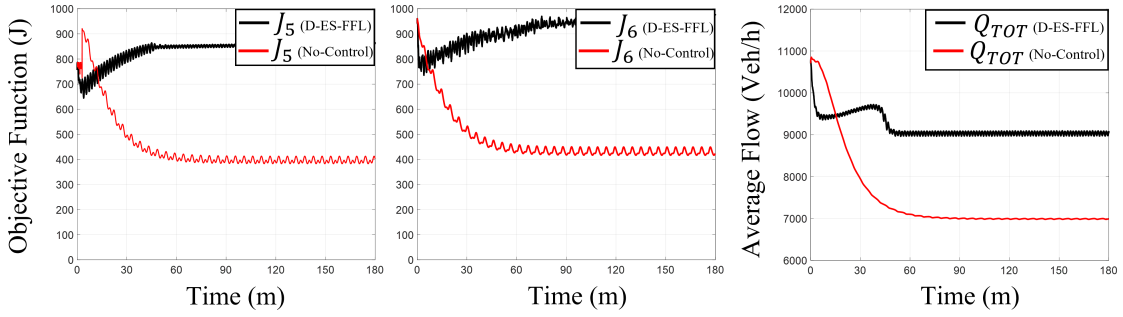

Figure 4.12: Objective functions of target cells 5 and 6 (sub-plot a) and the total average flow of all cells upstream of the bottleneck (sub-plot b).

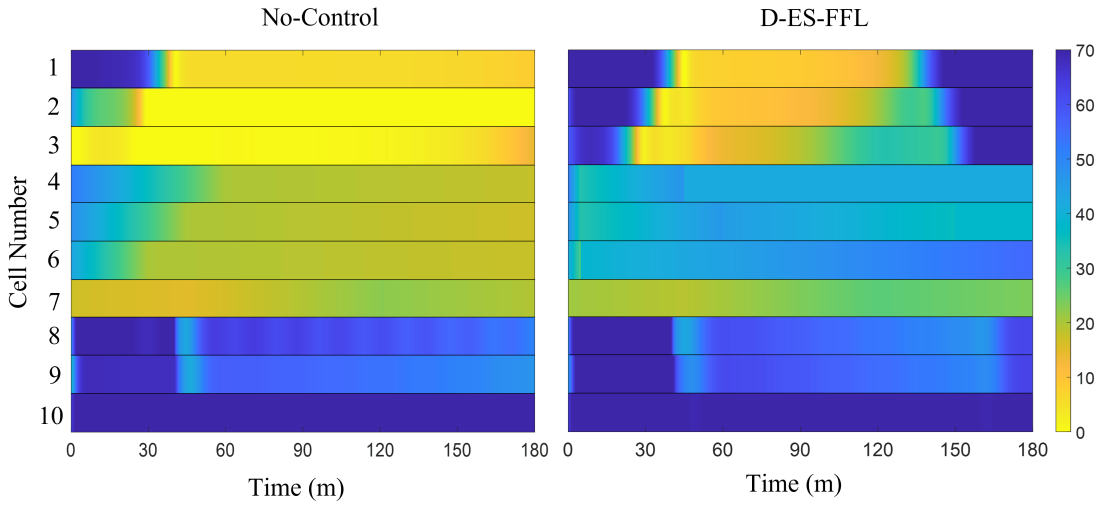

Figure 4.13: Visualization of the traffic velocity data for the whole network in "No-Control" and "D-ES-FFL" scenarios.

Simulink environment through the COM interface. Next, the local objective function of the congested cells is calculated and fed to the D-ES controller. Then, using the estimated optimal densities of D-ES in the Simulink, the suggested control commands are generated using the D-FFL controller. These commands are then passed to the MATLAB code and applied to the VISSIM through the COM interface to update the speed limit signs in the traffic network. We considered the same problem as case study 1. The highway link has ten cells with freeway link behavior type, and each cell is 1 mile in length. The inflow on the traffic network was set equal to 1980 veh/h with the stochastic volume type. The vehicle class of the vehicles in the traffic network was chosen to be "Car" with the driving behavior of "Freeway". To have a distributed traffic control network, we put the variable speed limit signs every 0.2 mile, so all vehicles in each cell get the suggested velocities information from the controller almost simultaneously. Also, in the first 12 minutes of the simulation, there is no active controller and effective communication between MATLAB and PTV VISSIM, so the desired initial conditions are reached. As shown in Fig. 4.14, by activating the "D-ES-FFL" controller, the average velocity in target cells is greater than the

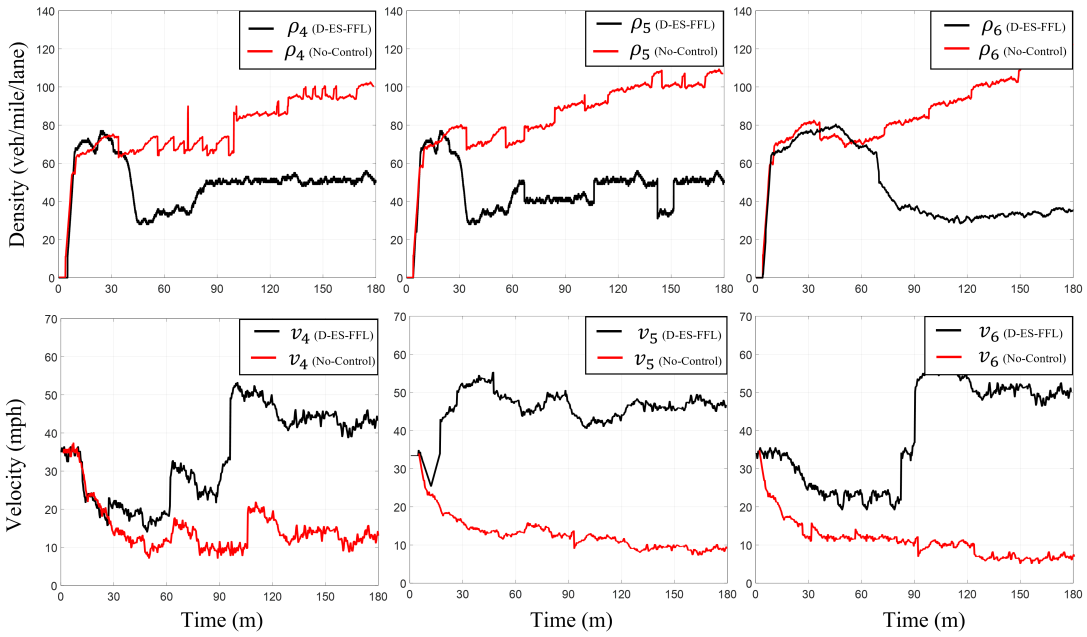

Figure 4.14: States (density and velocity) cells 4, 5 and, 6 are shown using PTV-VISSIM in both scenarios.

"No-Control" scenario while its density is less congested.

4.2.2 D-ES-FFL FOR HETEROGENEOUS TRAFFIC

4.2.2.1 CASE STUDY 1: EVALUATING THE EFFECTIVENESS OF D-ES-FFL

In this study, two traffic network scenarios are compared, where the first scenario assumes no active infrastructure controller, and the second scenario involves an active D-ES-FFL controller in the network. Cells 2, 5, 6, and 9, are in the congested phase in the traffic network during peak hours and are shown in Fig. 4.1. The high traffic inflow and an unknown downstream bottleneck contribute to this congestion. The V2I communication rate for AVs is set to 1 second, and the dynamic speed limit signs are updated every 30 seconds for HDVs.

The densities of AVs and HDVs in target cells 5 and 6 are presented in Fig. 4.15 for both the D-ES-FFL and No-Control scenarios. In the absence of control, congestion is observed to back-propagate, leading to more severe congestion and a higher likelihood of reaching jam density. In contrast, the implementation of the local D-ES-FFL

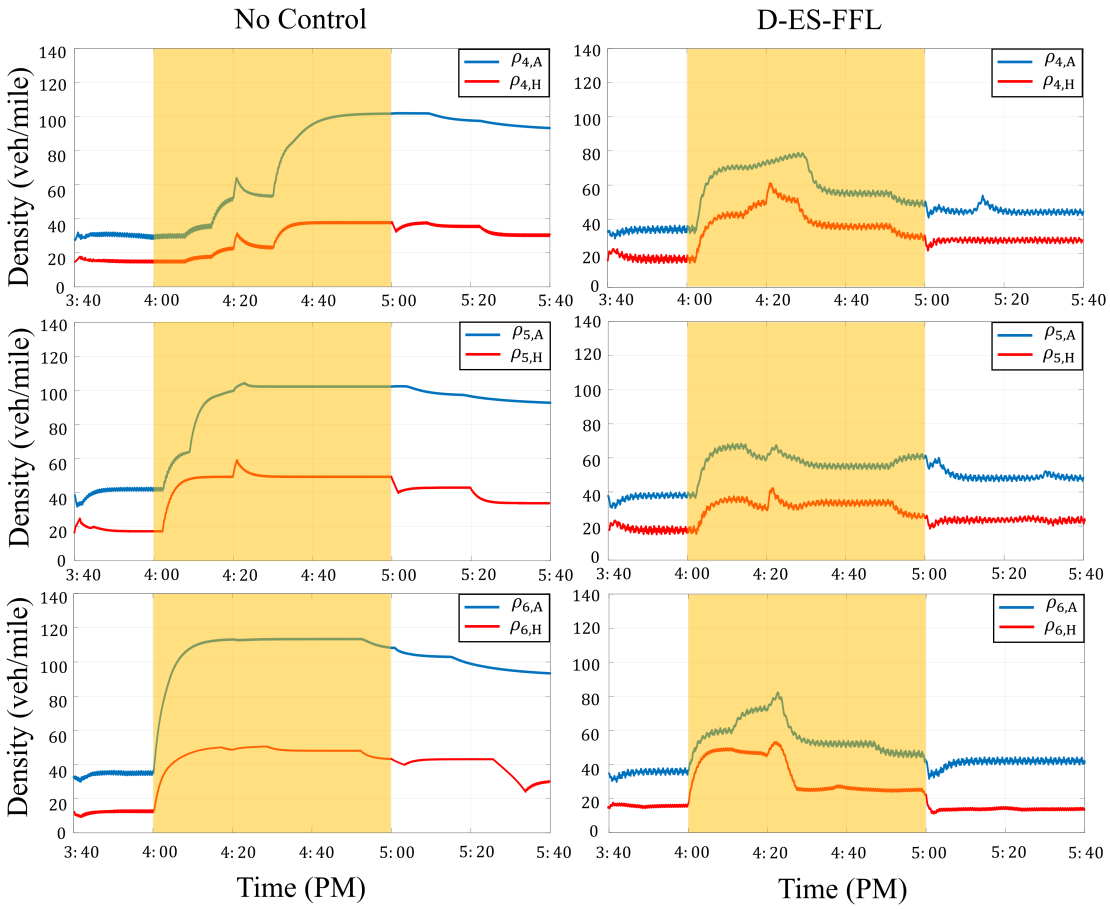

Figure 4.15: The densities of AVs and HDVs in target cells 5 and 6, as well as the upstream cell 4 are shown, under both the No-Control and D-ES-FFL scenarios. The solid blue line represents the density of AVs, while the solid red line represents the density of HDVs.

controller facilitates the estimation of optimal densities and enables tracking of both AVs and HDVs densities. As a result, target cells can avoid jam conditions, emphasizing the significance of utilizing the proposed D-ES-FFL control framework to manage traffic flow in congested networks. These results demonstrate the performance of the proposed multi-level control framework in improving traffic management and alleviating congestion in large-scale traffic networks. The optimization of the average flow rate of each target cell is achieved through a locally designed objective function, which minimizes the flow difference between the cell and its upstream cell, as expressed in (3.9). In Fig. 4.16, the values of the objective function for cells 5 and 6 are depicted

for both the No-Control and D-ES-FFL scenarios, along with the total average flow of the heterogeneous network.

Fig. 4.17 displays the density changes of AVs across the entire traffic network through a colormap representation for the full-time spectrum under both the No-Control and D-ES-FFL scenarios.

4.2.2.2 CASE STUDY 4: TESTING D-ES-FFL WITH PTV-VISSM

This study aimed to assess the efficiency of the proposed D-ES-FFL control framework in a real-world simulation using PTV-VISSIM. Fig. 4.24 provides a flowchart of the entire process for developing a direct MATLAB-VISSIM interface to implement the D-ES-FFL controller online. The process starts with setting up the traffic network and corresponding settings in VISSIM GUI, followed by saving the network and settings in the VISSIM project (INP) and initialization file (INI), respectively. The

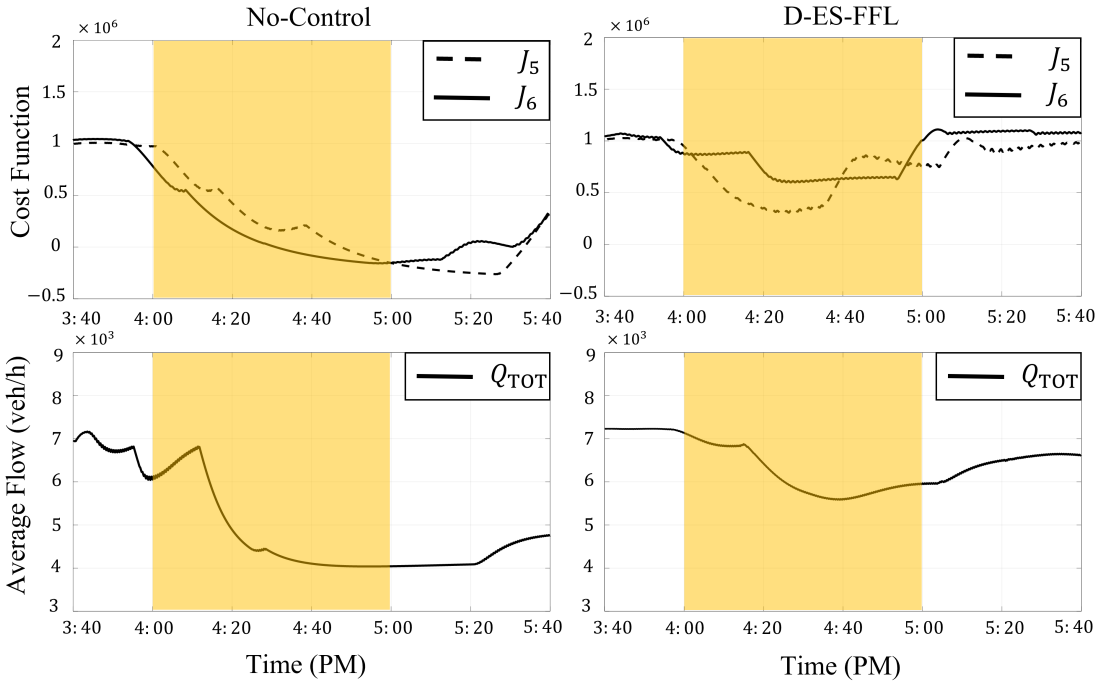

Figure 4.16: The values of the objective function (J) for the target cells 5 and 6 and the total average flow (Q_{TOT}) of the traffic network are presented in both scenarios of No-Control and D-ES-FFL.

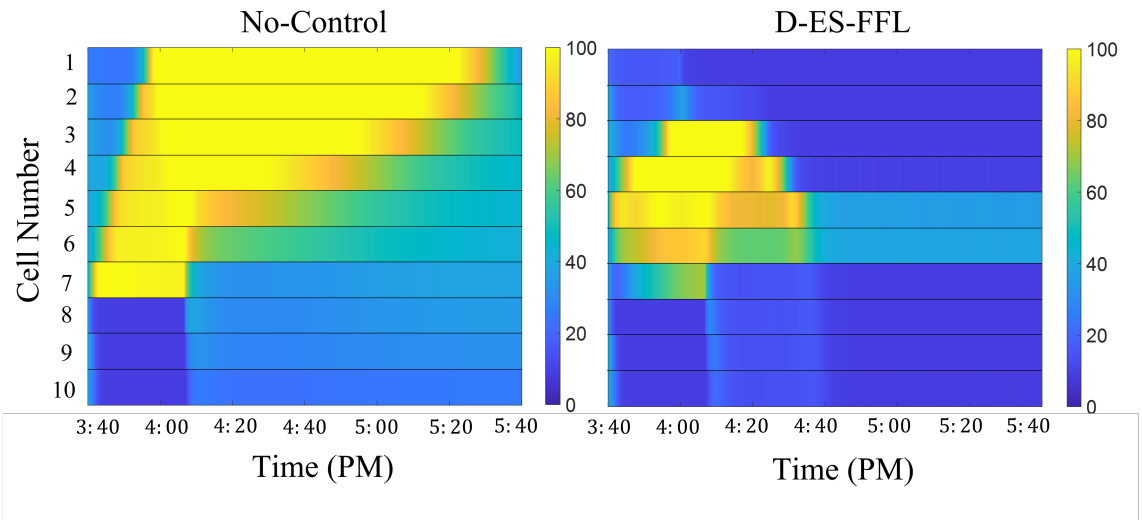

Figure 4.17: Visualization of the traffic density data for AVs across the entire network, under both the scenarios of having no control and using the D-ES-FFL controller.

MATLAB environment then controls the traffic network in the VISSIM microscopic simulator. To establish a direct MATLAB-VISSIM interface, two MATLAB codes are developed. The first code, a MATLAB script, controls the VISSIM simulator by sending commands from MATLAB and receiving traffic information from VISSIM. Specifically, this code activates the VISSIM server to create the COM object, takes INP and INI files as input, and accesses "network" and "simulation" through the COM object. The second code, a Simulink file, consists of the cost function model of the traffic network, the D-ES to estimate the desired densities of AVs and HDVs, and the D-FFL control to generate the control inputs.

In order to implement the D-ES-FFL controller, the study employs a single-step microscopic simulation with a step size of 10 minutes to adjust the state of signal controllers in real-time. At the end of each 10-minute cycle, the density of each cell is saved and transmitted to the MATLAB-Simulink environment using the COM interface. The saved densities are then used to update the cost function value in the Simulink file, which is used to generate the desired densities of AVs and HDVs through the D-ES controller. After generating desired densities of AVs and HDVs through the

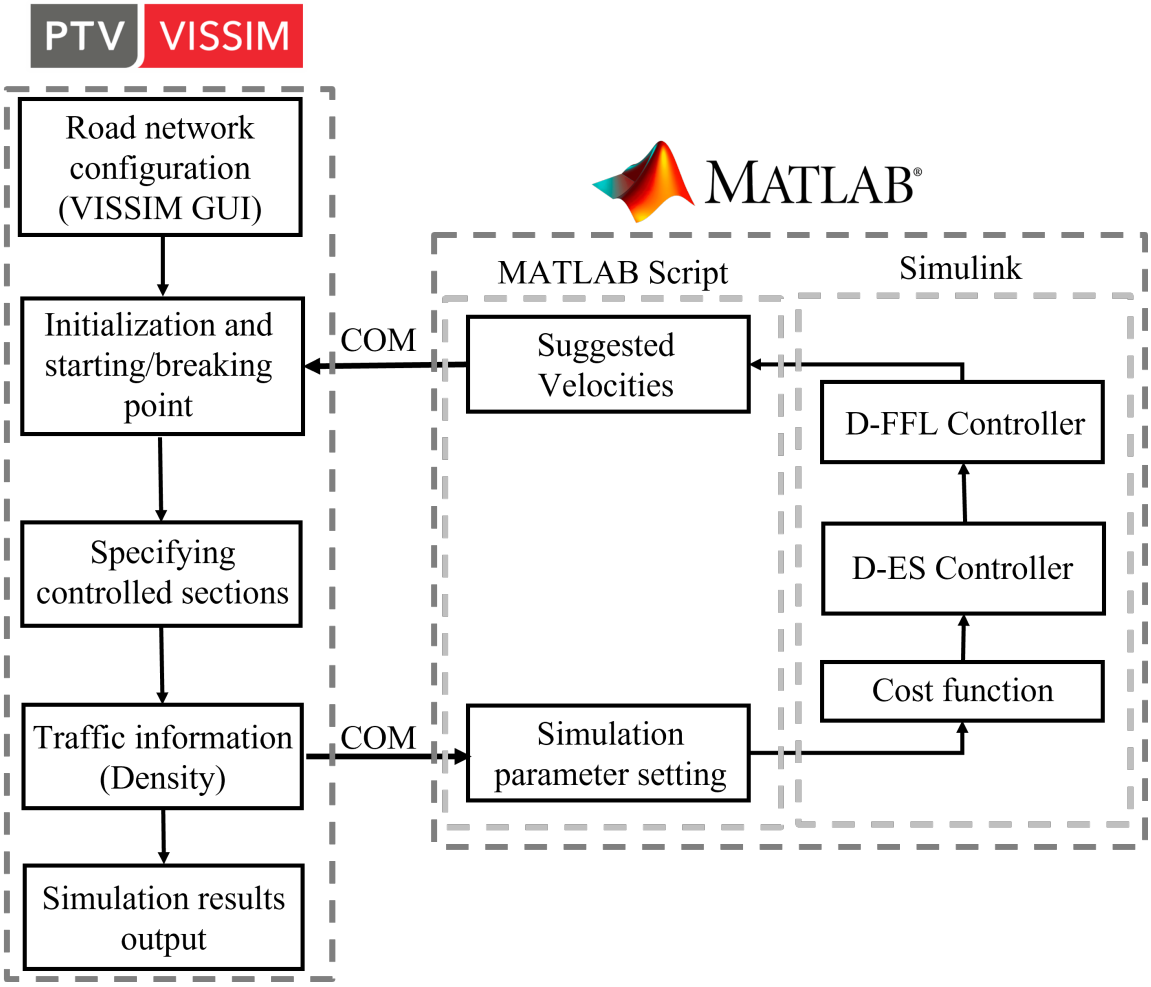

Figure 4.18: The structure of the simulation platform using MATLAB and VISSIM.

D-ES controller using the updated cost function value, the D-FFL controller generates control inputs based on these desired densities. These control inputs are then fed into the first code to calculate suggested velocities, which are subsequently applied to the VISSIM simulation. This process is repeated until the end of the simulation time, which is set to 120 minutes (12 cycles) for this particular study.

In this study, the same case as in case study 3 is considered, where the highway link consisted of ten cells with a freeway link behavior type and a length of 1 mile. The traffic network has an inflow of 3000 vehicles per hour with a stochastic volume type and a vehicle composition of 0.6 for AVs and 0.4 for HDVs. Flow and velocity information is collected at the end of each cell. Both HDVs and AVs are classified as

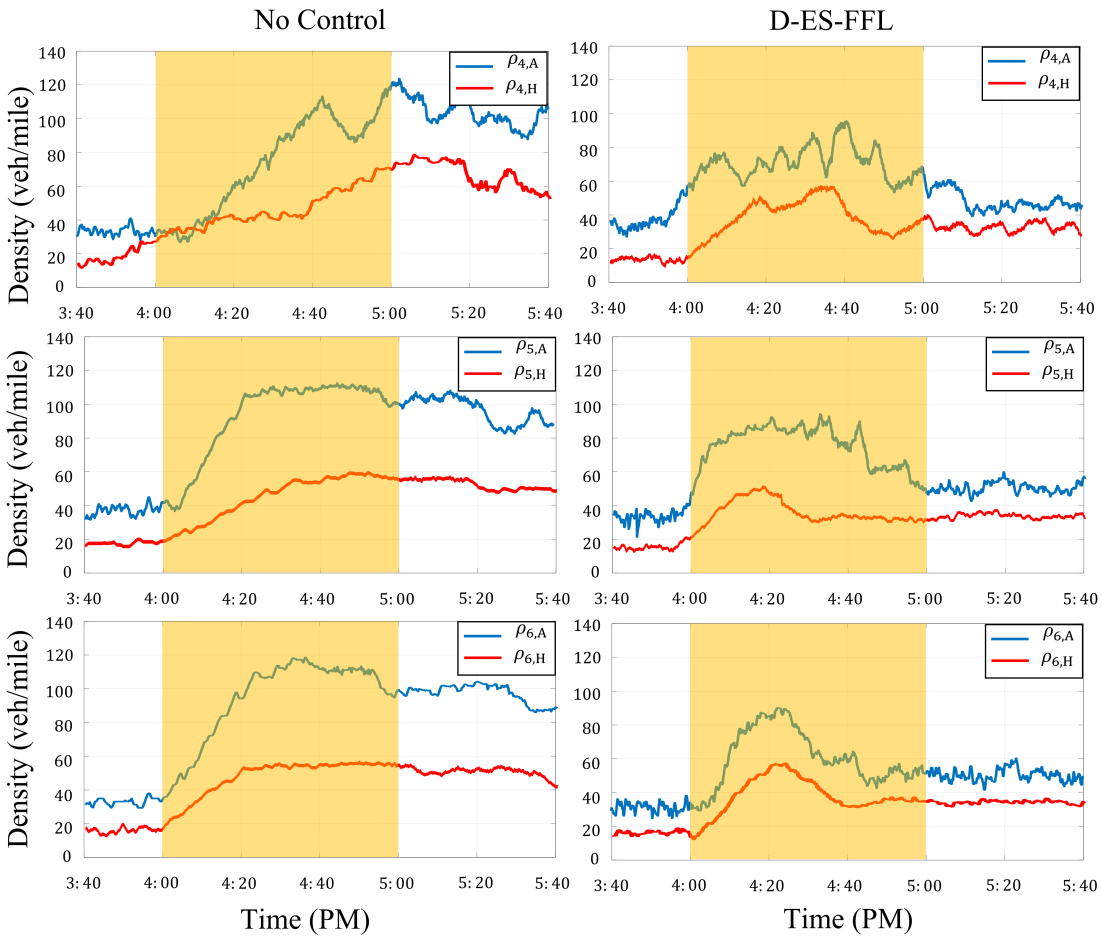

Figure 4.19: VISSIM Experimental Results. Densities of AVs and HDVs are shown for No-Control and D-ES-FFL scenarios.

"Car," with "Freeway" driving behavior for HDVs and "AV normal (CoEXist)" for AVs. Variable speed limit signs are placed every 0.1 miles for AVs and every 0.3 miles for HDVs to create a distributed traffic control network, allowing AVs to communicate at a faster rate compared to HDVs, as discussed in case study 3. The experimental results for the ten-cell heterogeneous traffic network are presented in Fig. 4.25.

4.2.3 D-LSNES-FFL FOR HETEROGENEOUS TRAFFIC

4.2.3.1 CASE STUDY 1: LSNES-FFL PERFORMANCE REVIEW

In this section, we begin our analysis by comparing the performance of the newly designed LSNES-FFL control system with the existing ES-FFL control system. This

comparison aims to demonstrate the enhanced capabilities of the improved upper-level controller in effectively managing large-scale traffic scenarios.

To start, we use a quadratic map, as denoted in (3.9), to contrast the gradient-based and Newton-based ES methods. It is important to note that we maintain uniformity in all parameters, with the sole exception of the gain matrix, to ensure a fair and unbiased comparison.

For the Newton-based approach, the convergence rate is influenced by the expression $-K_{\mathrm{N}}\Gamma(t)\mathcal{H}$. Notably, this rate can vary for different vehicle types within the traffic network. Conversely, the gradient-based scheme relies on the eigenvalues of $K_{\mathrm{G}}\mathcal{H}$. To maintain parity, we select K_{G} to be equivalent to $-K_{\mathrm{N}}\Gamma_0$.

Fig. 4.20 presents the density of AVs within target cell 5 while under the influence of three distinct active controllers in the traffic network. To ensure a just comparison among these methods, we initialize each scenario with identical initial conditions and model parameter values. Additionally, we uphold the equality of K_{G} and $-K_{\mathrm{N}}\Gamma_0$.

As observed in the results, the Newton ES method demonstrates a notably accelerated convergence towards the desired density when compared to the gradient-based ES approach, showcasing a significant 42% improvement. Furthermore, the incorporation of the Lyapunov-based switch contributes to a reduction in perturbation size once the system enters the vicinity of the desired density. This enhancement in control strategies ultimately leads to more effective traffic management and increased system robustness.

To further compare the designed control methods, we conducted a comprehensive traffic scenario analysis. This involved three scenarios: one with no traffic controller (akin to the section of I-485 as our benchmark case study), one with an active ES-FFL controller, and one with an active LSNES-FFL controller within the traffic network.

In Fig. 4.21, we depict the density changes of AVs and HDVs in target cells 5 and 6, as well as the upstream cell 4. This allows us to discern the performance

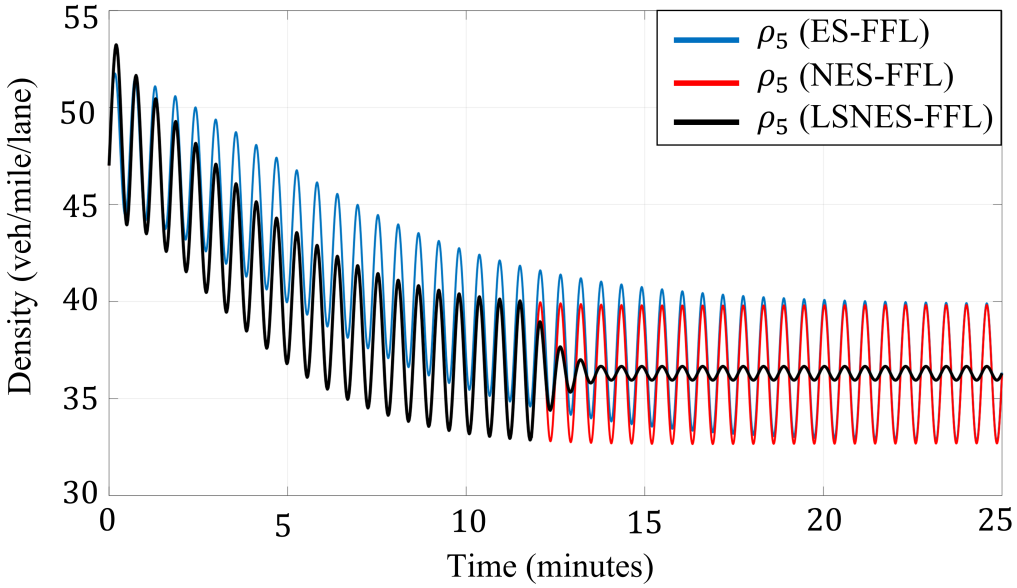

Figure 4.20: Target cell 5 AV density changes using ES-FFL (Blue), NES-FFL (Red), and LSNES (Black). The Newton-based ES has 42% faster convergence rate in comparison to gradient-based ES.

differences among these scenarios. Remarkably, the LSNES-FFL control approach outperforms the others by exhibiting a superior convergence rate in achieving the desired density for both AVs and HDVs in each cell. This outcome not only reduces overall congestion but also effectively prevents congestion from propagating backward, thereby enhancing traffic management significantly.

Following that, we proceed to validate the efficacy of the LSNES-FFL controller in alleviating congestion and hindering the back-propagation of congestion through another numerical demonstration. This case study entails a comparative analysis of three scenarios: the initial scenario, where no active infrastructure controller operates within the traffic network; the second scenario, deploying a localized hierarchical mainstream traffic flow controller for cells with unknown downstream bottlenecks; and the third scenario, implementing the local LSNES-FFL controller, as illustrated in Fig. 3.5, for designated cells within the traffic network. Specifically, cells 2, 5, 6, and 9 are singled out as susceptible to severe congestion owing to an unknown

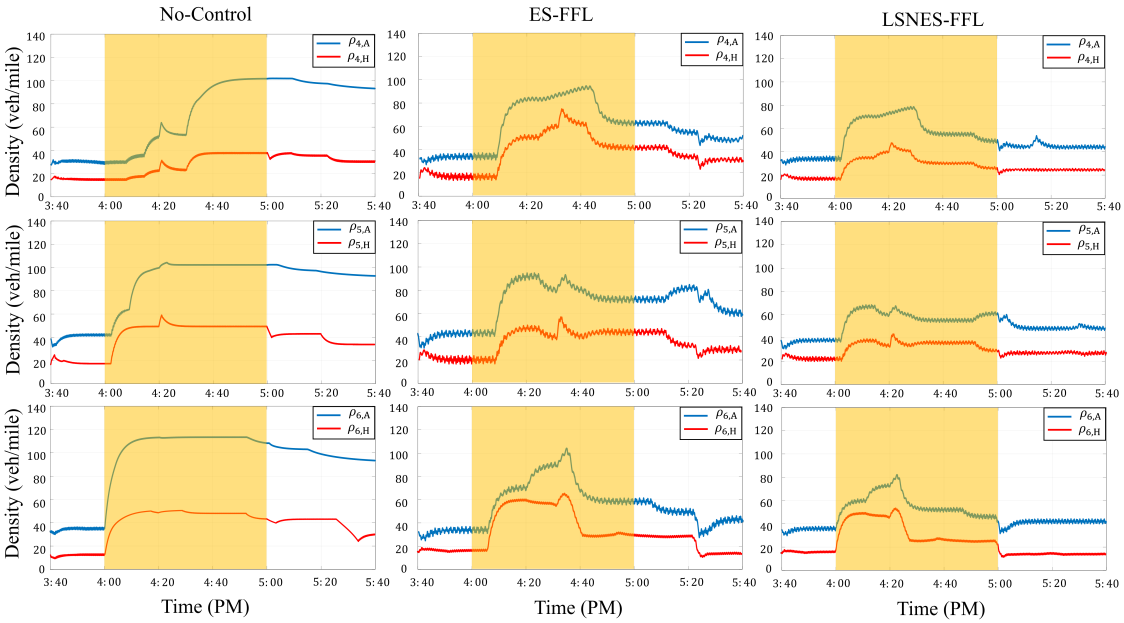

Figure 4.21: The densities of AVs and HDVs in target cells 5 and 6, as well as the upstream cell 4 are shown, in No-Control, ES-FFL, and LSNES-FFL scenarios. The solid blue line represents the density of AVs, while the solid red line represents the density of HDVs.

downstream bottleneck.

Among the array of local control strategies, the most prevalent methodologies involve hierarchical feedback traffic flow controllers. These strategies are predominantly founded on the formulation of desired traffic conditions and the execution of control measures aimed at maintaining the prevailing traffic state in proximity to predefined set-point values. Managing traffic in expansive networks frequently involves the utilization of a PID feedback controller for Mainstream Traffic Flow Control (MTFC) [86]. At a lower level, the control measures are calculated with feedback control laws that explicitly account for the presence of multiple vehicle classes and seek to concurrently alleviate congestion and prevent congestion back-propagation. These encompass Extended Multi-Class MTFC (EMC-MTFC) controllers, as depicted in Fig. 4.22, wherein control measures are explicitly depicted for each vehicle class, and the control methodology draws not only from downstream measurements of the

controlled cell but also from a broader range of system state measurements. These measurements are acquired within a defined region (termed a cluster) whose size varies dynamically, influenced by the upper level of the control scheme.

The PID gains are calculated to give us the best closed-loop command following for the problem. The calculated gains are Kp=13.2, Ki=0.78, and Kd=0.1.

In Fig. 4.23, we present the density profiles of cells 5 and 6, as well as the upstream cell 4, across three distinct scenarios: "LSNES-FFL," "EMC-MTFC," and "No-Control." It becomes evident that, in the absence of control, congestion initiates a retrogressive spread, exacerbating congestion levels as density escalates. However, with the activation of localized controllers, namely the "LSNES-FFL" and "EMC-MTFC" controllers, designed to estimate and maintain optimal densities, the target cells effectively evade congestion-related bottlenecks.

Upon a comparative assessment of the outcomes achieved by the LSNES-FFL controller and the EMC-MTFC controller, a notable distinction emerges in terms of settling time. Specifically, the LSNES-FFL controller demonstrates the ability to regulate the velocity of autonomous vehicles (AVs) within cell 5, and its upstream counterpart, achieving the desired density within a mere 85 seconds. In stark contrast, the EMC-MTFC controller necessitates a comparatively protracted 188 sec-

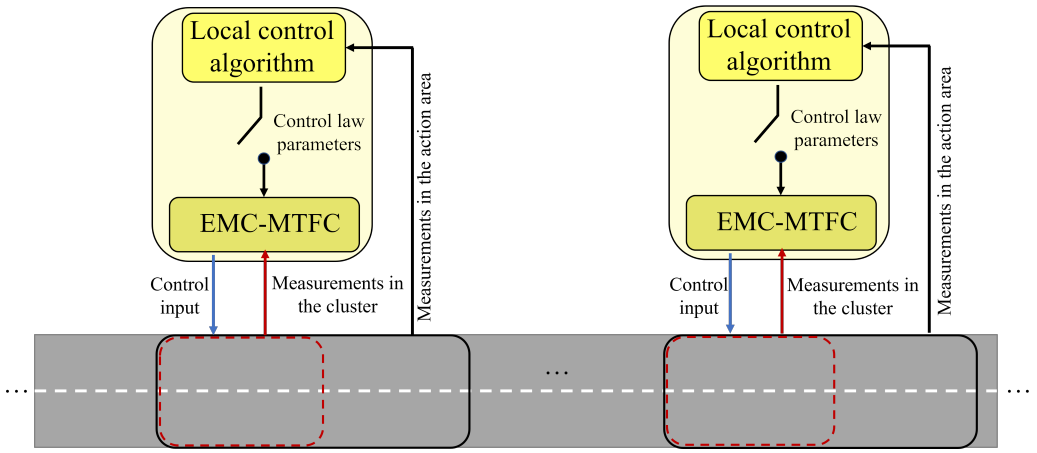

Figure 4.22: Distributed EMC-MTFC scheme

onds to reach the intended set-point. Furthermore, the designed controller exhibits enhanced efficiency in regulating the density of human-driven vehicles (HDVs), attaining the desired density in a mere 80 seconds, while the EMC-MTFC controller requires 115 seconds.

These findings underscore the superior effectiveness of the LSNES-FFL controller in managing the speed and density of both AVs and HDVs, holding substantial promise for optimizing traffic flow in densely congested networks. This superior performance can be attributed to the hierarchical framework's capacity to optimize control actions by exploiting the system's inherent dynamics. By harnessing the time constant of lower-level dynamics, the higher-level controller adeptly adjusts its perturbation frequency, resulting in a more precise and efficient system regulation when compared to the EMC-MTFC controller.

4.2.3.2 CASE STUDY 2: TESTING LSNES-FFL WITH PTV-VISSM

The primary objective of this case study is to assess the effectiveness of the proposed LSNES-FFL control framework through a real-world simulation conducted using PTV-VISSIM. As illustrated in Fig. 4.24, this study encompasses a comprehensive process for establishing a direct interface between MATLAB and VISSIM, facilitating the online implementation of the LSNES-FFL controller.

To implement the LSNES-FFL controller, a single-step microscopic simulation is employed in this study, with a time step of 10 minutes, enabling real-time adjustment of signal controllers. At the conclusion of each 10-minute cycle, the density of each cell is recorded and transmitted to the MATLAB-Simulink environment via the COM interface. These recorded densities are then utilized to update the cost function value within the Simulink file, which, in turn, determines the desired densities of both AVs and HDVs through the LSNES controller. Subsequent to generating the desired densities using the updated cost function value, the FFL controller generates control inputs based on these desired densities. These control inputs are subsequently fed into

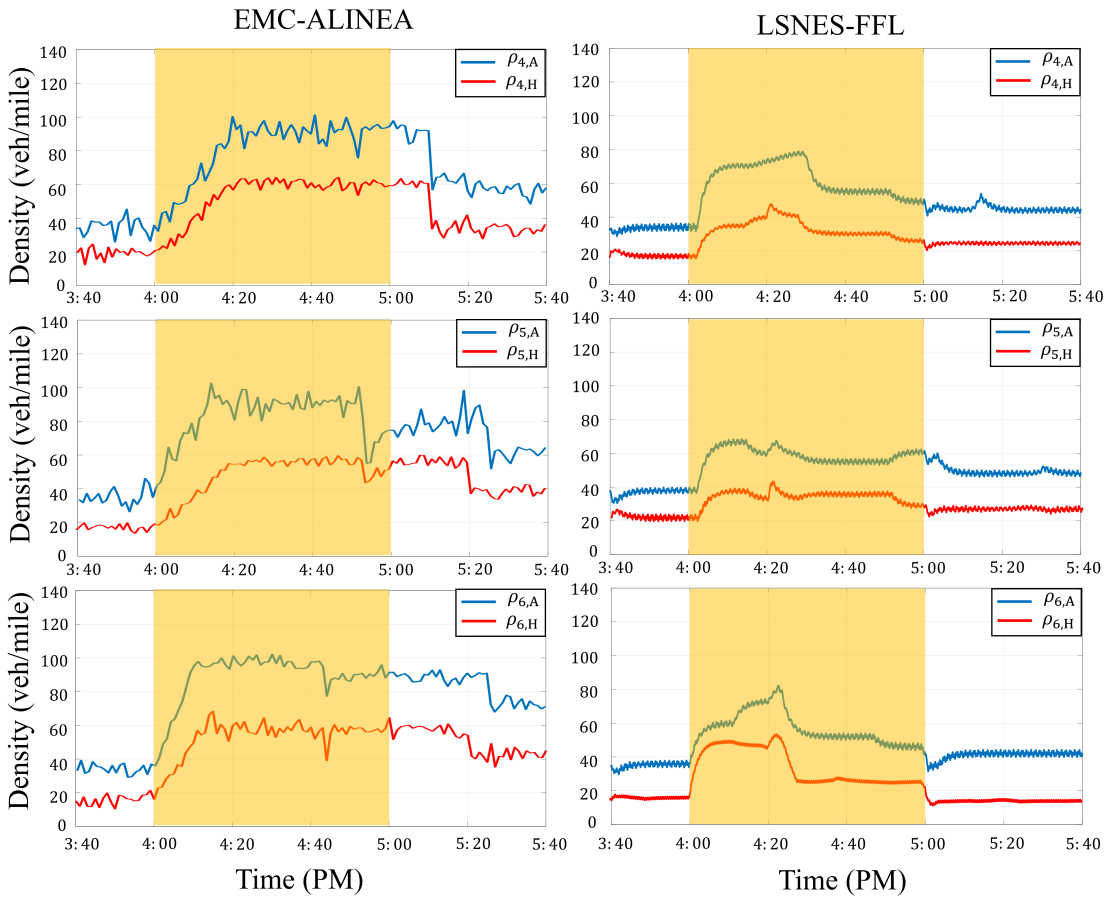

Figure 4.23: Density changes of target cells 5 and 6 and their upstream cell 4 in two cases; Active EMC-ALINEA control and Active LSNES-FFL control.)

the initial code, enabling the calculation of suggested velocities, which are then applied to the VISSIM simulation. This iterative process continues until the conclusion of the simulation period, which, in the context of this particular study, is set to 120 minutes (equivalent to 12 cycles).

In this research, we investigate the same scenario as described in case study 3, where the highway link comprises ten cells with a freeway link behavior type, each spanning a length of 1 mile. The traffic network experiences an inflow of 3000 vehicles per hour, characterized by a stochastic volume type, with a vehicle composition of 0.6 for AVs and 0.4 for HDVs. Measurements are taken at the end of each cell to gather data on traffic flow and velocity. Both HDVs and AVs are classified as "Car" and exhibit

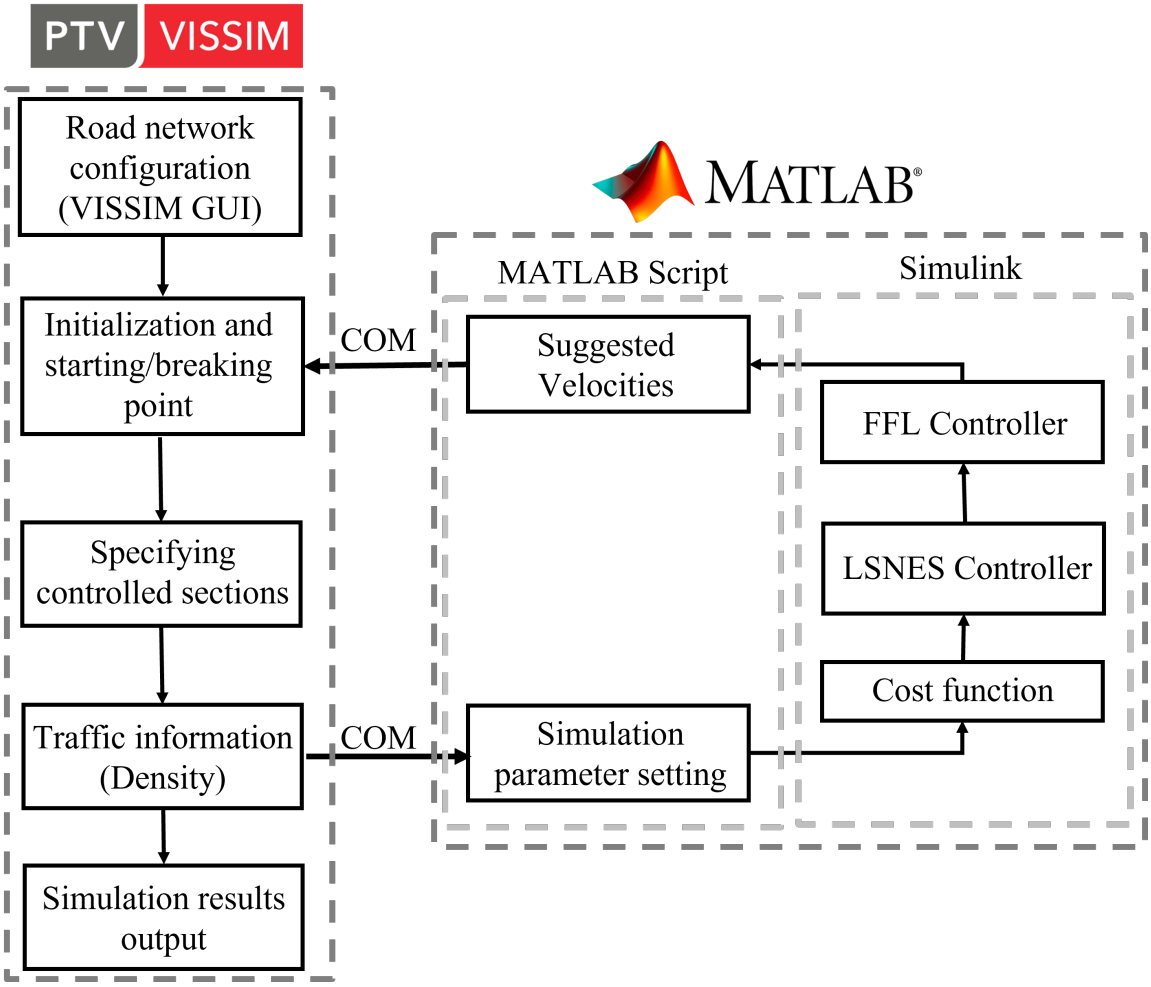

Figure 4.24: The structure of the simulation platform using MATLAB and VISSIM.

specific driving behaviors: HDVs adhere to the "Freeway" driving behavior, while AVs follow the "AV normal (CoEXist)" behavior. To establish a distributed traffic control network, variable speed limit signs are strategically placed every 0.1 mile for AVs and every 0.3 mile for HDVs. This configuration enables AVs to communicate faster than HDVs, as discussed in case study 3. The experimental findings concerning this heterogeneous traffic network, consisting of ten cells, are graphically presented in Figure 4.25.

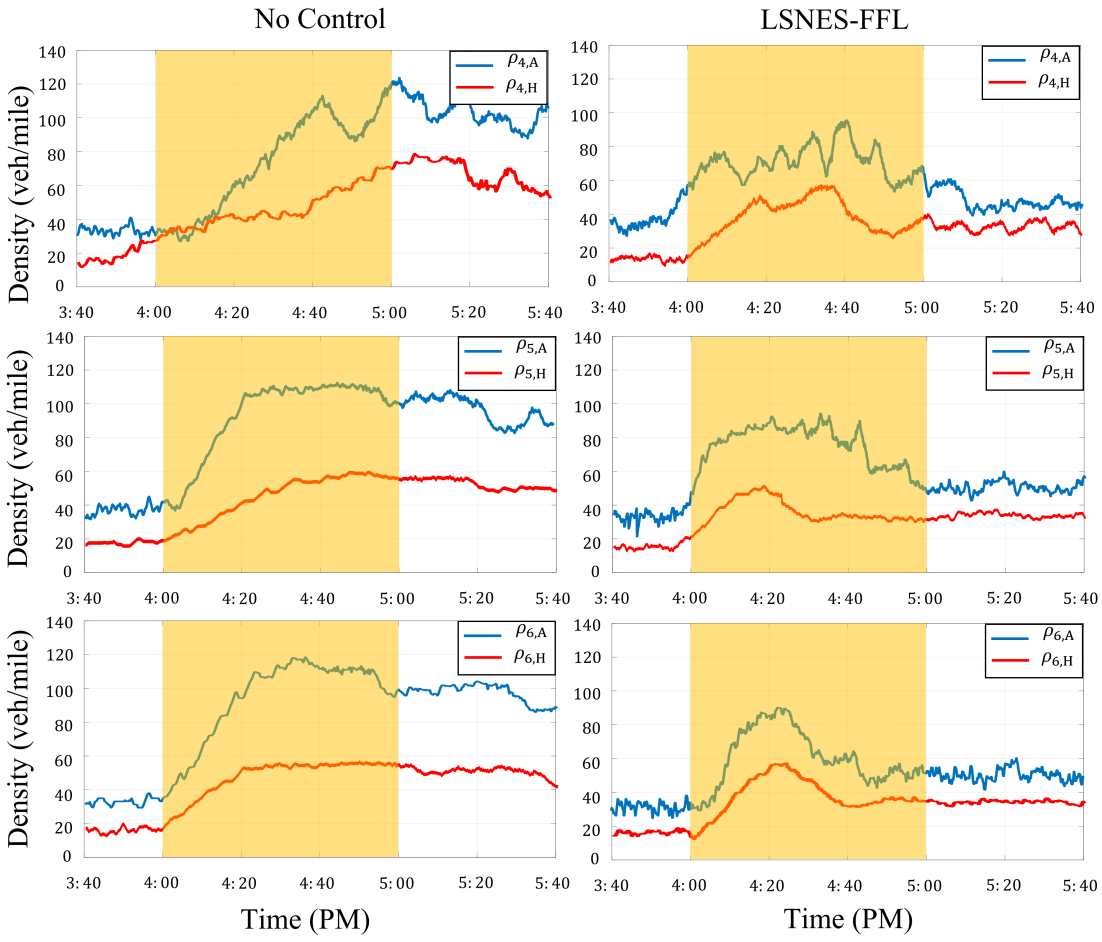

Figure 4.25: PTV-VISSIM Experimental Results. Densities of AVs and HDVs are shown for No-Control and LSNES-FFL scenarios.

CHAPTER 5: CONCLUSION AND FUTURE WORK

This dissertation focuses on modeling and controlling large-scale homogeneous and heterogeneous traffic networks. In this research, we defined heterogeneity as a multi-vehicle traffic network consisting of Human-Driven Vehicles (HDVs) and Autonomous Vehicles (AVs), distinguished by their operational characteristics and controllability. We used the homogeneous (single-class) and heterogeneous (multi-class) METANET models to describe the macroscopic behavior of the traffic within each cell. The METANET model is a second-order model in which the dynamic equations for both density and velocity changes in each cell in the traffic network are modeled. The density term is derived from the conservation of vehicles in a traffic network and the velocity term has three main terms; the relaxation term, convection term, and density gradient term. The relaxation term functions as a high-gain filter in the context of dynamic systems and it sets the time delay that drivers take to reach the desired speed. The convection term represents the impact of traffic from the upstream cell on the downstream cell, indicating the speed changes resulting from incoming and outgoing vehicle speeds. The density gradient term signifies that as the downstream density rises or falls, the speed in the current cell will correspondingly decrease or increase. There are several model parameters in the METANET model that are calibrated using the field data, however, in this research we considered all the model parameters to be state-and-class-dependent. Calibrating the model parameters based on each vehicle class and their states, helped us to have a higher fidelity traffic model with no extensive constraints on the inter-flow of vehicles. Furthermore, the velocity change dynamic equation in the METANET model contains the suggested velocity term which essentially serves as the parameter for speed control. In this research,

the suggested velocity term contains two terms; the control input which is set by the designed infrastructure-based controller, and the second term which is the steady-state macroscopic flow-density relationship based on the fundamental diagram. In order to set the suggested velocity for vehicles in each cell, we designed a hierarchical infrastructure-based controller to mitigate the traffic network's congestion despite the unknown disturbances in the system due to the i) complexity of mixed traffic networks, ii) slower V2I communication rates with HDVs, and iii) state- and class-dependent model parameters. At the lower level, the Distributed Filtered Feedback Linearization (D-FFL) is designed and implemented. The purpose of this controller is to track the desired density of each cell in time which is set by the upper level controller. D-FFL tracks the reference density by controlling the suggested velocity of vehicles in the target cell and its upstream cell. The implementation of the D-FFL control is dependent on the relative degree and dynamic inversion matrix. In this research, the relative degree between the control inputs to the output is two for each cell and its upstream cell. Moreover, the design of the D-FFL control approach is based on two underlying assumptions; i) The disturbance function is a continuous function and its derivative is accessible. ii) The input of the reference model (desired density of vehicles that are calculated by the upper-level controller) and their derivatives are assumed to be bounded. The controller inputs derived by the feedback linearization (ideal control inputs) and the control inputs generated by the FFL are mathematically equivalent. However, the feedback linearization method requires full knowledge of the plant model and measurement of the disturbance of the system. Instead, the D-FFL input control design relies on various factors, including the knowledge of the dynamic inversion matrix, the relative degree, and the parameters of the reference model. By considering these factors, the D-FFL control system can be optimized and implemented effectively in large-scale traffic networks with complex underlying dynamics that are challenging to get the full information of the model and measure

the disturbance of the system. At the upper-level, we designed multiple controllers to improve the overall performance of the hierarchical control. In our initial design, the Distributed Extremum-Seeking (D-ES) controller aims to find the optimal operating densities of each vehicle class in the target cells over time. D-ES is a real-time control method that seeks to optimize the steady-state dynamic of a system whose characteristics are not fully known. The gradient-based D-ES comprises three essential components: the dither signals, the gradient estimator, and the optimizer operating at progressively slower time scales. The primary objective of the upper-level controller in our research is to achieve two main goals simultaneously: the maximization of the average flow of the target cell to mitigate traffic congestion and the minimization of the flow difference between the target cell and the upstream flow to prevent the propagation of congestion in the backward direction. The desired densities are then fed into the lower-level controller as the reference model. The results obtained from our initial controller design revealed two significant insights: (i) the ES algorithm, which relies on gradient-based optimization, exhibits local convergence, and (ii) the speed of convergence is impacted by the second derivative (Hessian matrix) of the map which is unknown. To improve the performance of the designed hierarchical controller and reduce the convergence time, we designed and implemented Newton Extremum Seeking (NES) at the upper level of the hierarchy to feed the optimal density of target cells to the lower-level controller. One of the key distinctions between the Newton algorithm and the gradient algorithm is that the convergence of the former is not solely contingent on the second derivative (Hessian) of the cost map and it is user-assignable. In fact, this allows for the deliberate synchronization of all parameters to converge at a uniform pace, resulting in straightforward paths leading to the optimal point in a shorter time. The major improvement over the gradient-based D-ES implementation is that an additional loop is attached to the D-NES to obtain the estimate of the unknown Hessian matrix. However, the other obstacle

is that the inverse of the Hessian matrix is also required in the Newton algorithm. Since the Hessian matrix estimate, may not necessarily remain invertible, a dynamic system is also designed to asymptotically generate the inverse. This dynamic system takes the form of a Riccati differential equation filter. Finally, the existing ES methods including NES, often converge to a limited cycle around the desired state instead of achieving precise convergence. Thus, a significant challenge in utilizing the NES is eliminating the limit cycle behavior and achieving asymptotic convergence to the optimal set-point. To address the potential loss in optimality that may arise due to continuous sinusoidal perturbations around the optimal point, we proposed a switched control scheme to be added to the NES structure. The proposed switched control scheme involves reducing the amplitude of perturbations after convergence, specifically within a neighborhood around the desired state. The switch is determined by utilizing a Lyapunov function that is based on an averaged model of the NES feedback system. This Lyapunov function is designed to approximate the proximity to the desired state, and based on this estimate, the switch is activated to reduce the perturbation size. The simulation results showed that the Lyupanov-based Switch Newton Extremum Seeking-FFL (LSNES-FFL) control framework has a %42 faster convergence rate with respect to the conventional ES-FFL method. Finally, to show the effectiveness of the proposed methods, we tested and validated the effectiveness of the designed controllers in homogeneous and heterogeneous traffic networks in various test cases using MATLAB-SIMULINK and MATLAB-VISSIM with COM interface. First, we evaluated the efficiency of the lower-level controller (D-FFL) separately by quantifying its performance and comparing it with another common model-free traffic control method, the MTFC-PID control approach. We showed that our proposed controller design (D-FFL) has an overall faster convergence rate with respect to the MTFC-PID method. Furthermore, we evaluated the practical implementation of the D-FFL controller and the impact of discretization on the transportation infrastruc-

ture. We showed that by increasing the flow of AVs in heterogeneous traffic networks and minimizing the V2I communication rate for both AVs and HDVs, we can reach the maximum average flow of the traffic network. Finally, we used a real-world traffic simulator, PTV-VISSIM to show the effectiveness of the D-FFL controller. VISSIM serves as a widely employed microscopic traffic simulator, offering a graphical user interface for simulating both simple static controls (pre-timed or fixed-time) and the flexibility for dynamic simulation control through versatile programming languages. We showed that D-FFL generated the proper suggested velocities for the AVs in target cells and by sending it back to PTV-VISSIM, the traffic control system reached the desired densities. Moreover, we presented various test cases in order to show the effectiveness of the designed hierarchical controller for large-scale homogeneous and heterogeneous traffic networks. The performance of D-ES-FFL, D-NES-FFL, and D-LSNES-FFL were investigated and compared together and with common hierarchical traffic controllers. Furthermore, all of the designed controllers were tested in PTV-VISSIM using the MATLAB-VISSIM COM interface.

In summary, to highlight the contributions of this dissertation, we listed them here:

1: Modeling a Heterogeneous Traffic Network. The first aim of this thesis was to develop a modeling framework that can describe and predict the behavior of a heterogeneous traffic network including human-driven vehicles and autonomous vehicles. To capture the realistic nature of the heterogeneous traffic network under the study, we determined a proper way of coupling the dynamics of AVs and HDVs and deriving state- and class-dependent model parameters which led us to achieve a high-fidelity mathematical model for the large-scale traffic model.

2: Developing and Enhancing Traffic Management Strategies for Large-scale Traffic Networks. The second achievement of this research was enhancing the mobility in homogeneous and heterogeneous traffic networks. We de-

signed and enhanced a hierarchical macroscopic control framework to examine to what extent mobility can be improved for different levels of heterogeneity when facing congestion during traffic peak hours. The main contribution of our novel designed controller is that it only requires very limited knowledge about the complex underlying traffic model with no information about the disturbance of the system. Furthermore, we enhanced the control framework performance by improving the upper-level controller to reduce the convergence time and resolve congestion issues faster.

3: Test and Validation. We also tested and validated our proposed hierarchical control framework by using a real-world traffic simulator, PTV-VISSIM, using MATLAB-VISSIM COM interface on both homogeneous and heterogeneous traffic networks.

As for future work of this research, we have two main recommendations. First, we recommend combining the filtered feedback linearization method with MPC to handle the physical constraints like restricted speed or flow in a large-scale traffic network through nonlinear mapping of the feedback linearization in the optimization problem. In the case of minimum-phase systems, designing a feedback linearization control results in an exactly linearized system that can be used for MPC design. A predictive controller combined with an exact input-output linearization is applied to a target cell in a large-scale traffic network, which enables accurate density tracking and compliance with the constraints. Second, in order to capture the realistic nature of heterogeneous traffic systems, the uncertainties associated with the unmodeled dynamics (which can intrinsically be state- and control-dependent) must be considered. Traditionally, traffic management approaches consider worst-case scenarios, where the uncertainty is conservatively estimated offline from limited data. The offline estimation approaches require significant amounts of data and may fail to capture new changes in the system. Thus, the desired safety/robustness objective is usually achieved at

the expense of closed-loop performance. To address this shortcoming, we propose to develop a learning-based hierarchical predictive control paradigm. In particular, we define three objectives for this project. First, at the upper- (macroscopic) level, we suggest developing distributed learning- and scenario-based model predictive control (DLB-sMPC) methods wherein functional variational Bayesian neural networks (BNNs) will be used to model the state- and input-dependent uncertainty online. Moreover, to enhance the computational efficiencies of the proposed DLB-sMPC, we recommend developing a set of distributed optimization algorithms. Second, at the lower- (microscopic) level, to balance between the closed-loop performance and safety (collision avoidance) on the road, we propose to develop distributed cautious model predictive control (MPC) based approaches for heterogeneous multi-agent systems. Finally, to validate the paradigm's effectiveness on an integrated model of a heterogeneous traffic network for both urban and highway scenarios, using PTV-VISSIM traffic simulation software is recommended.

REFERENCES

[1] Bob Pishue. Inrix global traffic scorecard–appendices. *INRIX research*, 2021.

[2] Negar Mehr and Roberto Horowitz. How will the presence of autonomous vehicles affect the equilibrium state of traffic networks? *IEEE Transactions on Control of Network Systems*, 7(1):96–105, 2019.

[3] Ajith Muralidharan and Roberto Horowitz. Computationally efficient model predictive control of freeway networks. *Transportation Research Part C: Emerging Technologies*, 58:532–553, 2015.

[4] H Inose, H Fujisaki, and T Hamada. Theory of road-traffic control based on macroscopic traffic model. *Electronics Letters*, 3(8):385–386, 1967.

[5] Mauro Vallati, Daniele Magazzeni, Bart De Schutter, Lukás Chrpa, and Thomas McCluskey. Efficient macroscopic urban traffic models for reducing congestion: A pddl+ planning approach. In *Proceedings of the AAAI Conference on Artificial Intelligence*, volume 30, 2016.

[6] SK Zegeye, B De Schutter, J Hellendoorn, EA Breunesse, and A Hegyi. Integrated macroscopic traffic flow, emission, and fuel consumption model for control purposes. *Transportation Research Part C: Emerging Technologies*, 31:158–171, 2013.

[7] VL Knoop, SP Hoogendoorn, and JWC Van Lint. Routing strategies based on macroscopic fundamental diagram. *Transportation Research Record*, 2315(1):1–10, 2012.

[8] Borja Alonso, Ángel Ibeas, Giuseppe Musolino, Corrado Rindone, and Antonino Vitetta. Effects of traffic control regulation on network macroscopic fundamen-

tal diagram: A statistical analysis of real data. *Transportation Research Part A: Policy and Practice*, 126:136–151, 2019.

[9] Mohammad Hajiahmadi, Jack Haddad, Bart De Schutter, and Nikolas Geroliminis. Optimal hybrid macroscopic traffic control for urban regions: Perimeter and switching signal plans controllers. In *2013 European Control Conference (ECC)*, pages 3500–3505. IEEE, 2013.

[10] Ardalan Vahidi and Antonio Sciarretta. Energy saving potentials of connected and automated vehicles. *Transportation Research Part C: Emerging Technologies*, 95:822–843, 2018.

[11] Antonio Sciarretta and Ardalan Vahidi. Energy saving potentials of cavs. In *Energy-Efficient Driving of Road Vehicles*, pages 1–31. Springer, 2020.

[12] David J Chang and Edward K Morlok. Vehicle speed profiles to minimize work and fuel consumption. *Journal of transportation engineering*, 131(3):173–182, 2005.

[13] Erik Hellström, Jan Åslund, and Lars Nielsen. Design of an efficient algorithm for fuel-optimal look-ahead control. *Control Engineering Practice*, 18(11):1318–1327, 2010.

[14] Md Abdus Samad Kamal, Masakazu Mukai, Junichi Murata, and Taketoshi Kawabe. Model predictive control of vehicles on urban roads for improved fuel economy. *IEEE Transactions on control systems technology*, 21(3):831–841, 2013.

[15] Zhiyuan Du and Pierluigi Pisu. A fuel efficient control strategy for connected vehicles in multiple-lane urban roads. In *Conference on Decision and Control*, pages 715–720, 2016.

[16] Behrang Asadi and Ardalan Vahidi. Predictive cruise control: Utilizing upcoming traffic signal information for improving fuel economy and reducing trip time. *IEEE transactions on control systems technology*, 19(3):707–714, 2011.

[17] G Mahler and A Vahidi. Red light avoidance through probabilistic traffic signal timing prediction. *IEEE Transactions on Intelligent Transportation Systems*, 15:2516–2523, 2014.

[18] Sindhura Mandava, Kanok Boriboonsomsin, and Matthew Barth. Arterial velocity planning based on traffic signal information under light traffic conditions. In *IEEE Conference on Intelligent Transportation Systems*, pages 1–6, 2009.

[19] Hesham Rakha and Raj Kishore Kamalanathsharma. Eco-driving at signalized intersections using v2i communication. In *IEEE Conference on Intelligent Transportation Systems*, pages 341–346, 2011.

[20] Markos Papageorgiou, Christina Diakaki, Vaya Dinopoulou, Apostolos Kotsialos, and Yibing Wang. Review of road traffic control strategies. *Proceedings of the IEEE*, 91(12):2043–2067, 2003.

[21] Jackeline Rios-Torres and Andreas A Malikopoulos. A survey on the coordination of connected and automated vehicles at intersections and merging at highway on-ramps. *IEEE Transactions on Intelligent Transportation Systems*, 18(5):1066–1077, 2016.

[22] Yu-Chiun Chiou, Chen-An Sun, and Chih-Wei Hsieh. A macro-micro model under mixed traffic flow conditions. *Journal of the Eastern Asia Society for Transportation Studies*, 11:1931–1944, 2015.

[23] Sasan Amini, Ilias Gerostathopoulos, and Christian Prehofer. Big data analytics architecture for real-time traffic control. In *2017 5th IEEE international con-*

ference on models and technologies for intelligent transportation systems (MT-ITS), pages 710–715. IEEE, 2017.

[24] RP Alvarez Gil, Zsolt Csaba Johanyák, Tamás Kovács, et al. Surrogate model based optimization of traffic lights cycles and green period ratios using microscopic simulation and fuzzy rule interpolation. *Int. J. Artif. Intell*, 16(1):20–40, 2018.

[25] Tom Bellemans, Bart De Schutter, and Bart De Moor. Models for traffic control. *JOURNAL A*, 43(3/4):13–22, 2002.

[26] Markos Papageorgiou and Apostolos Kotsialos. Freeway ramp metering: An overview. *IEEE transactions on intelligent transportation systems*, 3(4):271–281, 2002.

[27] Mohammad Jannati, Sajad Abdollahzadeh Anbaran, Seyed Hesam Asgari, Wee Yen Goh, Ali Monadi, Mohd Junaidi Abdul Aziz, and Nik Rumzi Nik Idris. A review on variable speed control techniques for efficient control of single-phase induction motors: evolution, classification, comparison. *Renewable and Sustainable Energy Reviews*, 75:1306–1319, 2017.

[28] Yihang Zhang and Petros A Ioannou. Coordinated variable speed limit, ramp metering and lane change control of highway traffic. *IFAC-PapersOnLine*, 50(1):5307–5312, 2017.

[29] Fábio Duarte and Carlo Ratti. The impact of autonomous vehicles on cities: A review. *Journal of Urban Technology*, 25(4):3–18, 2018.

[30] Yair Wiseman. Autonomous vehicles. In *Research anthology on cross-disciplinary designs and applications of automation*, pages 878–889. IGI Global, 2022.

[31] Pouria Karimi Shahri, Amir H Ghasemi, and Vahid Izadi. Optimal lane management in heterogeneous traffic network using extremum seeking approach. Technical report, SAE Technical Paper, 2020.

[32] Yujie Li, Sikai Chen, Jiqian Dong, Aaron Steinfeld, Samuel Labi, et al. Leveraging vehicle connectivity and autonomy to stabilize flow in mixed traffic conditions: Accounting for human-driven vehicle driver behavioral heterogeneity and perception-reaction time delay. *arXiv preprint arXiv:2008.04351*, 2020.

[33] Mohsen Ramezani and Eric Ye. Lane density optimisation of automated vehicles for highway congestion control. *Transportmetrica B: Transport Dynamics*, 7(1):1096–1116, 2019.

[34] Lakshmi Dhevi Baskar, Bart De Schutter, and Hans Hellendoorn. Traffic management for automated highway systems using model-based predictive control. *IEEE Transactions on Intelligent Transportation Systems*, 13(2):838–847, 2012.

[35] Yicheng Zhang, Rong Su, Chunyang Sun, and Yi Zhang. Modelling and traffic signal control of a heterogeneous traffic network with signalized and non-signalized intersections. In *2017 IEEE Conference on Control Technology and Applications (CCTA)*, pages 1581–1586. IEEE, 2017.

[36] Ch Mallikarjuna and K Ramachandra Rao. Heterogeneous traffic flow modelling: a complete methodology. *Transportmetrica*, 7(5):321–345, 2011.

[37] Mallikarjuna Chunchu, Ramachandra Rao Kalaga, and Naga Venkata Satish Kumar Seethepalli. Analysis of microscopic data under heterogeneous traffic conditions. *Transport*, 25(3):262–268, 2010.

[38] Michael James Lighthill and Gerald Beresford Whitham. On kinematic waves ii. a theory of traffic flow on long crowded roads. *Proceedings of the Royal Society*

of London. Series A. Mathematical and Physical Sciences, 229(1178):317–345, 1955.

[39] Paul I Richards. Shock waves on the highway. *Operations research*, 4(1):42–51, 1956.

[40] Antonella Ferrara, Simona Sacone, and Silvia Siri. *Freeway traffic modelling and control*. Springer, 2018.

[41] Mohammed Al-Turki, Nedal T Ratrout, Syed Masiur Rahman, and Imran Reza. Impacts of autonomous vehicles on traffic flow characteristics under mixed traffic environment: Future perspectives. *Sustainability*, 13(19):11052, 2021.

[42] Laura Muñoz, Xiaotian Sun, Roberto Horowitz, and Luis Alvarez. Traffic density estimation with the cell transmission model. In *Proceedings of the 2003 American Control Conference, 2003.*, volume 5, pages 3750–3755. IEEE, 2003.

[43] Puspita Deo, Bart De Schutter, and Andreas Hegyi. Model predictive control for multi-class traffic flows. *IFAC Proceedings Volumes*, 42(15):25–30, 2009.

[44] Florence Giorgi, Ludovic Leclercq, and Jean-Baptiste Lesort. A traffic flow model for urban traffic analysis: extensions of the lwr model for urban and environmental applications. In *Transportation and Traffic Theory in the 21st Century*, pages 393–415. Emerald Group Publishing Limited, 2002.

[45] B Haut, G Bastin, and Y Chitour. A macroscopic traffic model for road networks with a representation of the capacity drop phenomenon at the junctions. *IFAC Proceedings Volumes*, 38(1):114–119, 2005.

[46] CF Daganzo. The cell transmission model. part i: A simple dynamic representation of highway traffic. berkeley, ca: Institute of transportation studies. *University of California, Berkeley*, 1993.

[47] Carlos F Daganzo. The cell transmission model: A dynamic representation of highway traffic consistent with the hydrodynamic theory. *Transportation Research Part B: Methodological*, 28(4):269–287, 1994.

[48] Carlos F Daganzo. The cell transmission model, part ii: network traffic. *Transportation Research Part B: Methodological*, 29(2):79–93, 1995.

[49] Jingqiu Guo, Senlin Cheng, and Yangzexi Liu. Merging and diverging impact on mixed traffic of regular and autonomous vehicles. *IEEE Transactions on Intelligent Transportation Systems*, 22(3):1639–1649, 2020.

[50] Markos Papageorgiou. Dynamic modeling, assignment, and route guidance in traffic networks. *Transportation Research Part B: Methodological*, 24(6):471–495, 1990.

[51] Markos Papageorgiou, Ioannis Papamichail, Albert Messmer, and Yibing Wang. Traffic simulation with metanet. In *Fundamentals of traffic simulation*, pages 399–430. Springer, 2010.

[52] Edward N Holland and Andrew W Woods. A continuum model for the dispersion of traffic on two-lane roads. *Transportation Research Part B: Methodological*, 31(6):473–485, 1997.

[53] Carlos F Daganzo. A continuum theory of traffic dynamics for freeways with special lanes. *Transportation Research Part B: Methodological*, 31(2):83–102, 1997.

[54] Wen-Long Jin. A kinematic wave theory of multi-commodity network traffic flow. *Transportation Research Part B: Methodological*, 46(8):1000–1022, 2012.

[55] Wen-Long Jin. A multi-commodity lighthill–whitham–richards model of lane-

changing traffic flow. *Transportation Research Part B: Methodological*, 57:361–377, 2013.

[56] S Logghe and Lambertus H Immers. Multi-class kinematic wave theory of traffic flow. *Transportation Research Part B: Methodological*, 42(6):523–541, 2008.

[57] Carlos F Daganzo. A behavioral theory of multi-lane traffic flow. part i: Long homogeneous freeway sections. *Transportation Research Part B: Methodological*, 36(2):131–158, 2002.

[58] JWC Van Lint, Serge P Hoogendoorn, and Marco Schreuder. Fastlane: New multiclass first-order traffic flow model. *Transportation Research Record*, 2088(1):177–187, 2008.

[59] Thomas Schreiter, Hans van Lint, and Serge Hoogendoorn. Multi-class ramp metering: Concepts and initial results. In *2011 14th International IEEE Conference on Intelligent Transportation Systems (ITSC)*, pages 885–889. IEEE, 2011.

[60] Mohinder S Grewal and Harold J Payne. Identification of parameters in a freeway traffic model. *IEEE Transactions on systems, man, and cybernetics*, (3):176–185, 1976.

[61] Carlos F Daganzo. Requiem for second-order fluid approximations of traffic flow. *Transportation Research Part B: Methodological*, 29(4):277–286, 1995.

[62] AATM Aw and Michel Rascle. Resurrection of" second order" models of traffic flow. *SIAM journal on applied mathematics*, 60(3):916–938, 2000.

[63] H Michael Zhang. A non-equilibrium traffic model devoid of gas-like behavior. *Transportation Research Part B: Methodological*, 36(3):275–290, 2002.

[64] Apostolos Kotsialos, Markos Papageorgiou, Christina Diakaki, Yannis Pavlis, and Frans Middelham. Traffic flow modeling of large-scale motorway networks using the macroscopic modeling tool metanet. *IEEE Transactions on intelligent transportation systems*, 3(4):282–292, 2002.

[65] Markos Papageorgiou, Jean-Marc Blosseville, and Habib Hadj-Salem. Macroscopic modelling of traffic flow on the boulevard périphérique in paris. *Transportation Research Part B: Methodological*, 23(1):29–47, 1989.

[66] Markos Papageorgiou, Jean-Marc Blosseville, and Habib Hadj-Salem. Modelling and real-time control of traffic flow on the southern part of boulevard peripherique in paris: Part i: Modelling. *Transportation Research Part A: General*, 24(5):345–359, 1990.

[67] Shuai Liu, Bart De Schutter, and Hans Hellendoorn. Model predictive traffic control based on a new multi-class metanet model. *IFAC Proceedings Volumes*, 47(3):8781–8786, 2014.

[68] Shuai Liu, Hans Hellendoorn, and Bart De Schutter. Model predictive control for freeway networks based on multi-class traffic flow and emission models. *IEEE Transactions on Intelligent Transportation Systems*, 18(2):306–320, 2016.

[69] Carlo Caligaris, Simona Sacone, and Silvia Siri. Optimal ramp metering and variable speed signs for multiclass freeway traffic. In *2007 European Control Conference (ECC)*, pages 1780–1785. IEEE, 2007.

[70] Cecilia Pasquale, Simona Sacone, and Silvia Siri. Two-class emission traffic control for freeway systems. *IFAC Proceedings Volumes*, 47(3):936–941, 2014.

[71] Cecilia Pasquale, Ioannis Papamichail, Claudio Roncoli, Simona Sacone, Silvia Siri, and Markos Papageorgiou. Two-class freeway traffic regulation to reduce

congestion and emissions via nonlinear optimal control. *Transportation Research Part C: Emerging Technologies*, 55:85–99, 2015.

[72] Cecilia Pasquale, Simona Sacone, Silvia Siri, and Bart De Schutter. A multi-class model-based control scheme for reducing congestion and emissions in freeway networks by combining ramp metering and route guidance. *Transportation Research Part C: Emerging Technologies*, 80:384–408, 2017.

[73] Muneer Muslih, Ahmed Abduljabbar, and Hasan Joni. Review of traffic demand management strategies. In *IOP Conference Series: Earth and Environmental Science*, volume 1232, page 012055. IOP Publishing, 2023.

[74] Markos Papageorgiou. *Applications of automatic control concepts to traffic flow modeling and control*. Springer, 1983.

[75] Markos Papageorgiou. Overview of road traffic control strategies. *IFAC Proceedings Volumes*, 37(19):29–40, 2004.

[76] Hong K Lo and Andy HF Chow. Control strategies for oversaturated traffic. *Journal of Transportation Engineering*, 130(4):466–478, 2004.

[77] András Hegyi. *Model predictive control for integrating traffic control measures*. Netherlands TRAIL Research School, 2004.

[78] Srinivas Peeta and T-H Yang. Stability issues for dynamic traffic assignment. *Automatica*, 39(1):21–34, 2003.

[79] Massimo Di Gangi, Giulio E Cantarella, Roberta Di Pace, and Silvio Memoli. Network traffic control based on a mesoscopic dynamic flow model. *Transportation Research Part C: Emerging Technologies*, 66:3–26, 2016.

[80] Xu Zhang and Thomas Riedel. Urban traffic control: present and the future. *International Journal of Urban Sciences*, 21(sup1):87–100, 2017.

[81] Konstantinos Ampountolas and Anastasios Kouvelas. Real-time estimation of critical values of the macroscopic fundamental diagram for maximum network throughput. In *TRB 94th Annual Meeting Compendium of Papers*, pages 15–1779. Transportation Research Board, 2015.

[82] Hansong Yu and Zhongsheng Hou. Two-level hierarchical optimal control for urban traffic networks. *Transportmetrica A: transport science*, 18(1):144–165, 2022.

[83] Pouria Karimi Shahri, Baisravan HomChaudhuri, Azad Ghaffari, and Amir H Ghasemi. Designing traffic management strategies for a heterogeneous traffic network. *IFAC-PapersOnLine*, 55(37):694–699, 2022.

[84] Pouria Karimi Shahri, Baisravan HomChaudhuri, Azad Ghaffari, and Amir H Ghasemi. Infrastructure-based hierarchical control design for congestion management in heterogeneous traffic networks. In *2023 American Control Conference (ACC)*, pages 4399–4404. IEEE, 2023.

[85] Pouria Karimi Shahri and Amir H Ghasemi. Heterogeneous traffic management using metanet model with filtered feedback linearization control approach. Technical report, SAE Technical Paper, 2022.

[86] Rodrigo C Carlson, Ioannis Papamichail, Markos Papageorgiou, and Albert Messmer. Optimal motorway traffic flow control involving variable speed limits and ramp metering. *Transportation science*, 44(2):238–253, 2010.

[87] Duo Li, Yifei Zhao, Prakash Ranjitkar, Haijiang Zhao, and Qiang Bai. Hybrid approach for variable speed limit implementation and application to mixed traffic conditions with connected autonomous vehicles. *IET Intelligent Transport Systems*, 12(5):327–334, 2017.

[88] Yina Wu, Mohamed Abdel-Aty, Ling Wang, and Md Sharikur Rahman. Combined connected vehicles and variable speed limit strategies to reduce rear-end crash risk under fog conditions. *Journal of Intelligent Transportation Systems*, 24(5):494–513, 2020.

[89] Rongsheng Chen, Tab Zhang, and Michael W Levin. Effects of variable speed limit on energy consumption with autonomous vehicles on urban roads using modified cell-transmission model. *Journal of Transportation Engineering, Part A: Systems*, 146(7):04020049, 2020.

[90] Miao Yu and Wei "David" Fan. Optimal variable speed limit control in connected autonomous vehicle environment for relieving freeway congestion. *Journal of Transportation Engineering, Part A: Systems*, 145(4):04019007, 2019.

[91] Andreas A Malikopoulos, Seongah Hong, B Brian Park, Joyoung Lee, and Seunghan Ryu. Optimal control for speed harmonization of automated vehicles. *IEEE Transactions on Intelligent Transportation Systems*, 20(7):2405–2417, 2018.

[92] Mofan Zhou, Xiaobo Qu, and Sheng Jin. On the impact of cooperative autonomous vehicles in improving freeway merging: a modified intelligent driver model-based approach. *IEEE Transactions on Intelligent Transportation Systems*, 18(6):1422–1428, 2016.

[93] Zhibin Li, Chengcheng Xu, Dawei Li, Pan Liu, and Wei Wang. Comparing the effects of ramp metering and variable speed limit on reducing travel time and crash risk at bottlenecks. *IET Intelligent Transport Systems*, 12(2):120–126, 2017.

[94] Péter Gáspár and Balázs Németh. Control strategy of the ramp metering in the

mixed traffic flow. In *Predictive Cruise Control for Road Vehicles Using Road and Traffic Information*, pages 121–132. Springer, 2019.

[95] Changyin Dong, Hao Wang, Ye Li, Wei Wang, and Zhe Zhang. Route control strategies for autonomous vehicles exiting to off-ramps. *IEEE Transactions on Intelligent Transportation Systems*, 2019.

[96] Qiangqiang Guo, Li Li, and Xuegang Jeff Ban. Urban traffic signal control with connected and automated vehicles: A survey. *Transportation research part C: emerging technologies*, 101:313–334, 2019.

[97] Biao Xu, Xuegang Jeff Ban, Yougang Bian, Wan Li, Jianqiang Wang, Shengbo Eben Li, and Keqiang Li. Cooperative method of traffic signal optimization and speed control of connected vehicles at isolated intersections. *IEEE Transactions on Intelligent Transportation Systems*, 20(4):1390–1403, 2018.

[98] Jihene Rezgui, Émile Gagné, Guillaume Blain, Olivier St-Pierre, and Maximilien Harvey. Platooning of autonomous vehicles with artificial intelligence v2i communications and navigation algorithm. In *2020 Global Information Infrastructure and Networking Symposium (GIIS)*, pages 1–6. IEEE, 2020.

[99] Jian Wang, Siyuan Gong, Srinivas Peeta, and Lili Lu. A real-time deployable model predictive control-based cooperative platooning approach for connected and autonomous vehicles. *Transportation Research Part B: Methodological*, 128:271–301, 2019.

[100] Siyuan Gong and Lili Du. Cooperative platoon control for a mixed traffic flow including human drive vehicles and connected and autonomous vehicles. *Transportation research part B: methodological*, 116:25–61, 2018.

[101] Junyan Hu, Parijat Bhowmick, Farshad Arvin, Alexander Lanzon, and Barry Lennox. Cooperative control of heterogeneous connected vehicle platoons: An

adaptive leader-following approach. *IEEE Robotics and Automation Letters*, 5(2):977–984, 2020.

[102] Marcel Sala and Francesc Soriguera. Macroscopic modeling of connected autonomous vehicle platoons under mixed traffic conditions. *Transportation Research Procedia*, 47:163–170, 2020.

[103] Mahyar Amirgholy, Mehrdad Shahabi, and H Oliver Gao. Traffic automation and lane management for communicant, autonomous, and human-driven vehicles. *Transportation research part C: emerging technologies*, 111:477–495, 2020.

[104] Pouria Karimi Shahri, Shubhankar Chintamani Shindgikar, Baisravan Hom-Chaudhuri, and Amir H Ghasemi. Optimal lane management in heterogeneous traffic network. In *Dynamic Systems and Control Conference*, volume 59162, page V003T18A003. American Society of Mechanical Engineers, 2019.

[105] Shengbo Eben Li, Feng Gao, Keqiang Li, Le-Yi Wang, Keyou You, and Dongpu Cao. Robust longitudinal control of multi-vehicle systems—a distributed h-infinity method. *IEEE Transactions on Intelligent Transportation Systems*, 19(9):2779–2788, 2017.

[106] Na Chen, Meng Wang, Tom Alkim, and Bart van Arem. A robust longitudinal control strategy of platoons under model uncertainties and time delays. *Journal of Advanced Transportation*, 2018, 2018.

[107] Cathy Wu, Alexandre M Bayen, and Ankur Mehta. Stabilizing traffic with autonomous vehicles. In *2018 IEEE International Conference on Robotics and Automation (ICRA)*, pages 1–7. IEEE, 2018.

[108] Fangfang Zheng, Can Liu, Xiaobo Liu, Saif Eddin Jabari, and Liang Lu. Analyzing the impact of automated vehicles on uncertainty and stability of the mixed

traffic flow. *Transportation research part C: emerging technologies*, 112:203–219, 2020.

[109] Mohsen Ramezani, Jack Haddad, and Nikolas Geroliminis. Dynamics of heterogeneity in urban networks: aggregated traffic modeling and hierarchical control. *Transportation Research Part B: Methodological*, 74:1–19, 2015.

[110] Youngjun Han, Danjue Chen, and Soyoung Ahn. Variable speed limit control at fixed freeway bottlenecks using connected vehicles. *Transportation Research Part B: Methodological*, 98:113–134, 2017.

[111] Alireza Talebpour, Hani S Mahmassani, and Amr Elfar. Investigating the effects of reserved lanes for autonomous vehicles on congestion and travel time reliability. *Transportation Research Record*, 2622(1):1–12, 2017.

[112] Maria Laura Delle Monache, Thibault Liard, Anaïs Rat, Raphael Stern, Rahul Bhadani, Benjamin Seibold, Jonathan Sprinkle, Daniel B Work, and Benedetto Piccoli. Feedback control algorithms for the dissipation of traffic waves with autonomous vehicles. In *Computational Intelligence and Optimization Methods for Control Engineering*, pages 275–299. Springer, 2019.

[113] Danjue Chen, Soyoung Ahn, Madhav Chitturi, and David A Noyce. Towards vehicle automation: Roadway capacity formulation for traffic mixed with regular and automated vehicles. *Transportation research part B: methodological*, 100:196–221, 2017.

[114] Zhibin Chen, Fang He, Lihui Zhang, and Yafeng Yin. Optimal deployment of autonomous vehicle lanes with endogenous market penetration. *Transportation Research Part C: Emerging Technologies*, 72:143–156, 2016.

[115] Marcello Montanino, Julien Monteil, and Vincenzo Punzo. From homogeneous

to heterogeneous traffic flows: Lp string stability under uncertain model parameters. *Transportation Research Part B: Methodological*, 146:136–154, 2021.

[116] Huan Yu, Shumon Koga, Tiago Roux Oliveira, and Miroslav Krstic. Extremum seeking for traffic congestion control with a downstream bottleneck. *Journal of Dynamic Systems, Measurement, and Control*, 143(3), 2021.

[117] Zhen Wang, Xiangmo Zhao, Zhigang Xu, Xiaopeng Li, and Xiaobo Qu. Modeling and field experiments on autonomous vehicle lane changing with surrounding human-driven vehicles. *Computer-Aided Civil and Infrastructure Engineering*, 2020.

[118] Dai Li and Zhongsheng Hou. Perimeter control of urban traffic networks based on model-free adaptive control. *IEEE Transactions on Intelligent Transportation Systems*, 22(10):6460–6472, 2020.

[119] Pouria Karimi Shahri, Baisravan HomChaudhuri, Srinivas S Pulugurtha, Ali Mesbah, and Amir H Ghasemi. Traffic congestion control using distributed extremum seeking and filtered feedback linearization control approaches. *IEEE Control Systems Letters*, 7:1003–1008, 2022.

[120] Pouria Karimi Shahri, Baisravan HomChaudhuri, Azad Ghaffari, and Amirhossein Ghasemi. Improving the performance of a hierarchical traffic flow control framework using lyapunov-based switched newton extremum seeking. *ASME Letters in Dynamic Systems and Control*, pages 1–6, 2023.

[121] Qian Chen, Shihua Li, Chengchuan An, Jingxin Xia, and Wenming Rao. Feedback linearization-based perimeter controllers for oversaturated regions. *IEEE Intelligent Transportation Systems Magazine*, 14(1), 2022.

[122] Kimia Chavoshi, Antonella Ferrara, and Anastasios Kouvelas. A feedback lin-

earization approach for coordinated traffic flow management in highway systems. *Control Engineering Practice*, 139:105615, 2023.

[123] Jesse B Hoagg and TM Seigler. Filtered-dynamic-inversion control for unknown minimum-phase systems with unknown-and-unmeasured disturbances. *International Journal of Control*, 86(3):449–468, 2013.

[124] Amir H Ghasemi. Slewing and vibration control of a single-link flexible manipulator using filtered feedback linearization. *Journal of Intelligent Material Systems and Structures*, 28(20):2887–2895, 2017.

[125] AH Ghasemi, Jesse B Hoagg, and TM Seigler. Decentralized vibration and shape control of structures with colocated sensors and actuators. *Journal of Dynamic Systems, Measurement, and Control*, 138(3):031011, 2016.

[126] Markos Papageorgiou, Habib Hadj-Salem, Jean-Marc Blosseville, et al. Alinea: A local feedback control law for on-ramp metering. *Transportation research record*, 1320(1):58–67, 1991.

[127] Farzam Tajdari, Claudio Roncoli, Nikolaos Bekiaris-Liberis, and Markos Papageorgiou. Integrated ramp metering and lane-changing feedback control at motorway bottlenecks. In *2019 18th European Control Conference (ECC)*, pages 3179–3184. IEEE, 2019.

[128] Azad Ghaffari, Miroslav Krstić, and Dragan Nešić. Multivariable newton-based extremum seeking. *Automatica*, 48(8):1759–1767, 2012.

[129] Kartik B Ariyur and Miroslav Krstic. *Real-time optimization by extremum-seeking control*. John Wiley & Sons, 2003.

[130] Mouhacine Benosman. *Learning-based adaptive control: An extremum seeking approach–theory and applications*. Butterworth-Heinemann, 2016.

[131] Jan Feiling, Shumon Koga, Miroslav Krstić, and Tiago Roux Oliveira. Gradient extremum seeking for static maps with actuation dynamics governed by diffusion pdes. *Automatica*, 95:197–206, 2018.

[132] Azad Ghaffari, Miroslav Krstić, and Sridhar Seshagiri. Power optimization and control in wind energy conversion systems using extremum seeking. *IEEE transactions on control systems technology*, 22(5):1684–1695, 2014.

[133] Martin Guay and Tao Zhang. Adaptive extremum seeking control of nonlinear dynamic systems with parametric uncertainties. *Automatica*, 39(7):1283–1293, 2003.

[134] Shu-Jun Liu and Miroslav Krstic. Stochastic averaging in discrete time and its applications to extremum seeking. *IEEE Transactions on Automatic control*, 61(1):90–102, 2015.

[135] Damir Rušiti, Giulio Evangelisti, Tiago Roux Oliveira, Matthias Gerdts, and Miroslav Krstić. Stochastic extremum seeking for dynamic maps with delays. *IEEE control systems letters*, 3(1):61–66, 2018.

[136] Miroslav Krstić and Hsin-Hsiung Wang. Stability of extremum seeking feedback for general nonlinear dynamic systems. *Automatica*, 36(4):595–601, 2000.

[137] Joon-Young Choi, Miroslav Krstic, Kartik B Ariyur, and Jin Soo Lee. Extremum seeking control for discrete-time systems. *IEEE Transactions on automatic control*, 47(2):318–323, 2002.

[138] Dragan Nešić. Extremum seeking control: Convergence analysis. *European Journal of Control*, 15(3-4):331–347, 2009.

[139] Chunlei Zhang and Raúl Ordóñez. *Extremum-seeking control and applications:*

a numerical optimization-based approach. Springer Science & Business Media, 2011.

[140] Ronny Kutadinata, Will Moase, Chris Manzie, Lele Zhang, and Tim Garoni. Enhancing the performance of existing urban traffic light control through extremum-seeking. *Transportation Research Part C: Emerging Technologies*, 62:1–20, 2016.

[141] Zejiang Wang, Xingyu Zhou, and Junmin Wang. Extremum-seeking-based adaptive model-free control and its application to automated vehicle path tracking. *IEEE/ASME Transactions on Mechatronics*, 2022.

[142] Darryl DeHaan and Martin Guay. Extremum-seeking control of state-constrained nonlinear systems. *Automatica*, 41(9):1567–1574, 2005.

[143] Martin Guay and Denis Dochain. A time-varying extremum-seeking control approach. *Automatica*, 51:356–363, 2015.

[144] Huan Yu, Jean Auriol, and Miroslav Krstic. Simultaneous downstream and upstream output-feedback stabilization of cascaded freeway traffic. *Automatica*, 136:110044, 2022.

[145] Yang Tian, Ning Pan, Maobo Hu, Haoping Wang, Ivan Simeonov, Lyudmila Kabaivanova, and Nicolai Christov. Newton-based extremum seeking for dynamic systems using kalman filtering: Application to anaerobic digestion process control. *Mathematics*, 11(1):251, 2023.

[146] Alireza Bafandeh and Chris Vermillion. Altitude optimization of airborne wind energy systems via switched extremum seeking—design, analysis, and economic assessment. *IEEE Transactions on Control Systems Technology*, 25(6):2022–2033, 2016.

[147] HJ Payne. Models of freeway traffic and control, simulation councils proc. *Ser.: Mathematical Models of Public Systems*, 1(1).

[148] Hassan K Khalil. Control of nonlinear systems.

[149] M Cremer and Markos Papageorgiou. Parameter identification for a traffic flow model. *Automatica*, 17(6):837–843, 1981.

[150] Albert Messner and Markos Papageorgiou. Metanet: A macroscopic simulation program for motorway networks. *Traffic engineering & control*, 31(8-9):466–470, 1990.

[151] Carlos F Daganzo and Nikolas Geroliminis. An analytical approximation for the macroscopic fundamental diagram of urban traffic. *Transportation Research Part B: Methodological*, 42(9):771–781, 2008.

[152] Xu Wang, Derek Yin, and Tony Z Qiu. Applicability analysis of an extended metanet model in traffic-state prediction for congested freeway corridors. *Journal of Transportation Engineering, Part A: Systems*, 144(9):04018046, 2018.

[153] Sylvie Benzoni-Gavage and Rinaldo M Colombo. An-populations model for traffic flow. *European Journal of Applied Mathematics*, 14(5):587–612, 2003.

[154] Stéphane Chanut and Christine Buisson. Macroscopic model and its numerical solution for two-flow mixed traffic with different speeds and lengths. *Transportation research record*, 1852(1):209–219, 2003.

[155] Steven Logghe. Dynamic modeling of heterogeneous vehicular traffic. *Faculty of Applied Science, Katholieke Universiteit Leuven, Leuven*, 2, 2003.

[156] Zhen Sean Qian, Jia Li, Xiaopeng Li, Michael Zhang, and Haizhong Wang. Modeling heterogeneous traffic flow: A pragmatic approach. *Transportation Research Part B: Methodological*, 99:183–204, 2017.

[157] Jesse B Hoagg and TM Seigler. Decentralized filtered dynamic inversion for uncertain minimum-phase systems. *Automatica*, 61:192–200, 2015.

[158] Yulie Gong, Guangping Liu, and Zhenneng Lu. Extremum seeking control for real-time optimization of high temperature heat pump systems incorporating vapor injection. *Thermal Science and Engineering Progress*, 42:101867, 2023.

[159] Xin-Yue Guo, Geng Zhang, and Ai-Fang Jia. Study on mixed traffic of autonomous vehicles and human-driven vehicles with different cyber interaction approaches. *Vehicular Communications*, 39:100550, 2023.

[160] Shubhankar Chintamani Shindgikar, Pouria Karimi Shahri, and Amir H Ghasemi. Modelling and control of multi-vehicle traffic networks using an integrated vissim-matlab simulation platform. Technical report, SAE Technical Paper, 2020.